Massive neutrinos and spherical collapse in ΛCDM and DGP gravity

by

Odd Petter Sand

Thesis

for the degree of

Master of Science in Astronomy

Institute of Theoretical Astrophysics
University of Oslo

September 2016

Abstract

Spherical collapse is a crude, but useful toy model for structure formation in an expanding universe. Previous works have looked at this model in ΛCDM with massive neutrinos, where the primary findings were that massive neutrinos in general delay the formation of structure in the universe, but this is to some small extent counteracted by neutrinos clustering in the dark matter halo. One has also studied spherical collapse in DGP gravity, a form of modified gravity without a cosmological constant, where weakened gravity on large scales instead explain the accelerated expansion of the universe.

This thesis aims to take the next step and look at combining the two approaches into one: Modelling spherical collapse with massive neutrinos and DGP gravity at the same time. Previous studies give us reason to expect certain degeneracies here - data might well be explained by both effects, making it difficult to pinpoint to what extent each influences observations. Investigating these degeneracies is therefore our goal.

We design and implement an algorithm to investigate spherical collapse in Python 2, with initial conditions from a modified version of the CAMB code. We find that top-hat overdensities in DGP gravity with a similar background to ΛCDM in general collapse much later. In particular, for massless neutrino collapse in DGP to look like massive neutrino collapse in ΛCDM, the sum of neutrino masses needs to be at least 0.8 eV, well in excess of current cosmological upper bounds.

In the absence of neutrino clustering, we observe the same difference of 0.8 eV with massive neutrinos in both cosmologies, but note a significant dependency on this number of the choice of h and r_c in DGP gravity. For an alternate parameter set, we need an even higher difference in total neutrino mass. This suggests that massive neutrinos with realistic masses may be unable to completely mask the effects of a modified theory of gravity, but we cannot rule out that there exists a combination of DGP parameters that cancels this effect.

Preface

What a long and winding road it has been.

It seems strange to look at the finished result and knowing that half of the text didn't even make it into the thesis you hold in your hands. If this work has taught me anything, it is that research is not linear. Going off on a tangent of possibility, hitting the brick wall of reality and starting over is not only part of the process, but central to it. Yet in the end, so much of that effort is hidden away, leaving only the things that worked, or worked well enough. And even then, the hours of debugging, checking calculations and results are only implicit. I now find it a little strange that one puts in all this effort and then attempts to present it as effortless. Perhaps that is how this misconception arose to begin with.

I have also learned a lot about the flawed concept of perfection. I used to be very goal-oriented and concerned with how to reach those goals. Now I find myself focusing more on the activities that get you there, and taking care of the human in that process. It has been a liberating experience. And I think the key is that when you worry and suffer enough, you eventually get tired of it and decide to try something different. Not that there's anything *wrong* with trying too hard per se. It may well be a necessary step to bring attention to what you are doing. Struggle is a great teacher.

In this context, I am thankful to have been given a challenging project for my master's thesis, although I didn't know that when I started. If I had, I might have taken an easier way out, and those lessons might have gone unlearned, at least for now.

I am proud of the process that led me here. That's not to say I'm not satisfied with the result as well. Just know it for what it is: Not the whole story.

Acknowledgements

First and foremost I would like to thank my supervisor and sensei, professor Øystein Elgarøy, for taking the time to take care not just of the student, but also the person. A true mentor, I eventually learned to trust in your stubborn optimism on behalf of the work I was doing, and in so doing started to trust myself more. That is a great gift.

Also a big thank you Signe Riemer-Sørensen, who helped me find a place to start when poking around the maze that is the CAMB code, which turned out to be a fun experience, and to the many contributors at StackExchange, which turned out to be a fantastic repository for figuring out technical details.

I am most grateful to Kiyotomo Ichiki (University of Nagoya, Japan) and Masahiro Takada (Kavli IPMU, Tokyo, Japan), who took the time to receive me in person and discuss my project during my exchange semester in Japan, and who most generously shared the details of their work. Their insights helped push me in the right direction. I am also grateful to Marilena LoVerde (C. N. Yang Institute of Theoretical Physics, Stony Brook University, New York, USA) for patiently answering my e-mails about details in her articles.

Thank you to the Institutes of Astrophysics and Mathematics, who gave me the opportunity to teach while working on this thesis. Not only did it give me the means to support myself, but also gave me something constructive to focus on for a while whenever I found myself stuck. Thank you to all the students in my math and astronomy classes during these years - you really made me feel appreciated and that I made a positive difference.

Big thanks to Ursi Canentes, who provided much needed diversions after long days in the study room, and to my understanding fellow master students there, for giving me some quiet alone time when I needed it. And to my family, for always being there for each other.

Last, but not least, warm thanks to my girlfriend Marie, for your unwavering support. Thank you for taking care of me during the intense final weeks, for inspiring me and for sharing your own considerable experience. But most of all, just for being you. You'll never walk alone. ♡

Contents

List of Figures

Chapter 1

Introduction

Even as the universe expands, structures form by gravitational attraction.

One proposed way to explain that the expansion seems to currently be accelerating, is to employ modified theories of gravity. If Newton's gravitational constant grows gradually weaker as one approaches scales significantly larger than the Solar System, the universe will expand faster the larger it becomes. However, this effect may well even affect scales much smaller than the horizon of the observable universe, as overdense clouds of matter will collapse more slowly to galaxies compared to a standard gravity theory with mysterious dark energy.

The rate at which these structures form also depends on the masses of neutrinos, potentially both as a background component and through the extent that neutrinos cluster in gravity wells made up of dark and baryonic matter. Increasing the mass of massive neutrinos will make the background universe decelerate more slowly, delaying structure formation somewhat[1], whereas neutrino clustering will have the opposite effect.

When using galaxy formation as a probe of both of these effects, one therefore expects them to be degenerate[1]. If both are present, one effect may mask the other to some extent or even completely, making it potentially extremely challenging to use observations such as the planned Euclid mission[2] to fulfil its goal of looking for both.

The best way to examine degeneracies such as these is to use N-body simulations for a range of parameters. However, these are complex and relatively time-intensive. Hence, the much simpler model of spherical collapse is a way to get a faster preliminary handle on these degeneracies. In this thesis, we perform spherical collapse in a massive neutrino background, in standard gravity and a flavour of modified gravity named DGP gravity[2]. These simulations are run with

[1]This sounds counterintuitive at first glance, but we will explain why this happens in subsection 2.8.1 Note for now that we are considering the collapse of a fixed mass M_{cb} of cold dark matter and baryons. Neutrinos only contribute to the background and, optionally, clustering in the potential set up by the collapsing sphere.

[2]Named after its originators Dvali, Gabadadze and Porrati.[3]

and without neutrino clustering.

In this thesis, the first chapters are devoted to the theoretical framework of cosmology, massive neutrinos, DGP gravity and spherical collapse. We then describe the algorithms used in the implementation of the simulations, before presenting the results and discussing what they may mean and how useful they will turn out to be.

1.1 Notation and conventions

Units are denoted in square brackets, for example: $[t] = \mathrm{s}$.

1.2 Symbols with multiple uses

Symbol		
η	Conformal time (section 2.3)	Neutrino clustering (section 7.4)
β	DGP gravity (chapter 5)	Neutrino clustering (section 7.4)
λ	Wavelength (chapter 2)	Proper time (chapter 3)
μ	Chemical potential (chapter 3)	Unitless neutrino mass (chapter 4)
S	Entropy (chapter 4)	Spin (chapter 4)
k	Wave number (chapter 2 and section 7.2)	Unitless momentum (section 7.4)

Part I

Theory

Chapter 2

Cosmological Background

"Friendships, even the best of them, are frail things. One drifts apart."

— Virginia Woolf, To the Lighthouse

This chapter is mostly based on Øystein Elgarøy's lecture notes[4] and Scott Dodelson's book[5]. We assume familiarity with certain concepts of special relativity, most notably the **Minkowski line element**:

$$ds^2 = -c^2dt^2 + dx^2 + dy^2 + dz^2 \tag{2.1}$$

As in special relativity, it is common in cosmology to use unitless velocities, normalized to $c = 1$, so that time and distance may both be measured in (light) seconds. However, in this chapter I have chosen to make an exception and include instances of c in the formulas so it should never be ambiguous which convention is used. Besides, converting to unitless velocities is straightforward under most circumstances.

This chapter only deals with cosmology in **general relativity (GR)**. We will examine modified (DGP) gravity in chapter 5.

2.1 The Cosmological Principle

It is generally assumed in cosmology that the universe we inhabit is **isotropic** and **homogeneous** on large scales. Homogeneity means that the physical properties are the same everywhere in the universe, so there is nothing special about our location in the universe. Isotropy means that the universe has no preferred direction. On smaller scales, structures such as galaxies and clusters, the spatial averages within a box depends on the placement and orientation of the box. Not so on large scales.

The consequence of these assumptions is that the universe should always look the same in all directions and at all distances. We call this the **cosmological principle**.

2.2 The Friedmann-Robertson-Walker Line Element

In an expanding universe, it is convenient to work with **co-moving coordinates**. This is a coordinate grid that is itself expanding at the same rate as the universe itself, so that we can distinguish between movement due to expansion (in which case the co-moving coordinates remain unchanged) and **peculiar motion** relative to the expansion (in which case the co-moving coordinates *do* change). In a non-expanding universe, all motion is peculiar.

For the remainder of this chapter, we will employ co-moving spherical coordinates r, θ, ϕ[1] so that whenever the radial distance r is used, it is assumed to be co-moving unless otherwise specified. This is not a given in later chapters.

By applying the cosmological principle to a universe where spacetime itself may expand (or contract), one may derive the **Friedmann-Robertson-Walker (FRW) metric** (sometimes called the **line element**), which in spherical coordinates is

$$ds^2 = -c^2dt^2 + a^2(t)\left(\frac{dr^2}{1-kr^2} + r^2\left[d\phi^2 + \sin^2\phi d\theta^2\right]\right) \tag{2.2}$$

Here $\sqrt{-ds^2}$ (**proper time**[2]) is a measure of separation in spacetime between two events, which should be independent of the observer's frame of reference. As in special relativity, $ds^2 < 0$ corresponds to **timelike** events (which can be causally connected) and $ds^2 > 0$ to **spaceelike** events, (which cannot). The limit between these cases are then the **lightlike** events, with $ds^2 = 0$, which describes the movement of photons. Note that t is **cosmic time**, measured by an observer moving with the expansion of the universe (i.e. one whose co-moving coordinates remain the same at all times).

What is different from special relativity's Minkowski line element 2.1 is that this line element also allows for spacetime itself expanding or contracting as time passes: The time-dependent scale factor $a(t)$ incorporates this property. If the universe doubles in size between times t_1 and t_2, we write this as $a(t_2) = 2 \cdot a(t_1)$. It is common to denote the magnitude of the scale factor at the present time t_0

[1] For the angular coordinates, I use the notation θ for the azimuth in the xy plane and ϕ for the inclination. The opposite is often used in physics texts, but old habits die hard.

[2] With another sign convention, where the signs on the left side of Eq. (2.2) are reversed, ds would become the proper time.

as $a_0 = a(t_0)$ and use this for normalization. Thus $\frac{a(t)}{a_0}$ will give us the relative size of the universe at some point in time t compared to the size of the universe today. We will use overdots to denote time derivatives: The rate at which the universe expands is then $\dot{a} \equiv \frac{da}{dt}$ and its acceleration as $\ddot{a} \equiv \frac{d^2a}{dt^2}$.

k in Eq. (2.2) is here the geometrical **curvature** of the universe, where we must distinguish between the following cases allowed by general relativity:

- $k = 1$: A **closed** universe, with finite volume. This is the three-dimensional equivalent to the surface of a sphere, which is also closed: It has no boundaries, yet its area is finite. On such a surface, lines that are parallel somewhere will inevitably intersect at some point: Two expeditions both moving strictly north (in parallel) from the equator will end up meeting at the North Pole, for instance. Also, if one travels in straight line, one ends up at the origin because of the geometry of the closed surface. Both these terrestrial examples can be extended to three dimensions.

- $k = 0$: A **flat** universe, with infinite volume (otherwise, it would have an edge somewhere, in which case our assumption of isotropy breaks down). Parallel lines remain parallel, and the geometry is Euclidean, which can not be assumed for non-flat universes.

- $k = -1$: An **open** universe, also with infinite volume, where initially parallel lines diverge. In two dimensions, such a universe would be shaped like a saddle.

So, which is it? Observations are inconclusive at present: The universe seems flat, yet it may well be that the curvature is simply not detectable on the scales we have managed to probe so far (including the results from the **Planck** satellite [6] [7]).

2.2.1 A note about units

If the universe is curved, $k = \pm 1$, it may be *more* or *less* curved. For instance, a closed universe may have a smaller or greater radius. What we have done above to get only those three choices for k is to normalize it to make it unitless. We require both terms in the denominator of (2.2), that is, $1 - kr^2$, to have the same units. The only way to achieve this with unitless k is to also have r be unitless, but that has the side effect of making everything inside the parentheses that enclose the spatial dimensions unitless as well. As such, our only way to make the units of the time term $[-c^2dt^2] = \mathrm{m}^2$ match the units of the space terms is that $[a(t)] = \mathrm{m}$ as well.[3]

[3]For unitless velocities, such that $c = 1$, we would get $[a(t)] = \mathrm{s}$, light seconds.

However, in the case that the universe is flat, $k = 0$, we are free to allow $[r] = \mathrm{m}$, in which case $a(t)$ is allowed to be unitless, as well as the other way around.

The importance of making this distinction comes into play when we consider the custom of setting the present value of the scale factor to unity, $a_0 = 1$. We are free to do so only when a is a unitless quantity, which means that this is possible *only* if the universe is flat! If it is not, we have to choose between normalizing a or k; we cannot normalize both at once without sacrificing information about the size of the universe. Of course, the ratio $\frac{a}{a_0}$ will still be unitless with value 1 at the present time, and may serve the same purpose.

2.2.2 Proper distance

How does one then measure distances when the universe itself is expanding? The **proper distance** D_P is found by placing one point at the origin and then employing spherical co-moving coordinates. The shortest distance between the points is the **geodesic** (what we call a straight line in flat space), where only the radial co-moving coordinate r varies (since we placed one of the points at the origin); we can then ignore the θ and ϕ contributions to the line element. At a fixed time t, the spatial distance for an infinitesimal displacement along the geodesic is $|ds| = a(t)\frac{dr'}{\sqrt{1-kr'^2}}$, and integrating over these contributions yields

$$D_P(r,t) = \int |ds| = a(t) \int_0^r \frac{dr'}{\sqrt{1-kr'^2}} \tag{2.3}$$

where r' is also given in co-moving coordinates. Note that this results in a separation of variables, where $a(t)$ carries the entire time dependency and the integral only depends on r. Thus, it is convenient to introduce the shorthand

$$\mathcal{S}^{-1}(r) \equiv \int_0^r \frac{dr'}{\sqrt{1-kr'^2}} \tag{2.4}$$

For the three cases that concern us, integrating the expression above results in

- $k = 1$: $\mathcal{S}^{-1}(r) = \sin^{-1}(r)$.
- $k = 0$: $\mathcal{S}^{-1}(r) = r$, which results in the quite intuitive expression $D_P(r,t) = a(t) \cdot r$. Note that on small enough scales that where curvature can be neglected, this is a valid approximation in any model (in this case we say that spacetime is **locally flat**).
- $k = -1$: $\mathcal{S}^{-1}(r) = \sinh^{-1}(r)$.

And we can simplify

$$D_P(r,t) = a(t)\mathcal{S}^{-1}(r) \tag{2.5}$$

With this notation, a point located at proper distance r_{PD} from wherever we choose to place the origin[4], will have co-moving radial coordinate

$$r = \mathcal{S}\left(\frac{r_{PD}}{a}\right)$$

In a flat universe, this simplifies to

$$r = \frac{r_{PD}}{a} \tag{2.6}$$

If the particle follows along with the expansion (no peculiar motion), then $r_{PD} \propto a$ and thus $r =$ constant.

2.3 Conformal time

In an expanding universe, we can even observe **superluminal motion** ($v_r > c$) for sufficiently distant objects. One may easily assume (as Erwin Hubble himself supposedly did) that special relativity should be employed once the radial velocity approaches the speed of light, but this does not agree with observations. The explanation lies in the fact this motion does not occur in any observer's inertial frame. In fact, general relativity was the answer to the question of what one should do when no such frame is available. Thus, special relativity only applies in the context of peculiar motion: Peculiar velocity v_{pec} may never exceed the speed of light, but there seems to be no upper limit to the radial velocity v_r caused by cosmic expansion.[8] In this case, a light signal from one point may never make it to the other: As space keeps expanding, the more it moves toward its destination, the further it has to go.

In universes where the past expansion has been sufficiently fast, light that reaches us can only have been emitted from locations within the **particle horizon**[5], which marks the boundary of the **observable universe**. Light emitted from outside the particle horizon cannot yet have reached us (and may in fact

[4] And we are free to choose under the assumption that the cosmological principle applies, since the universe has no preferred center in such a case.

[5] Hereafter referred to simply as the horizon. In general, this is a little dangerous, as one risks ambiguity between this and the cosmological **event horizon**, but in this thesis the event horizon is of little interest and will not be discussed.

never reach us, depending on the future expansion of the intervening spacetime). We find the co-moving distance to the particle horizon by setting the proper time $ds^2 = 0$ for a ray of light and assuming only radial motion towards an observer at the origin, so that $d\theta^2 = d\phi^2 = 0$. When we insert this into Eq. (2.20) and separate the resulting differential equation. Remembering to use Eq. (2.4), we get

$$r_{PH}(t) = \mathcal{S}\left(\int_0^t \frac{c}{a(t')}dt'\right) \tag{2.7}$$

and if we want the proper distance, we can use (2.5) and find

$$D_{P,PH}(t) = a(t)\int_0^t \frac{c}{a(t')}dt' \tag{2.8}$$

The **Hubble parameter** is defined by

$$H \equiv \frac{\dot{a}}{a} \tag{2.9}$$

so that

$$dt = \frac{1}{aH}da$$

and we can rewrite Eq. (2.8) in terms of the scale factor as

$$D_{P,PH}(a) = a\int_0^a \frac{c}{(a')^2 H}da' \tag{2.10}$$

A common way to rewrite the line element (2.2) is to factor out the scale factor from the time term as well:

$$ds^2 = a^2\left(\underbrace{-\frac{c^2}{a^2}dt^2}_{d\eta^2} + \frac{dr^2}{1-kr^2} + r^2\left[d\theta^2 + \sin^2\theta d\phi^2\right]\right) \tag{2.11}$$

where we call η **conformal time** since it make this factoring possible. It can be written as a differential equation

$$\frac{d\eta}{dt} = \frac{c}{a} \tag{2.12}$$

But the right hand side is the same quantity that we integrated over to find the co-moving distance to the particle horizon in Eq. (2.7), so if we impose the initial condition $\eta(t = 0) = 0$, we can write that integral in terms of conformal time as

$$r_{PH}(\eta) = \mathcal{S}\left(\int_0^t \frac{d\eta}{dt'}dt'\right) = \mathcal{S}\left(\int_0^\eta d\eta'\right) = \mathcal{S}(\eta) \tag{2.13}$$

hence if the universe is flat, conformal time is exactly the co-moving distance to the particle horizon! Thus our choice of initial condition is justified: At $t = 0$, light would not have had time to travel any distance, so $\eta = 0$ at that point in time (this holds even if the particle horizon does not exist at later times, but not if the model contains no Big Bang).

We can rewrite (2.12) as

$$\frac{c}{a} = \frac{d\eta}{dt} = \frac{d\eta}{da}\frac{da}{dt} = \frac{d\eta}{da}aH$$

which means

$$\frac{d\eta}{da} = \frac{c}{a^2 H} \tag{2.14}$$

which is actually identical to what is inside the integral in Eq. (2.10), so that

$$D_{P,PH}(a) = a\int_0^a \frac{d\eta}{da'}da' = a \cdot \eta(a) \tag{2.15}$$

Interestingly, we have not supposed the universe to be flat in this case. If it is, a is unitless, so η will have the same units as $D_{P,PH}$. If the universe is not flat, we found that $[a] = \text{m}$, but in this case we see from Eq. (2.11) that η must be unitless. In either case the product of these quantities will have the same unit as the proper distance to the particle horizon.

This means that conformal time is a scaled measure of the maximum physical distance light could have travelled since the Big Bang provided it could do so without being scattered or absorbed. In a flat universe where we can set $a_0 = 1$, the result is that conformal time is the same as the proper distance to the particle

horizon today. In a curved universe, we could similarly define $\eta_0 = 1$ to measure conformal time in units of today's horizon.

Finally, if we measure this distance in units of light seconds, we get the amount of time it would take for light to travel to the current particle horizon provided the universe did not expand further in the meantime.

2.4 Cosmological redshift

As mentioned in the previous section, we cannot use the Doppler formula from special relativity when studying non-peculiar velocity. However, in the same way that we distinguish between peculiar motion and expansion, we take **cosmological redshift** to mean redshift after correcting for peculiar motion, i.e. the contribution to the total redshift from cosmic expansion. We postulate that the wavelength of a photon in space necessarily expands at the same rate as space itself - we can then say that the **co-moving wavelength** $\frac{\lambda(t)}{a(t)}$ is constant in the absence of peculiar motion.

Since we make observations in the present epoch, we denote $a_{obs} = a_0$ and $a_{source} = a$ for convenience. The cosmological redshift is given by the Doppler formula

$$z = \frac{\lambda_{obs} - \lambda_{source}}{\lambda_{source}} \tag{2.16}$$

and is thus related to the scale factor a by the relation

$$1 + z = \frac{\lambda_{obs}}{\lambda_{source}} = \frac{a_0}{a} \tag{2.17}$$

Note that while we must use the special relativistic Doppler equation for high peculiar velocities, the formula above is valid for cosmological redshift even if $v_r \geq c$.

2.5 The Friedmann equations

The central equations in cosmology stem from the theory of general relativity, more specifically the **Einstein field equations**[6], which relate the geometry in the universe to its energy content:

[6]Plural as they apply component-wise for each combination of 4-dimensional indices μ and ν.

$$E_{\mu\nu} = \frac{8\pi G}{c^4} T_{\mu\nu} + \Lambda g_{\mu\nu} \tag{2.18}$$

Here $E_{\mu\nu} = R_{\mu\nu} - \frac{1}{2} g_{\mu\nu} \mathcal{R}$ is the **Einstein tensor**, which describes the geometry of the universe, Λ is a **cosmological constant** to be explained later in this section and $g_{\mu\nu} = \hat{e}_\mu \hat{e}_\nu$ is the **metric tensor**, the scalar product of unit vectors. It is related to the line element by

$$ds^2 = g_{\mu\nu} dx^\mu dx^\nu \tag{2.19}$$

where dx^μ and dx^ν are infinitesimal vector components along some curve and we have used the **Einstein summation convention**: implicit summing over repeated indices[7]. Applying Eq. (2.2) we may then write the FRW metric tensor in diagonal matrix form:

$$g_{\mu\nu} = \begin{bmatrix} -c^2 & 0 & 0 & 0 \\ 0 & \frac{a^2}{1-kr^2} & 0 & 0 \\ 0 & 0 & a^2 r^2 & 0 \\ 0 & 0 & 0 & a^2 r^2 \sin^2 \phi \end{bmatrix} \tag{2.20}$$

From the metric, one may also directly, if not trivially[8], find the **Ricci tensor** $R_{\mu\nu}$ and the **Ricci scalar** $\mathcal{R} = g^{\mu\nu} R_{\mu\nu}$. $g^{\mu\nu}$ is a **contravariant tensor**[9], whose components are

$$g^{\mu\nu} = \begin{bmatrix} \frac{1}{c^2} & 0 & 0 & 0 \\ 0 & \frac{1-kr^2}{a^2} & 0 & 0 \\ 0 & 0 & \frac{1}{a^2 r^2} & 0 \\ 0 & 0 & 0 & \frac{1}{a^2 r^2 \sin^2 \phi} \end{bmatrix}$$

Returning to the Eq. (2.18), $T_{\mu\nu}$ is the **stress-energy tensor**, describing the energy content of the universe. For a **perfect isotropic fluid** (that is, a fluid with no viscosity, shear stress or heat conductivity) it is

[7] For the remainder of the thesis, this convention will be used unless stated otherwise.
[8] A common route is to apply the **Cartan formalism**, as described in [9].
[9] See [10] for a very intuitive explanation of covariance, contravariance and tensors in general.

$$T_{\mu\nu} = (g_{\mu\nu})^{-1} \begin{bmatrix} -\bar{\rho} & 0 & 0 & 0 \\ 0 & \bar{P} & 0 & 0 \\ 0 & 0 & \bar{P} & 0 \\ 0 & 0 & 0 & \bar{P} \end{bmatrix} \tag{2.21}$$

where $\bar{P}$ is isotropic pressure and $\bar{\rho}$ is the total matter-energy density given in units of mass density[10]. Note that this applies in any coordinate system, the specifics of which are hidden in the metric factor $(g_{\mu\nu})^{-1}$. To convert this to units of energy density, we can use the conversion $\bar{\rho}_E = \bar{\rho}c^2$, which follows naturally from the special relativistic mass-energy relation $E = mc^2$.

In short, the Einstein field equations relate the geometry of the universe (left hand side) directly to the energy content of the universe (right hand side), making them mutually dependent. Using the time-time component of these equations (and setting $\Lambda = 0$ for the time being)

$$G_{00} = \frac{8\pi G}{c^4} T_{00} \tag{2.22}$$

one can derive the first **Friedmann equation**, which is a first-order differential equation describing the evolution of the scale factor a with time:

$$\dot{a}^2 + kc^2 = \frac{8\pi G\bar{\rho}}{3} a^2 \tag{2.23}$$

This matter-energy density is a sum of contributions from matter and radiation components. In addition, the universe may contain **dark energy** components, which like matter and radiation can influence how the universe evolves. In epochs where the matter-energy density from other sources is relatively low, this term will then dominate how the scale factor $a(t)$ evolves.

Vacuum energy has been proposed as a candidate for dark energy. However, the energy densities derived in quantum field theory are many orders of magnitude larger than what we expect from dark energy's effect on the universal expansion. This mismatch is so large that it has been termed the **vacuum catastrophe** (see for instance [11]). One way to reconcile this problem is to make corrections to GR itself. **Modified gravity** are such corrections that recover GR on small scales, yet seeks to explain the observed current accelerated expansion on larger scales. We will get back to these theories in section 5; for the remainder of this

[10]The reason for the bars above these quantities is that the universe is decidedly not homogeneous and isotropic on small scales. To take these perturbations into account, we will hereafter denote the spatial averages or unperturbed quantities by bars.

section, we will simply keep in mind that what we call dark energy may not necessarily be a form of energy with an associated density, though we will keep using this notation in the Friedmann equations for now.

The vacuum energy contribution is commonly expressed in terms of the cosmological constant from Eq. (2.18):

$$\Lambda = \frac{8\pi G}{c^2}\bar{\rho}_\Lambda \tag{2.24}$$

As we saw, it may appear as a constant on either side of the equation and not as a contribution to the stress-energy tensor itself[11]. In this case one can split the energy density into contributions from matter and radiation $\bar{\rho}_{mr} = \bar{\rho}_m + \bar{\rho}_r$ and vacuum energy $\bar{\rho}_\Lambda$ and write

$$\bar{\rho} = \bar{\rho}_{mr} + \bar{\rho}_\Lambda = \bar{\rho}_{mr} + \frac{c^2\Lambda}{8\pi G} \tag{2.25}$$

Thus one may often encounter versions of equation (2.23) that look like

$$\dot{a}^2 + kc^2 = \left(\frac{8\pi G}{3}\bar{\rho}_{mr} + \frac{\Lambda c^2}{3}\right)a^2 \tag{2.26}$$

2.5.1 The second Friedmann equation

Going back to the Einstein field equations, but now looking at the sum of the space-space components, i.e. the trace

$$G_{ii} = 8\pi G T_{ii} \tag{2.27}$$

and combining this with Eq. (2.23), one may also derive a second Friedmann equation, sometimes called the **Friedmann acceleration equation** to distinguish it from the first:

$$\frac{\ddot{a}}{a} = -\frac{4\pi G}{3}\left(\bar{\rho} + \frac{3\bar{P}}{c^2}\right) \tag{2.28}$$

To be able to express what the pressure is for the various components that

[11] Where vacuum energy is not included by definition. One could in principle construct a stress-energy tensor for the vacuum as well, but as Eqs. (2.18) and (2.24) suggest, it would simply be equal to $\Lambda g_{\mu\nu}$.

make up our model universe, we will also need an equation of state for each component.

2.5.2 Equation of state

We will assume that each component behaves as a perfect isotropic fluid fluid at all times. Thus, the density $\bar{\rho}$ and pressure $\bar{P}$ give a complete description of how the fluid behaves. Then, looking at only one component of interest, we can use the relation between mean-square velocity and temperature from statistical mechanics (which also defines **Boltzmann's constant** k_B):

$$m\left\langle v^2\right\rangle = 3k_BT \tag{2.29}$$

where m, T and v are the mass, temperature and velocity, respectively, of a single particle. One can then apply the ideal gas law and solve for pressure to obtain

$$\bar{P} = \frac{\langle v^2\rangle}{3c^2}\bar{\rho}c^2 \tag{2.30}$$

We then define

$$\omega \equiv \frac{1}{3}\frac{\langle v^2\rangle}{c^2} = \frac{k_BT}{mc^2} \tag{2.31}$$

where the final equality comes from Eq. (2.29). This gives us the desired equation of state:

$$\bar{P} = \omega\bar{\rho}c^2 \tag{2.32}$$

Here ω depends only on the mean-square velocity of the particle species we are interested in. It turns out that this simple equation of state is sufficient to describe most cases of interest in cosmology.

2.5.3 Relativistic components

When we say that a component is relativistic, we will in general mean that its average kinetic energy is equal to or greater than its rest energy:

$$\langle E_k\rangle = \left(\sqrt{\frac{1}{1-\frac{\langle v^2\rangle}{c^2}}} - 1\right)mc^2 \geq mc^2 \tag{2.33}$$

where the first equality comes from special relativity. Combining this with Eq. (2.29), we find that a massive particle species is defined to be relativistic when

$$\frac{k_B T}{mc^2} \geq \frac{1}{4} \tag{2.34}$$

or, using Eq. (2.31):

$$\omega \geq \frac{1}{4} \tag{2.35}$$

We will not use this binary limit in practice, but it helps making clear what we mean by relativistic and non-relativistic matter components.

2.5.4 Evolution of density components

It is now possible, using both Friedmann equations (2.23) and (2.28) together with our equation of state, (2.32), to derive a formula for the evolution of the energy density with time, $\dot{\bar{\rho}}$. We then get a separable differential equation that can be solved analytically:

$$\dot{\bar{\rho}}_i = -3\frac{\dot{a}}{a}(1+\omega_i)\bar{\rho}_i \tag{2.36}$$

Note that we used $\bar{\rho}_i$ instead of $\bar{\rho}$ in the equation above: The density is a sum of components $\bar{\rho}_i$ so that $\bar{\rho} = \sum \bar{\rho}_i$, and we are making the rather daring assumption that each component $\bar{\rho}_i$ evolves independently of the others[12]. This means that apart from the scale factor a, which affects each component according to the equation of state, the density evolution only depends on $\bar{\rho}_i$ and ω_i for that particular component. Thus we get a set of independent equations, and we can write $\bar{\rho}_i$ instead $\bar{\rho}$ in the equation above. The solution of these equations are

$$\bar{\rho}_i = \bar{\rho}_{i,0}\left(\frac{a_0}{a}\right)^{3(1+\omega_i)} \tag{2.37}$$

[12]This assumption means that there are no processes converting energy from one component to another, which is clearly not the case at all stages in the evolution of the universe (nucleosynthesis, for example). For a more accurate treatment, we will need the Boltzmann equations, which will be introduced in the next chapter. However, once a component drops out of equilibrium and decouples from the others, the approximation that it evolves independently is valid for that component. We will assume that this approximation holds for all components since recombination, roughly 300 000 years after the Big Bang, when matter and radiation parted ways. This will be examined closer in section 3.3.

where $\bar{\rho}_{i,0}$ and a_0 are the present epoch values of the density of a particular component and the scale factor, respectively (we use these as boundary conditions). At this point, we need to know what the constituent components and their ω_i values are.

2.6 Matter and radiation components

In this thesis, we will concern ourselves with the following cosmological components:

- Matter components (also known as **dust**): $\bar{\rho}_m = \bar{\rho}_c + \bar{\rho}_b$
  - $\bar{\rho}_c$ stands for **cold dark matter (CDM)** density. "Cold" stems from the assumption that this component is completely non-relativistic today (as opposed to **warm dark matter**, which would be relativistic). This as yet unidentified component makes up the bulk of the total matter density in the universe, but since it only interacts with other components via gravity (and perhaps the weak nuclear force), it is very hard to observe directly, as opposed to components interacting with the electromagnetic force (may emit radiation) and the strong nuclear force (interacts strongly with other forms of matter). Note that non-relativistic neutrinos today would be detected as cold dark matter, given that they are limited to weak interactions.
  - $\bar{\rho}_b$ stands for **baryon** density. This is all "regular" matter. Note that while in particle physics the term "baryons" is limited to fermions consisting of three quarks (such as protons and neutrons), the cosmological definition is wider. Here we will take it to include every particle in the standard model except neutrinos.[4]
- Ultrarelativistic components (also known as **radiation**): $\bar{\rho}_r = \bar{\rho}_\gamma + \bar{\rho}_{\nu,massless}$
  - $\bar{\rho}_\gamma$ stands for **photon** density, the contribution from electromagnetic radiation in the universe.
  - $\bar{\rho}_{\nu,massless}$ stands for **massless neutrinos.** Although neutrinos certainly have mass (see section 4.1), we could in theory want to run a simulation with one or more neutrinos massless. In this case, they count as a radiation component.
- Massive neutrinos: $\bar{\rho}_\nu$
  - **Massive** neutrino species have a time-dependent ω_ν as defined by Eq. (2.32). They will be ultrarelativistic in the very early universe and non-relativistic today (unless their masses are smaller than $\frac{4k_BT}{c^2}$, as Eq. (2.34) suggests).

- Dark energy: $\bar{\rho}_\Lambda$.
- Effective energy density from modified gravity: $\bar{\rho}_{rc,eff}$. See chapter 5 for details; all we need to know at the moment is that it is not a physical energy density.

The total energy-matter density is the sum of these components: $\bar{\rho} = \bar{\rho}_m + \bar{\rho}_r + \bar{\rho}_\nu + \bar{\rho}_\Lambda + \bar{\rho}_{rc,eff}$. In practice, one or the other of the last two components will always be 0 - they will not appear together in the context of this thesis[13]. Note that these subscripts will also be used in other contexts than energy density, one example being the spatially averaged radiation pressure, $\bar{P}_r$.

2.6.1 Dust ($\omega = 0$)

For non-relativistic massive particles (or **dust**), $\langle v_m^2 \rangle \ll c^2$, hence $\omega \approx 0$ for dust components. Inserting this into equation (2.32) reveals that $\bar{P}_m \approx 0$, hence in the following, we will assume dust to be pressureless.

2.6.2 Radiation ($\omega = 1/3$)

For **ultrarelativistic** particles (such as photons and massless neutrinos), $\langle v^2 \rangle \approx c^2$, hence $\omega \approx 1/3$ for radiation components, yielding the familiar expression for radiation pressure

$$\bar{P}_r = \frac{1}{3}\bar{\rho}_{rad} \tag{2.38}$$

where $\bar{\rho}_{rad}$ is the **radiation density** given in units of energy density, so that $\bar{\rho}_{rad} = \bar{\rho}_r c^2$.

2.6.3 Massive neutrinos ($\omega = \frac{\bar{P}_\nu(t)}{\bar{\rho}\_\nu(t)}$)

Massive neutrinos will be covered in section 4.5.

2.6.4 Vacuum energy ($\omega = -1$)

For the vacuum stress-energy tensor in Eq. (2.21) to be Lorentz invariant, it has to be proportional to the Minkowski metric from special relativity. It follows that $\bar{P}_\lambda = -\bar{\rho}_\Lambda$ and $\omega_\Lambda = -1$.[14]

[13] There is nothing wrong per se with including a small vacuum energy even if modified gravity is taken to be responsible for accelerated expansion today, but it goes beyond the scope of this project.

[14] See for instance [9] for more on Lorentz invariance and special relativity.

Many theories of dark energy allow for $\omega_\Lambda \neq -1$, however, and even time-dependent values of ω_Λ.[15] Still, $\omega_\Lambda = -1$ is well within the current measurement uncertainties.[12]

2.7 Critical density and density parameters

One can show using the first Friedmann equation (2.23) that the universe will be flat ($k = 0$) only when the density[16] is exactly the **critical density** defined in terms of the Hubble parameter as

$$\bar{\rho}_{crit} = \frac{3H^2}{8\pi G} \tag{2.39}$$

We can then define the unitless **cosmological density parameters** as density in terms of this critical density, even if dark energy and curvature are present. For components that have a density $\bar{\rho}_i$, we define:

$$\Omega_i \equiv \frac{\bar{\rho}_i}{\bar{\rho}_{crit}} = \frac{8\pi G}{3H^2}\bar{\rho}_i \tag{2.40}$$

Why is this notation convenient? If we insert the present epoch values $a = a_0$ and $H = H_0$ into the previous equations, we will get the present epoch values of all these parameters, which we denote $\bar{\rho}_{crit,0}$, Ω_{m0}, $\Omega_{\Lambda 0}$ and so on. Let us now introduce the substitutions

$$\frac{8\pi G}{3} = \frac{H_0^2}{\bar{\rho}_{crit,0}} \qquad \text{and} \qquad \bar{\rho}_i = \bar{\rho}_{i,0}\left(\frac{a_0}{a}\right)^{3(1+\omega_i)} \tag{2.41}$$

where we have used (2.39) and (2.37), respectively. These substitutions, along with the definition (2.40) allow us to write the first Friedmann equation in terms of the density parameters at the present epoch as

$$\left(\frac{H}{H_0}\right)^2 = \sum_i \Omega_{i0}\left(\frac{a_0}{a}\right)^{3(1+\omega_i)} + \Omega_{k0}\left(\frac{a_0}{a}\right)^2 \tag{2.42}$$

where for convenience we have defined a similar "curvature density"[17] parameter:

[15] See for instance [2], section 1.2.1.

[16] This density must include $\bar{\rho}_\Lambda$ in the presence of a cosmological constant - matter and radiation densities are not by themselves sufficient.

[17] This density has no physical significance in itself, beyond being the surplus or deficit density

$$\Omega_k \equiv -\frac{kc^2}{a^2H^2} \tag{2.43}$$

so that Eq. (2.26) can be recovered. We can also use (2.17) to substitute $\left(\frac{a_0}{a}\right) = (1+z)$ if we find it more convenient to work with redshifts directly.

Inserting $H = H_0$ and $a = a_0$, it is easily seen that the sum of all density parameters in the present epoch is $\Omega_0 \equiv \sum_i \Omega_{i0} + \Omega_{k0} = 1$, which provides a handy way to eliminate a density parameter from the equations if the sum of all the other density parameters is known.

In fact, this is true even in other epochs other than the present. To see this, we note that the critical density has a time dependence through H:

$$\bar{\rho}_{crit}(t) = \left(\frac{H(t)}{H_0}\right)^2 \bar{\rho}_{crit,0} \tag{2.44}$$

and using this together with Eq. (2.37), we can now rewrite Eq. (2.40) as

$$\Omega_i = \frac{\bar{\rho}_i}{\bar{\rho}_{crit}} = \frac{\bar{\rho}_{i,0}\left(\frac{a_0}{a}\right)^{3(1+\omega_i)}}{\bar{\rho}_{crit,0}\left(\frac{H}{H_0}\right)^2} = \Omega_{i,0}\left(\frac{H_0}{H}\right)^2\left(\frac{a_0}{a}\right)^{3(1+\omega_i)} \tag{2.45}$$

and for the curvature parameter, Eq. (2.43) similarly gives us

$$\Omega_k = \left(\frac{H_0}{H}\right)^2 \Omega_{k0}\left(\frac{a_0}{a}\right)^2 \tag{2.46}$$

which makes the sum of all the parameters

$$\Omega \equiv \sum_i \Omega_i + \Omega_k = \left(\frac{H_0}{H}\right)^2\left[\sum_i \Omega_{i0}\left(\frac{a_0}{a}\right)^{3(1+\omega_i)} + \Omega_{k0}\left(\frac{a_0}{a}\right)^2\right] \tag{2.47}$$

Now we may recognize the terms in the square brackets from equation (2.42). Substituting this, we get

$$\Omega = \left(\frac{H_0}{H}\right)^2\left(\frac{H}{H_0}\right)^2 = 1 \tag{2.48}$$

of the curved universe compared to a flat one.

Thus the sum Ω is time invariant, and the component density parameters are normalized at all times.

2.8 Model cosmologies

There are several cosmological models that can be constructed using different values for the density parameters. We will look at the ones that are most directly relevant for the numerical simulations that will follow.

2.8.1 Flat universe with one dominant component

A very simple model (with neat closed form solutions) comes from assuming a flat universe ($\Omega_{k0} = 0$) where one class of component Ω_j with $j \in m, r, \Lambda$ dominates all the others completely. In this case, the first Friedmann equation becomes simply

$$\left(\frac{H}{H_0}\right)^2 = \Omega_{j0}\left(\frac{a_0}{a}\right)^{3(1+\omega_j)} \tag{2.49}$$

This is a separable differential equation which can be solved for $a(t)$, giving

$$a(t) = a_0\left(\frac{t}{t_0}\right)^{\frac{2}{3(1+\omega_j)}} \qquad (\omega_j \neq -1) \tag{2.50}$$

where the present time is given by

$$t_0 = \frac{2}{3(1+\omega_j)H_0} \tag{2.51}$$

Using the Friedmann equations, it can be shown that our universe has been matter dominated for most of its history (excepting a radiation dominated phase in its youth and a relatively recent switch to dark energy dominance). In the case of total matter dominance (often termed an **Einstein-de Sitter universe**), we can insert $w_j = 0$ (pressureless matter) and get

$$a(t) = a_0\left(\frac{t}{t_0}\right)^{2/3} \tag{2.52}$$

This universe is clearly decelerating:

$$\ddot{a} = -\frac{2a_0}{9t_0^2}\left(\frac{t}{t_0}\right)^{-4/3} \tag{2.53}$$

Likewise, a radiation dominated universe with $\omega_j = 1/3$ expands even slower:

$$a(t) = a_0\left(\frac{t}{t_0}\right)^{1/2} \tag{2.54}$$

This helps explain why massive neutrinos delay structure formation: Massive neutrinos behave as CDM at late times, whereas massless neutrinos behave like radiation. In chapter 8, we will see later that in the ΛCDM model, this effect is negligible when we only look at the evolution of the scale factor, since the neutrino contributing to the total energy density of the universe is small.

As for structure formation, we shall see in section 4.5[18] that increasing the neutrino mass means an increase in the background density $\bar{\rho}_\nu$. This means that a larger fraction of the CDM we observe today consists of massive neutrinos, who once were relativistic. Relativistic particles will free-stream out of overdensities, slowing down the rate at which they can cluster. We discover in chapter 8 that the effect turns out to be more dramatic for spherical collapse than for the background - with greater neutrino mass the collapse is significantly delayed.

Note that in the special case $\omega_j = \omega_\Lambda = -1$, the solution of equation (2.49) is instead

$$a(t) = a_0 e^{H_0(t-t_0)} \tag{2.55}$$

which is commonly referred to as the **de Sitter universe**, containing only vacuum energy.

2.8.2 The standard model of Big Bang cosmology (ΛCDM)

It is more realistic, however, to abandon the assumption that only one type of component dominates all the others. In doing so, however, we sacrifice the possibility of closed form solutions to the Friedmann equations and have to settle for solving them numerically. Note that the ΛCDM model is still flat ($\Omega_k = 0$). The matter-energy components present in this model are:

- Cold dark matter: Ω_c
- Baryons: Ω_b

[18] Eq. (4.22).

- Radiation (including massless neutrinos): Ω_r
- Dark energy: Ω_Λ

2.8.3 Extended standard model with massive neutrinos

If neutrinos have mass (which they must have to oscillate between flavours, a behaviour that is observed in solar neutrinos), then at some point they will become non-relativistic. Extending the ΛCDM model to allow for this, we add the following parameter:

- Massive neutrinos: Ω_ν

2.8.4 Closed matter-dominated universe (Spherical collapse)

Being a central point in this thesis, chapter 6 is dedicated to a discussion of a universe with positive curvature ($k = 1$), once we have more background material covered.

2.9 Cosmological scales

We have already considered the universe on many different **scales**, notably when we discussed the validity of the cosmological principle. To quantify what we mean with a scale, it is convenient to use the language of Fourier transforms and associate a scale with a co-moving wavelength[19] λ, or more specifically by a **wave number**

$$k = \frac{2\pi}{\lambda} \tag{2.56}$$

The relation between k and the proper[20] wavelength λ_{PD} is then given by Eq. (2.6) in a flat universe:

$$k = a(t)\frac{2\pi}{\lambda_{PD}} \tag{2.57}$$

Such a scale is also commonly referred to as a **mode.**

[19] We discussed this in section 2.4. See also [13].
[20] As in "proper distance".

Chapter 3

The Boltzmann equation

"If you are out to describe the truth, leave elegance to the tailor."
— Ludwig Boltzmann

Up until now, we have stuck to the cosmological principle and considered a homogeneous universe, where the components only interact through gravitational potentials. We are now about to depart from this simplified view of cosmology: Not only will we consider other types of interactions (like Coulomb interactions between baryons and photons, for instance), we will also introduce **perturbations** to the homogeneous background and consider the resulting **anisotropies**.

In contrast to the previous chapter, we will use natural units[1] and denote the spatial parts of the co-moving coordinates by x^i, where $X^i \equiv \left[\begin{array}{cccc} x^1, & x^2, & x^3 \end{array}\right] = \left[\begin{array}{cccc} x, & y, & z \end{array}\right]$. Similarly, for momentum, $P^i \equiv \left[\begin{array}{cccc} p^1, & p^2, & p^3 \end{array}\right] = \left[\begin{array}{cccc} p_x, & p_y, & p_z \end{array}\right]$ is not only co-moving, but also relativistic[2]).

The most important source for this chapter is Dodelson[5], which has been used implicitly throughout.

3.1 The distribution function

Each component of the universe may be described by a **distribution function** f in **phase space**.

The phase space is a seven-dimensional space with three dimensions for position and for momentum, plus a time component: $f(t, X^i, P^i)$. This can be written more concisely in vector notation, and in order to apply GR, we will use the 4-vectors

[1] $c = k_B = \hbar = 1$

[2] In contrast to $p^i \equiv m\frac{dx^i}{d\lambda}$, where λ is proper time for massive particles. Massless particles such as photons have no proper time. In these cases, λ is interpreted simply as a parametrization of the particle's path.[9] Hence the change of symbol from the previous chapter.

$$X^\mu = \left[\begin{array}{cc} -t, & X^i \end{array} \right] \qquad P^\mu = \frac{dX^\mu}{d\lambda} = \left[\begin{array}{cc} E, & P^i \end{array} \right] \tag{3.1}$$

We define[3]

$$p^2 \equiv g_{ij} P^i P^j \tag{3.2}$$

so that p is the absolute value of the momentum and take $\hat{p}$ to be the unit vector for the momentum's direction, so that $\hat{p}^i = \frac{P^i}{p}$ and $\hat{p}^i \hat{p}_i = 1$. Then we have

$$P^\mu = p \left[\begin{array}{cccc} \frac{E}{p}, & \hat{p}^x, & \hat{p}^y, & \hat{p}^z \end{array} \right] \tag{3.3}$$

Relativistic energy in natural units is given by

$$E = \sqrt{p^2 + m^2} \tag{3.4}$$

so for a massless particle, $E = p$. For massive particles we find it more convenient to work with E directly, since p is the only variable (the particle species' rest mass and the speed of light are constant).

The distribution function simply counts the number density of particles with momentum (p_x, p_y, p_z) at position (x, y, z) at the time t. We express this as[4]

$$f = f(t, X^i, E, \hat{p}) \tag{3.5}$$

Integrating over positions, directions and energies gives us a the total number of particles at a given time, $f(t)$. The **Boltzmann equation** simply states that the total derivative of the distribution f is a function of f itself:

$$\frac{df}{dt} = C\left[f\right] \tag{3.6}$$

When working numerically, it is more convenient to work with partial derivatives:

[3]Not to be confused with $P^2 \equiv g_{\mu\nu} P^\mu P^\nu$.

[4]If f is properly normalized, this may be interpreted as a probability distribution. In this chapter we omit normalization factors for readability.

$$\frac{df}{dt} = \frac{\partial f}{\partial t} + \frac{\partial f}{\partial x^i}\frac{dx^i}{dt} + \frac{\partial f}{\partial E}\frac{dE}{dt} + \frac{\partial f}{\partial \hat{p}^i}\frac{d\hat{p}^i}{dt} \tag{3.7}$$

3.1.1 0th order: Equilibrium

In a universe that is isotropic and homogeneous, the distribution function may only depend on time, not position. Furthermore, there can be no momentum toward any specific direction for any component. This allows us to simplify the above equation to

$$\frac{df}{dt} = \frac{\partial f}{\partial t} + \frac{\partial f}{\partial E}\frac{dE}{dt} \tag{3.8}$$

In equilibrium, the temperature of a component is T_i everywhere (homogeneity). However, at low temperatures, different kinds of particles respond to the cooling differently. For bosons (such as photons), the quantum mechanical distribution is the **Bose-Einstein** distribution

$$f_{BE} = \frac{1}{\exp\left(\frac{E_i - \mu_i}{T_i}\right) - 1} \tag{3.9}$$

while fermions (such as protons and electrons) obey the **Fermi-Dirac** distribution

$$f_{FD} = \frac{1}{\exp\left(\frac{E_i - \mu_i}{T_i}\right) + 1} \tag{3.10}$$

where μ_i is the chemical potential. $E_i \gg \mu_i$ turns out to be a good approximation for almost all particles at all times, hence we will neglect the chemical potential for 0th order processes, such as annihilation and pair creation.

In a homogeneous, expanding universe (without perturbations), E_i and T_i do not depend on position and direction of momentum, but both depend on time and magnitude of momentum.

3.2 Temperatures

For photons, one can use Eq. (3.9) to show that the temperature is related to the energy density by the relation

$$\bar{\rho}_\gamma = a_B T_\gamma^4 \tag{3.11}$$

where $a_B \equiv \pi^2/15$ is the radiation constant. This result, when combined with Eq. (2.37) and $\omega_\gamma = 1/3$, becomes

$$T_\gamma = \left(\frac{\rho_\gamma}{\bar{\rho}_{\gamma 0}}\right)^{1/4} T_{\gamma 0} = \frac{a_0}{a} T_{\gamma 0} \tag{3.12}$$

Inserting this back into Eq. (3.11) results in

$$\bar{\rho}_\gamma = a_B \left(\frac{a_0}{a} T_{\gamma 0}\right)^4 = \bar{\rho}_{\gamma,0} \left(\frac{a_0}{a}\right)^4 \tag{3.13}$$

A review of current measurements of the **cosmic microwave background (CMB)** radiation give a photon temperature today of $T_{\gamma 0} = 2.72548 \pm 0.00057\,\mathrm{K}$ [14].

For compleley relativistic neutrinos, using Eq. (3.10) leads to *almost* the same relation:

$$\rho_\nu = \frac{7}{8} a_B T_\nu^4 \tag{3.14}$$

The extra factor of 7/8 stems from the following relation between the fermion and boson integrals:

$$\int_0^\infty \frac{u^3}{e^u + 1} du = \int_0^\infty \frac{u^3}{e^u - 1} du - 2\int_0^\infty \frac{u^3}{e^{2u} - 1} du = \frac{7}{8}\int_0^\infty \frac{u^3}{e^u - 1} du \tag{3.15}$$

See [4] for a detailed derivation. For this thesis it is sufficient to note that that the quantity u will make a reappearance in subsection 4.5, so consider it a teaser of what is to come.

3.3 Multi-component universe

When multiple components are present at once, there may be additional interactions between them besides the way they interact with the scale factor through gravitational effects. To begin with, there are **scattering** phenomena, such as:

- Compton/Thomson scattering of photons off of free electrons: $\gamma + e \rightleftharpoons \gamma + e$

- Coulomb interactions between protons and electrons: $p + e \rightleftharpoons p + e$

Scattering does not change the co-moving number densities of the particle species involved, but **annihilation** processes will:

- Electron-positron annihilation (and creation): $\gamma \rightleftharpoons e + \bar{e}$
- Ionization/recombination: $e + p \rightleftharpoons H + \gamma$
- Weak neutron-proton interactions: $p + e^- \rightleftharpoons n + \nu$

So far, when we have looked at how each component evolves independently of the others[5], we have ignored these effects.

3.3.1 Decoupling

For a homogeneous universe with interacting particle species, the Boltzmann equation can be written in the following form

$$a^{-3}\frac{d\left(n_1 a^3\right)}{dt} = n_1^{(0)} n_2^{(0)} \langle \sigma v \rangle \left(\frac{n_3 n_4}{n_3^{(0)} n_4^{(0)}} - \frac{n_1 n_2}{n_1^{(0)} n_2^{(0)}} \right) \tag{3.16}$$

as long as we also assume that the system is in **kinetic equilibrium**[6] and at temperatures $T < (E - \mu)$, which mask the quantum mechanical effects of the Bose-Einstein and Fermi-Dirac distributions. Here $n_i^{(0)}$ and n_i are the number densities of a species in the reaction $1 + 2 \longleftrightarrow 3 + 4$ in and out of equilibrium, respectively, whereas $\langle \sigma v \rangle$ denotes the thermally averaged cross section[7].

When the reaction rates are large compared to the expansion rate, the terms inside the curly brackets have to cancel each other out. However, as the temperature (average kinetic energy) and number densities drop with the expansion, $n_i n_j \langle \sigma v \rangle$ will drop so far that the assumption of kinetic equilibrium no longer holds.

At the point where this has happened to *all* reactions connecting a pair of cosmological components, we say that the components on each side of the reaction

[5] except through the evolution of the scale factor

[6] Scattering happens so frequently that the distributions are given by (3.9) and (3.10).

[7] Strictly speaking, $\langle \sigma \rangle$ would be the average cross section. *This* average has units of volume per time, and is in fact the average *volume* a particle passes through (per time unit) in which a collision/reaction can occur. Thus $n_i \langle \sigma v \rangle$ has units of reactions per time unit and is the reaction rate, while $n_i n_j \langle \sigma v \rangle$ has units of inverse time times inverse volume and is the number of reactions per unit volume per time unit.

decouple from one another - they evolve independently[8] from that point on, interacting only through gravity's effect on the geometry of spacetime.

3.3.2 Electron-positron annihilation

Matter and antimatter will annihilate and produce photons, and at high energies this process is reversible: $e^+e^- \longleftrightarrow \gamma\gamma$. However, at the point where the expansion drops the average photon energy below the rest energy for an electron/positron, this process becomes increasingly one-sided and annihilation becomes dominant until all the available positrons have been converted to photon energy (a surplus of electrons remain at this point, thanks to asymmetry in the matter-antimatter number densities).

This annihilation converts the rest energy of the electrons and positrons to kinetic energy (momentum) for the photons, thus contributing to a significant increase in the temperature of the photon gas and all components thermally coupled to it at this point ($T \approx 1\,\mathrm{MeV}$). This is closely related to **neutrino decoupling**, which we take a closer look at in section 4.4.

3.4 Perturbations

When we go beyond the unperturbed distributions of Eqs. (3.9) and (3.10) and introduce perturbations to this distributions (such as overdense and underdense regions in space), things quickly get complicated. Changing the density in a region of space perturbs the metric from the homogeneous-isotropic FRW metric we encountered in Eq. (2.20) - we usually refer to this as **gravity**. Through the spatial dependence in Eq. (3.5), this affects the distribution functions. The picture is complicated further by scattering and annihilation processes that link the distribution functions together. To account for all this, one solves the **coupled Boltzmann-Einstein equations**, where these connections are inherent.

This sounds like quite a task - and it is - but fortunately there are a couple of factors that can make this task significantly easier:

- **No collision term for neutrinos:** The weak force collisional cross-section for cosmological neutrinos is vanishingly small, unlike solar and atmospherical neutrinos which are actually possible to detect.[9] This simplifies the

[8] That is to say, they can still interact, but so rarely that the majority of particles on one side of the reaction is not affected by the other side - most notably, they drop out of *thermal* equilibrium with one another and their temperatures evolve independently because they have very few opportunities to exchange energy.

[9] In fact, the neutrino cross section scales as $\sigma \propto E_{cm}^2$, where E_{cm} is the centre of momentum energy of the incoming neutrino. This drastically reduces the possibility non-relativistic neutrinos interacting both with each other and other particles, such as the ones in detectors.[15]

calculations considerably, as we can ignore scattering and annihilation processes.

- **Linearized equations:** As long as the perturbations are small, we can solve the equations to first order and ignore higher order contributions. This leads to many terms vanishing. However, once a perturbation becomes large, such as in the late stages of spherical collapse (chapter 6), linearized equations may not necessarily be accurate enough. Fortunately, for our purposes, they will suffice, as by this point the collapse dynamics are completely dominated by the CDM and baryon components[16].

3.4.1 Massive neutrinos around a spherical overdensity

This subsection makes extensive use of an article by LoVerde and Zaldarriaga[17].

Using the Newtonian equation of motion[10], one introduces a gravitational potential with two terms:

- The potential due to the Hubble flow, taking into account the expansion of the background: $\Psi_H(r,t) = -\frac{1}{2}\left(\dot{H} + H^2\right) r^2$
- The peculiar gravitational potential around the collapsing sphere with radius $R = R(t)$:

$$\Psi_{pec}(r,t) = \begin{cases} \frac{G\delta M}{2}\frac{r^2}{R^3} & r \leq R \\ -\frac{G\delta M}{r} + \frac{3}{2}\frac{G\delta M}{R} & r > R \end{cases} \tag{3.17}$$

Here δM is the **matter perturbation**, the excess matter when the unperturbed background density is subtracted, see Eq. (6.21) in chapter 6 for details.

While a full derivation goes beyond the scope of this thesis, the non-relativistic Boltzmann equation for massive neutrinos at late times is

$$\frac{\partial f}{\partial t} + \frac{\mathbf{p}}{a m_\nu} \cdot \nabla_x f - \left(\mathbf{p}\left(H - \dot{\Psi}_{pec}\right) + \frac{m_\nu}{a}\nabla_x \Psi_{pec}\right) \cdot \nabla_p f = 0 \tag{3.18}$$

where $\mathbf{x}$ is the neutrino's position. With a variable change to $\mathbf{q} = a\mathbf{p}$ and writing the function as a sum of the unperturbed distribution [11] and a perturbation term,

$$f(\mathbf{q}, \mathbf{x}, t) = f_0(q, a) + f_1(\mathbf{q}, \mathbf{x}, t)$$

[10] Under the assumption that only a non-relativistic neutrino would be significantly perturbed by a dark matter halo. It is shown in [17] that this assumption is justified.

[11] Satisfying the homogeneous equation where $\Psi_{pec} = 0$.

the Boltzmann equation for massive neutrinos becomes

$$\frac{\partial f_1}{\partial t} + \frac{\mathbf{q}}{a^2 m_\nu} \cdot \nabla_x f_1 - m_\nu \nabla_x \Psi_{pec} \cdot \nabla_q (f_0 + f_1) = 0$$

A final approximation[12] is then to drop the final $\nabla_q f_1$ term:

$$\frac{\partial f_1}{\partial t} + \frac{\mathbf{q}}{a^2 m_\nu} \cdot \nabla_x f_1 - m_\nu \nabla_x \Psi_{pec} \cdot \nabla_q f_0 = 0 \tag{3.19}$$

It should be noted that this approach does not accurately treat neutrinos whose trajectories are significantly affected by the collapsing sphere, most notably those who become bound. Nevertheless, it is shown in [16] that for our purposes, the linearized solution with this approximation is correct to about one percent for neutrino masses up to $m_\nu = 1\,\mathrm{eV}$, well beyond current cosmological upper limits. And now, the time has come to take a closer look at the neutrinos themselves.

[12]Known as the BKT approximation after its originators Brandenberger, Kaiser and Turok.[18]

Chapter 4

Massive neutrinos

"Neutrinos have mass? I didn't even know they were Catholic."
— based on a quote by Woody Allen

4.1 Why neutrinos have mass

In the Standard Model of particle physics, neutrinos are considered massless and thus always relativistic [13]. However, there are many extensions to the Standard Model in which neutrinos are massive. A consequence of massive neutrinos are processes called **flavour oscillations,** in which any of the neutrino flavours can turn into any of the others. Typically, we include three neutrino species: electron (ν_e), muon (ν_μ) and tau (ν_τ) neutrinos - the number of neutrino species that can take part in weak interactions are found by LEP[1] to be $N_\nu = 2.994 \pm 0.012$. Additional neutrino species that do *not* take part in weak interactions may exist, however: we call these **sterile** neutrinos [19] . We will, however, restrict ourselves to the three weakly interacting species in this thesis.

Measurements on the flux of **solar** neutrinos in the Homestake experiments did show a deficit in the number of electron neutrinos, ν_e. This is the only flavour of neutrino produced by the fusion processes in the Sun's core. However, once ν_μ and ν_τ could be reliably detected, the deficit was shown to be due to flavour oscillations on the path from the solar core to the detectors [20].

We will make an important distinction between the neutrino **mass eigenstates** $\nu_i = \nu_{1,2,3}$ (which would never oscillate) and the **flavour eigenstates** $\nu_f = \nu_{e,\mu,\tau}$, which correspond to the physical particles[2]. The latter are linear combinations of the mass eigenstates

[1]The Large Electron-Positron collider at CERN.

[2]Or, more accurately, to their interactions with each of the charged leptons in the Standard Model

$$\nu_f = \sum_i U_{fi}\nu_i \tag{4.1}$$

and as such may experience oscillations between the mass eigenstates [13, 21]. This is often referred to as **neutrino mixing** (U_{fi} is often called the mixing matrix)**.** When we refer to neutrino masses, we will from this point on assume the context of mass eigenstates unless otherwise specified.

Oscillation data provides constraints on the squared difference between neutrino masses, $\Delta m_{ij}^2 = m_i^2 - m_j^2$. Meanwhile, we have constraints on the sum $\sum_i U_{fi}^2 m_i$ from neutrinoless beta decay experiments. However, no known experiment provides constraints on the absolute masses of each of the species themselves (m_i) [21].

4.2 Degenerate neutrino mass eigenstates

If oscillation data for atmospheric neutrinos gives a much larger mass difference than for solar neutrinos, $(\Delta m_{\text{atm}})^2 \gg (\Delta m_{\text{sun}})^2$, we have two possibilities for the mass eigenstates:

- $\Delta m_{\text{sun}}^2 = \Delta m_{21}^2$ and $\Delta m_{\text{atm}}^2 = \Delta m_{32}^2$: This is called the **normal mass hierarchy**, since $m_3 > m_2 > m_1$.
- $\Delta m_{\text{sun}}^2 = \Delta m_{21}^2$ and $\Delta m_{\text{atm}}^2 = \Delta m_{13}^2$: This is called the **inverted mass hierarchy**, since $m_2 > m_1 > m_3$.

The measured values by oscillation experiments[22] are

$$\Delta m_{21}^2 = (7.53 \pm 0.18) \cdot 10^{-5}\,\text{eV}^2 \qquad \left|\Delta m_{31}^2\right| = (2.42 \pm 0.06) \cdot 10^{-3}\,\text{eV}^2 \tag{4.2}$$

where the absolute value takes into account that Δm_{31}^2 in the normal hierarchy is equivalent to $\Delta m_{13}^2 = -\Delta m_{31}^2$ in the inverted hierarchy. In the normal hierarchy, $\Delta m_{32}^2 = \Delta m_{31}^2 - \Delta m_{21}^2$, so for the observed values, $(\Delta m_{\text{atm}})^2 \gg (\Delta m_{\text{sun}})^2$ still holds there.

Recent measurements of mixing angles in neutrino oscillations suggest a lower bound for the lightest neutrino mass at $m_{\nu,1} = 3 \cdot 10^{-3}\,\text{eV}$ [23]. This is assuming the masses are distributed in the normal hierarchy, which is slightly favoured as the highest allowed sum of neutrino masses are $\sum m_{\nu,i} \approx 0.05\,\text{eV}$ and $\sum m_{\nu,i} \approx 0.1\,\text{eV}$ for the normal and inverted hierarchy, respectively. One can at the time of writing not exclude the inverted hierarchy entirely, however, a recent constraint on this upper bound is $\sum m_{\nu,i} \approx 0.11\,\text{eV}$ which is close to the limit of what is allowed for the inverted hierarchy[24]. This constraint comes from cosmology,

however, and such bounds usually come with a host of assumptions that are problematic for this thesis (ΛCDM is normally assumed, for instance). Beta decay experiments place an upper limit for the lightest neutrino as high as $m_{\nu 1} < 2.2\,\text{eV}$.[13, 25] This does not mean that a sum of masses of 0.1 eV is completely unrealistic, but it at least justifies also looking at higher masses[3]. It should also be noted that these limits do not take into account sterile neutrinos with no weak interactions.

For a small sum of neutrino masses, $\sum_i m_i < 0.3\,\text{eV}$, it is shown in [13][4] that the choice of hierarchy has a large effect on the distribution of the masses. For larger $\sum_i m_i$, the differences become so small that all the neutrino eigenstates have approximately the same mass. In this case we say that the masses are **degenerate**.

4.3 Massive neutrinos and cosmology

From a cosmological point of view, massive neutrinos differ from massless ones in a very important way: While initially relativistic (and so eligible to be treated as radiation in early times), there comes a point where the expansion of the background leads to the massive neutrinos becoming non-relativistic. For the range of neutrino masses we are interested in, this occurs during the matter dominated epoch. We will assume this to happen instantly, so there will be a discontinuity in the time derivatives $\dot{\Omega}_r$ and $\dot{\Omega}_c$ as we instantly transfer some of Ω_ν from one to the other: in short, we treat relativistic massive neutrinos as radiation and non-relativistic ones as cold dark matter. It can be shown that in the non-relativistic limit $m_{\nu,i} \gg T_{\nu,i}$ the energy density of the neutrinos are $\rho_{\nu,i} = n_{\nu.i} m_{\nu,i}$ (not surprisingly, since temperature is a measure of kinetic energy and the rest energy dominates in this limit). [13]

At late times, we thus expect all the eigenstates to have $m_{\nu,i} \gg T_{\nu 0} = 1.94535\,\text{K} = 1.6763 \cdot 10^{-4}\text{eV}$, so that they are all non-relativistic today.

4.4 Neutrino temperature and decoupling

This section is based on the sources [21], [26] and [27].

Even massive neutrinos would still be in thermal equilibrium with the photon-baryon plasma at early times - the photon temperature and neutrino temperature (and all other temperatures of plasma constituents) are identical. Neutrinos are initially (at temperatures exceeding the point just above $k_B T = 1\,\text{MeV}$) kept coupled to the baryon-photon plasma through the scattering process $\nu e \longleftrightarrow \nu e$. However, as the universe expands and particles in the plasma move further apart,

[3] In this thesis, we follow [16] and look at sums of neutrino masses up to 1.2 eV.

[4] Fig. 2, to be exact.

the weak interaction rate drops below the expansion rate of the universe. As the weak interactions are the only ones affecting neutrinos, they drop out of thermal equilibrium[5] about 1 second after the Big Bang: The can no longer adjust their energy faster than the plasma temperature is changing. Shortly thereafter (about 10 seconds after the Big Bang), the plasma temperature drops below the energies required for electron-positron creation, and as a result electrons and positrons annihilate en masse, spending their mass energies to heat the plasma. This does not affect the neutrinos, however, as they have dropped out of equilibrium with the plasma already. Hence, while the photons are heated by the annihilations, the neutrinos are largely unaffected.

For particles in thermal equilibrium, the entropy S stays constant as the universe expands[6]. This means that in a co-moving volume $\propto a^3$, the **entropy density** $s = S/V$ obeys

$$sa^3 = \text{constant} \tag{4.3}$$

When working with species in thermal equilibrium, a common assumption is to only include the relativistic species, since the contributions from non-relativistic components are exponentially smaller. In these cases, one can define the **number of relativistic degrees of freedom for entropy:**

$$g_{\star S} = \sum_{j=bosons} g_j \left(\frac{T_j}{T_\gamma}\right)^3 + \frac{7}{8} \sum_{j=fermions} g_j \left(\frac{T_j}{T_\gamma}\right)^3 \tag{4.4}$$

where g_j is the degrees of freedom of a species[7], T_j is its temperature (which may differ from the photon temperature), and the factor 7/8 takes into account the difference between Bose-Einstein and Fermi-Dirac statistics[8]. As relativistic species dominate with their contributions to the entropy density, we may approximate it by disregarding the non-relativistic ones, and get[9]

$$s = \frac{2\pi^2}{45} g_{\star S} T_\gamma^3 \tag{4.5}$$

[5]Or "freeze out", as some like to call it.

[6]This is shown in [26] under the assumption that we can assume all chemical potentials to be zero, or more precisely, $|\mu| \ll T$, which is certainly justified during the epoch in question

[7]The spin contribution to g_j is $2S + 1$ for a massive spin S particle (do not confuse S in this footnote with entropy above). For massless particles that are constrained to move at the speed of light, such as photons, it would be equal to $2S$. Other contributions include various charges, such as electric and colour charge.[4].

[8]See Eq. (3.15) in section 3.2 for a more detailed explanation of this number.

[9]Again, we refer to [26] for the full derivation.

Combining this with Eq. (4.3), we get

$$g_{\star S}\,(aT_\gamma)^3 = \text{constant} \tag{4.6}$$

Thus, a sudden drop in $g_{\star S}$ means that $(aT_\gamma)^3$ must increase. Since the end of $e^\pm$ annihilation in itself would not have caused a sudden expansion of the universe[10], the net result must be an increase in T_γ. To be more specific, just before the temperature crosses the electron-positron annihilation threshold, the species in equilibrium with the photons are the photons themselves ($g_\gamma = 2$), and the electron-positron pairs ($g_{e^\pm} = g_{e^+} + g_{e^-} = 4$ and $T_{e^\pm} = T_\gamma$). In this case Eq. (4.4) gives us $g_{\star S} = 11/2$ before the threshold, and $g_{\star S} = 2$ afterwards. Thus:

$$\frac{11}{2}(aT_\nu)^3 = \frac{11}{2}(aT_{\gamma,before})^3 = 2(aT_{\gamma,after})^3$$

for neutrinos, photons before annihilation and after annihilation, respectively. The result of this is that after annihilation the photon and neutrino temperatures are related by

$$T_\nu = \left(\frac{4}{11}\right)^{1/3} T_\gamma \tag{4.7}$$

provided the scale factor a did not have time to change much during the threshold crossing (we will in fact assume the crossing to be instantaneous). Using Eqs. (3.11) and (3.14), we can also relate the energy densities in a similar way, but only as long as the mass eigenstate ν_i can be considered completely relativistic (i.e. $\omega_{\nu i} \approx 1/3$):

$$\bar{\rho}_{\nu i} = \frac{7}{8}\left(\frac{4}{11}\right)^{4/3} \bar{\rho}_\gamma \tag{4.8}$$

4.4.1 Effective number of neutrinos

Up until this point, we have assumed that the decoupling of the neutrinos (9 seconds earlier) was instantaneous as well. The time has come to drop this assumption. Taking into account the fact that there is still a slight interaction between the neutrinos and the electromagnetic plasma, a more accurate calculation shows that the neutrinos receive a small portion of the entropy from the electron-positron annihilations. As we saw in the previous chapter, it turns out that weak

[10]The Friedmann equations relate the expansion history to energy density, not entropy.

interactions get stronger with higher energy[15], hence higher-momentum neutrinos are heated more than their lower-momentum counterparts.

To account for this effect, one introduces an extra factor c_i for in Eq. (4.8):

$$\bar{\rho}_{\nu i} = \frac{7}{8}\left(\frac{4}{11}\right)^{4/3} c_i \bar{\rho}_\gamma \tag{4.9}$$

The equivalent version of Eq. (4.7) is then

$$T_{\nu i} = \left(\frac{4}{11}\right)^{1/3} c_i^{1/4} T_\gamma = c_i^{1/4} T_\nu \tag{4.10}$$

It is common to relate this the **effective number of neutrino species** N_{eff} as follows:

$$N_{eff} = \sum_i N_i c_i \tag{4.11}$$

where N_i is the number of degenerate neutrino mass eigenstates that share the same value of c_i.[11] This formula is only valid while the neutrinos are relativistic. If *all* the eigenstates are degenerate, we have simply

$$c_i = \frac{N_{eff}}{N_i} \tag{4.12}$$

For three massless neutrino species, we would have $N_{eff} = 3$ in the limit of instantaneous decoupling. However, due to the extra energy transferred to the neutrinos from annihilating $e^\pm$ pairs, their energy density increases, and so we obtain $N_{eff} = 3.034$ from this effect.

Similarly, there is a finite temperature correction from quantum electrodynamics (QED) to consider: Electromagnetic interactions lowers the energy density of the electromagnetic plasma, so the entropy released by the $e^\pm$ annihilation turns out to be a little less than it would be in the non-interactive case, thus T_γ and T_ν (and correspondingly, the energy densities) end up even closer together than if this effect were absent. In the instantaneous decoupling limit, this effect alone would give $N_{eff} = 3.011$.

[11] This differs notably from the notation of [28]. I made the changes $c_i \to N_i$ and $g_i \to c_i$ to avoid using the symbol g_i for both the degrees of freedom for a particle species and the factor that appears when we drop the assumption of instantaneous decoupling. However, c_i is freed up since I prefer N_i for the number of actual eigenstates to make it clear that we are counting something. I feel these changes are justified as they remove needless ambiguity.

If this effect had been completely independent of the non-instantaneous neutrino decoupling, one could simply add these contributions and get $N_{eff} = 3.045$. However, since a few neutrinos that still interact with the plasma at this point, these are also heated a little less, and in [27] it is shown that both effects simultaneously give $N_{eff} = 3.0395$.

4.5 Neutrino mass eigenstates

Being fermions, unperturbed neutrinos have the Fermi-Dirac distribution from Eq. 3.10, which is

$$f_0 \equiv \frac{1}{e^{E_{\nu i}/T_{\nu i}} - 1} \tag{4.13}$$

when we neglect the chemical potential. We can then determine the unperturbed quantities for a single neutrino mass eigenstate as in [5], chapter 2:

$$\bar{n}_{\nu i} = g_\nu \int f_0 \frac{d^3p}{(2\pi)^3} \tag{4.14}$$

$$\bar{\rho}_{\nu i} = g_\nu \int E_{\nu i}(p) \cdot f_0 \frac{d^3p}{(2\pi)^3} \tag{4.15}$$

$$\bar{P}_{\nu i} = g_\nu \int \frac{p^2 f_0}{3E_{\nu i}(p)} \frac{d^3p}{(2\pi)^3} \tag{4.16}$$

Here, $g_\nu = 2 \cdot \frac{1}{2} + 1 = 2$ is the number of internal degrees of freedom (spin degeneracy) for neutrinos with spin 1/2 discussed in section 4.4. We can interpret this as each mass eigenstate having either spin up or spin down, by the Pauli exclusion principle. The factors $(2\pi)^3$, or $(2\pi\hbar)^3$ in ordinary units, comes from Heisenberg's uncertainty principle, which puts a limit on the unit size of phase space volumes. We will encounter these whenever we integrate over momentum.

According to [21], neutrinos within the mass ranges discussed here ($< 1\,\text{eV}$) are definitely relativistic at decoupling, hence we will bake the factor c_i into the neutrino temperature as Eq. (4.10) suggests - we repeat this equation here for clarity:

$$T_{\nu i} = \left(\frac{4}{11}\right)^{1/3} c_i^{1/4} T_\gamma = c_i^{1/4} T_\nu \tag{4.17}$$

Here T_ν is the thermal result calculated from the CMB temperature T_γ, whereas $T_{\nu i}$ takes into account that decoupling is not instantaneous, plus QED corrections. Using the substitution[12]

$$u = \frac{p}{T_{\nu i}} = \frac{ap}{T_{\nu i0}} \tag{4.18}$$

$$dp = \frac{T_{\nu i0}}{a} du$$

and assuming spherical symmetry, we rewrite the number density, energy density and pressure of a single mass eigenstate for a neutrino species. For all three integrals there is a common prefactor

$$\mathcal{P}(a, n) = \frac{T_{\nu i}^n}{\pi^2} = \frac{T_{\nu i0}^n}{\pi^2 a^n} \tag{4.19}$$

For the number density, we have the analytic solution

$$\bar{n}_{\nu i} = 2 \int \frac{1}{e^{p/T_{\nu i}} + 1} \frac{d^3p}{(2\pi)^3} = \frac{T_{\nu i}^3}{\pi^2} \int_0^\infty \frac{u^2}{e^u + 1} du = \mathcal{P}(a, 3) \cdot \frac{3}{2} \xi(3) \tag{4.20}$$

where $\xi(x)$ is the Riemann zeta function[13]. The value of $\xi(3)$ is well known as **Apery's constant**. In place of the mass $m_{\nu i}$ we may similarly substitute

$$\mu_i = \frac{m_{\nu i}}{T_{\nu i}} = \frac{m_{\nu i} a}{T_{\nu i0}} \tag{4.21}$$

and get

$$\bar{\rho}_{\nu i}(a, \mu_i) = 2 \int \frac{\sqrt{p^2 + m_{\nu i}^2}}{e^{p/T_{\nu i}} + 1} \frac{d^3p}{(2\pi)^3} = \mathcal{P}(a, 4) \int_0^\infty \frac{u^2 \sqrt{u^2 + \mu_i^2}}{e^u + 1} du \tag{4.22}$$

whose unitless equivalent is

[12] This is the very same substitution used in Eq. (3.15) in section 3.2. At that point, we had not introduced g_i and $T_{\nu i}$ yet, but we could still have used T_ν under the assumption of instantaneous decoupling and no electromagnetic interactions.

$$\Omega_{\nu i}\left(a,\mu_i\right) = \frac{8T_{\nu i0}^4 G}{3\pi a^4 H^2}\int_0^\infty \frac{u^2\sqrt{u^2+\mu_i^2}}{e^u+1}du \tag{4.23}$$

(where no sum is implied in the indices), and

$$\bar{P}_{\nu i}\left(a,\mu_i\right) = \frac{2}{3}\int \frac{p^2}{\left(e^{p/T_{\nu i}}+1\right)\sqrt{p^2+m_{\nu i}^2}}\frac{d^3p}{\left(2\pi\right)^3}$$

$$= \frac{\mathcal{P}(a,4)}{3}\int_0^\infty \frac{u^4}{\left(e^u+1\right)\sqrt{u^2+\mu_i^2}}du \tag{4.24}$$

Note that we recover the usual equation of state (2.38) for energy density and radiation pressure in the limit $\mu_i \to 0$ where the neutrinos are massless or ultra-relativistic (at small a). In this case the integrals themselves are identical, and have the numerical solution

$$\bar{\rho}_{\nu i} = 3\bar{P}_{\nu i} = \mathcal{P}(a,4)\int_0^\infty \frac{u^3}{e^u+1}du = \mathcal{P}(a,4)\frac{7}{8}\frac{\pi^4}{15} \tag{4.25}$$

We again refer to [4] for a derivation of the final equality, as we did for Eq. (3.15). Note that the Fermi-Dirac integral in that equation is actually Eq. (4.22) in the massless limit.

Chapter 5

DGP gravity

"I am somewhat preoccupied with telling the laws of physics to sit down and shut up."
— Vaarsuvius, Order of the Stick

One motivation for modified theories of gravity is to explain the late-time acceleration of the universe without resorting to dark energy in the form of a cosmological constant. If the zero point energy from quantum field theory does not gravitate, vacuum energy with negative pressure cannot explain the accelerated expansion, and the vacuum catastrophe is no longer an issue.

Regardless, in high-density areas of space such as the solar neighbourhood out to a few AU, modified gravity needs to recover GR, which has been tested thoroughly on these scales. On intermediate scales of a few to tens of Mpc, however, structure formation might well be affected in ways that GR does not explain.[29]

5.1 sDGP gravity

This section is based on the articles [30] and [29].

The basic idea of **Braneworld gravity** is that extra dimensions may modify the Friedmann equation. In the simplest case, one imagines a 4-dimensional FRW universe embedded as a brane[1] in a 5-dimensional universe. This fifth dimension is only evident on scales larger than a crossover scale r_c, below which the universe is indistinguishable from a true 4-dimensional one and GR is thus recovered. Only on scales larger than r_c will the expansion accelerate.

Braneworld gravity comes in two flavours: **Self-accelerating** models, where no dark energy is needed to explain late-time acceleration, and **normal** models, in which dark energy with negative pressure[2] is required. DGP gravity, which we

[1] An $(n-1)$-dimensional subspace in n-dimensional space. The reason we avoid the term "surface" is that it is usually taken to imply only two dimensions.

[2] In the form of brane tension, for instance.

mentioned back in chapter 1, comes in both flavours, termed sDGP and nDGP, respectively. This chapter is concerned with outlining the basics of the former.

sDGP gravity modifies the Friedmann equation (2.23) in the following way: For a matter field in four dimensions characterized by $\bar{\rho}_m(t)$, the Hubble parameter relates to the crossover scale[3] r_c by

$$H^2 \pm \frac{H}{r_c} = \frac{8\pi G\bar{\rho}_m}{3} \tag{5.1}$$

so that the extradimensional effects carried by the second term on the left hand side are only noticeable at late times, when H becomes small compared to r_c. Here the plus sign applies to normal models and the minus sign to self-accelerating ones, so we will use it in the following form:

$$H^2 - \frac{H}{r_c} = \frac{8\pi G\bar{\rho}_m}{3} \tag{5.2}$$

If we insist, we may rewrite the modified gravity contribution in terms of an effective dark energy component

$$\bar{\rho}_{rc,eff} \equiv \frac{3H}{8\pi G}\frac{1}{r_c} = \frac{1}{Hr_c}\rho_{crit} \tag{5.3}$$

(where Eq. (2.39) was used for the final equality), so that we recover the familiar form

$$H^2 = \frac{8\pi G}{3}\left(\bar{\rho}_m + \bar{\rho}_{rc,eff}\right)$$

During and after matter domination, the modified Friedmann equation may be written as

$$H = H_0\left(\sqrt{\Omega_{rc0}} + \sqrt{\Omega_{m0}a^{-3} + \Omega_{rc0}}\right) \tag{5.4}$$

where

$$\Omega_{rc} \equiv \frac{1}{4H^2r_c^2} \tag{5.5}$$

[3]Note that r_c is not a co-moving distance.

There are a few things to note about this definition: First, comparing this with Eq. (5.3), we see that

$$\frac{\bar{\rho}_{rc,eff}}{\rho_{crit}} = \frac{1}{Hr_c} = 2\sqrt{\Omega_{rc}} \tag{5.6}$$

which is *not* equal to Ω_{rc} unless $\Omega_{rc} = 1/4$. The usual relationship between a density and its Ω component does not apply here. Second, note that $\Omega_{rc0} = 0$ in Eq. (5.4) recovers the Einstein-de Sitter universe, whereas $H/H_0 \to 2\sqrt{\Omega_{rc0}}$ in the limit $a \to \infty$. This is the reason for the factor of 4 in Eq. (5.5) - inserting for Ω_{rc0} in Eq. (5.4) for this limit, we obtain

$$H = \frac{1}{r_c}$$

so Eq. (5.2) becomes

$$H^2 - \frac{H}{r_c} = \frac{1}{r_c^2} - \frac{1}{r_c^2} = 0$$

as expected since $\bar{\rho}_m \to 0$ in this limit. Finally, the relation between Ω_{rc} and Ω_{rc0} follows from Eq. (5.5):

$$\Omega_{rc} = \left(\frac{H_0}{H}\right)^2 \Omega_{rc0} \tag{5.7}$$

A final note: While it may seem that we have simply replaced one constant (Λ) by another (r_c), but the main difference is that unlike Λ, r_c is stable under quantum corrections[30]. It is not of great consequence for this thesis, however, and so we refer to texts on quantum field theory for a more thorough explanation.

5.2 Extension: Radiation and massive neutrinos

What follows in this section is entirely my own work.

We may expand Eq. (5.2) by simply adding the missing energy densities for a flat universe with modified gravity, massive neutrinos, radiation and matter (but without dark energy in the form of a cosmological constant):

$$H^2 - \frac{H}{r_c} = \frac{8\pi G}{3}\left(\bar{\rho}_r + \bar{\rho}_{cb} + \bar{\rho}_\nu\right) \tag{5.8}$$

where as before we recover $H \to \frac{1}{r_c}$ in the limit $a \to \infty$. This quadratic equation in H may be made unitless by dividing by H_0^2 and then applying Eq. (5.6):

$$\left(\frac{H}{H_0}\right)^2 - 2\sqrt{\Omega_{rc0}}\left(\frac{H}{H_0}\right) - \frac{8\pi G}{3H_0^2}\left(\bar{\rho}_r + \bar{\rho}_{cb} + \bar{\rho}_\nu\right) = 0$$

which can then be solved directly:

$$\frac{H}{H_0} = \sqrt{\Omega_{rc0}} \pm \sqrt{\Omega_{rc0} + \frac{8\pi G}{3H_0^2}\left(\bar{\rho}_r + \bar{\rho}_{cb} + \bar{\rho}_\nu\right)} \tag{5.9}$$

Since all the constants on the right hand side are positive, there is always one and only one positive real solution as required by the expectation that our universe should expand and not contract. Recognising $8\pi G/3H_0^2$ to be the inverse critical density of Eq. (2.39), we may write the above result in a form more similar to Eqs . (5.4) and (2.42):

$$H = H_0\left(\sqrt{\Omega_{rc0}} + \sqrt{\Omega_{r0}a^{-4} + \Omega_{cb0}a^{-3} + \Omega_{\nu 0}a^{-3(1+\omega_{\nu,eff})} + \Omega_{rc0}}\right) \tag{5.10}$$

where $\omega_{\nu,eff}$ is a time-dependent parameter defined by Eq. (2.32):

$$\omega_{\nu,eff} \equiv \frac{\bar{P}_\nu}{\bar{\rho}_\nu} \tag{5.11}$$

This is effectively a measure of how relativistic the massive neutrinos are at a point in time, starting at $\omega_{\nu,eff} = \frac{1}{3}$ in the ultrarelativistic limit and dropping to zero for nonrelativistic neutrinos. This quantity is calculable provided we can calculate the spatially averaged energy density and pressure of the massive neutrinos at any given time.[4]

A peculiarity of DGP gravity is that the Ω parameters don't generally add up to one: Eq. (2.48) does not hold. Rather, from Eq. (5.10) , we have that

$$\sqrt{\Omega_{rc0}} + \sqrt{\Omega_{r0} + \Omega_{cb0} + \Omega_{\nu 0} + \Omega_{rc0}} = 1$$

[4]We show in subsection 4.5 how this is done.

or

$$\Omega_{r0} + \Omega_{cb0} + \Omega_{\nu 0} = 1 - 2\sqrt{\Omega_{rc0}} = 1 - \frac{1}{H_0 r_c} = 1 - \frac{\bar{\rho}_{rc,eff,0}}{\rho_{crit,0}} \tag{5.12}$$

where the final equality comes from Eq. (5.6). We have discovered that this peculiarity comes from the way that $\rho_{rc,eff}$ and Ω_{rc} are defined. If they had been defined in the way we have come to expect from ΛCDM, the sum of Ω parameters would in fact have been 1:

$$\Omega_{r0} + \Omega_{cb0} + \Omega_{\nu 0} + \frac{\bar{\rho}_{rc,eff,0}}{\rho_{crit,0}} = 1 \tag{5.13}$$

We could have extended this further to a curved background universe with the inclusion of an Ω_{k0} parameter[5]. In any event, the take-home message is that the sum of all *other* parameters equalling one only means the universe is flat if $\Omega_{rc0} = 0$, that is, in the limit $r_c \to \infty$.

5.3 Criticisms

It should be well noted that sDGP gravity is not a problem-free solution to the mystery of dark energy. The most serious of issues affecting it is that it does not agree well with observations: A likelihood study of data from CMB, supernovae and Hubble constant measurements, sDGP predicts anisotropies in the CMB that have not been seen. Adjusting the initial conditions to remove these anisotropies brings the results in conflict with observations from the WMAP satellite [31].

A more recent analysis uses Planck data to arrive at the same conclusion. A phenomenological approach from [30] introduces a parameter α so that Eq. (5.1) may be written

$$H^2 - \frac{H^\alpha}{r_c^{2-\alpha}} = \frac{8\pi G}{3}\rho_m \tag{5.14}$$

so that $\alpha = 1$ is pure sDGP gravity. In [12], combining Planck's observations with supernovae, one obtains the constraint

$$\alpha < 0.20$$

[5]The details may be found in [31].

at 95% confidence, implying that the flat sDGP model is not compatible with current cosmological data.

As if that was not enough, [32] show that ghost particles with negative energy density appear at the linearized level of sDGP gravity, making the spacetime unstable. Whether non-linear effects may stabilize it remains an open question, but it is certainly enough to make one question the validity of the sDGP model.

Nonetheless, in this context, we consider sDGP a useful example of a modified theory of gravity for its relative simplicity: Allowing a self-accelerating expansion of universe with no need for dark energy and still allowing a top-hat to retain its shape during collapse. Furthermore, spherical collapse has already been studied[6] for this model in [29], so we do not have to start entirely from scratch.

In a full N-body simulation of massive neutrinos in modified gravity, models that agree more closely with observations become more attractive, but given the simplified nature of spherical collapse, we are not running a very realistic simulation to begin with. And the time has finally come to dedicate the next chapter to look at spherical collapse.

[6] Although not with massive neutrinos.

Chapter 6

Spherical collapse models

"Gravity is a habit that is hard to shake off."
— Terry Pratchett, Small Gods

The **spherical collapse** models are approximations to the collapse of self-gravitating matter. Most often used to make simple models of non-linear structure formation, one looks at an isolated, uniform sphere of matter of a certain mass M (usually a mix of CDM and baryons) that is overdense compared to the **background** universe. The density as a function of radius then becomes a step function, giving it a characteristic **top-hat** shape. In addition to this, one sets the further constraint that M is conserved throughout the collapse - this means that no matter of the forms that make up M is allowed to cross the boundary between the collapsing sphere and the background[1].

In GR, an initial top-hat density distribution will remain a top-hat for the duration of the collapse. This is a result of **Birkhoff's theorem**[2], which states that there are no time-dependent solutions with spherical symmetry. There is only one, unique time-independent **vacuum solution**[3], which is known as the **Schwarzschild metric**. Thus, a spherically symmetric distribution such as a top-hat must be time independent under GR. As we shall see, this is not generally the case for modified theories of gravity[35, 36].

A more important, but subtler consequence of Birkhoff's theorem is that a top-hat will evolve completely independently from the background universe: A freely falling test particle inside the collapsing sphere will have an equation of

[1]Components that do *not* make up M will be allowed to cross the boundary, however, as we will see in section 6.2. [33] shows, for instance, how massive neutrinos are distributed within a collapsing sphere of CDM and baryons during different stages of the collapse.

[2]Though it should be noted that a relatively unknown Norwegian physicist by the name of Jørg Tofte Jebsen published this result two years before Birkhoff himself.[34]

[3]Contrary to what the name sugests, a vacuum solution *does* allow for a massive central object that bends spacetime around it - it just prohibits massive objects anywhere *else*. The Schwarzschild metric is only a vacuum solution outside the central object - the *interior* Schwarzschild solution (see for instance [9]) is not a vacuum solution.

motion that is independent of the background universe outside the sphere, and the sphere can therefore be described by its own FRW metric with its own, independent scale factor[37][4].

6.1 Einstein-de Sitter background

The simplest case is to take a flat, matter-dominated universe (Einstein-de Sitter) as the background. This is obviously too simple to describe the universe we live in, since such a universe will not experience late-time acceleration[5]. Still, it is of interest for the following reasons:

- No structures will form in the radiation dominated epoch ($z \approx 3600$), which ends well before recombination ($z \approx 1100$). Thus, ignoring radiation for the duration of the collapse is not a far-fetched assumption.[4]
- As far as we can tell, the universe is flat today. If it is not, it was even closer to the critical density in the past[4]. Hence ignoring curvature for the background universe is safe, at least until today.
- In modified gravity theories such as DGP gravity, we may set the cosmological constant to zero, as in an Einstein-de Sitter universe, and still get accelerated expansion at late times. Hence, this simple case is a decent approximation before the acceleration kicks in.

Giving the scale factor of the overdense sub-universe the suggestive label R, Amendola ([38], p. 348-349) points out that one can derive its evolution from Newtonian mechanics alone. It is straightforward to do for the second Friedmann equation (2.28), however. For a pressureless fluid of CDM and baryons, we get

$$\ddot{R} = -\frac{4\pi G}{3}\left(\rho_{cb}\right) R$$

or

$$\frac{\ddot{R}}{R} = -\frac{4\pi G}{3}\left(\rho_{cb}\right) \tag{6.1}$$

and assuming the mass $M = \frac{4}{3}\pi R^3 \rho_{cb}$ to be invariant throughout the collapse[6],

[4] p. 421

[5] See Eq. (2.53) in subsection 2.8.1.

[6] This is equivalent to assuming the sphere to be isolated, with no infalling or outgoing matter crossing the boundary as it collapses.

$$\frac{\ddot{R}}{R} = -\frac{GM}{R^3}$$

Following Amendola, we multiply both sides by $2R\dot{R}$ to make the differential equation first order:

$$2\dot{R}\ddot{R} = -\frac{2GM}{R^2}\dot{R} \tag{6.2}$$

$$\frac{d}{dt}\left(\dot{R}^2\right) = \frac{d}{dt}\left(\frac{2GM}{R}\right)$$

$$\dot{R}^2 = \frac{2GM}{R} - C \tag{6.3}$$

where we keep Amendola's choice of sign for the integration constant (this equation is in general known as the **cycloid equation**. Inserting for the mass again, we see that

$$\dot{R}^2 = \frac{8\pi G R^2}{3}\rho_{cb} - C$$

And if the density ρ_{cb} is exactly critical, we have from (2.39) that

$$\dot{R}^2 = R^2 H_{sub}^2 - C$$

Since $H_{sub} \equiv \dot{R}/R$ by definition, this means that $C = 0$ and we would follow the background instead of getting collapse. Likewise, for any supercritical sub-universe that may undergo collapse, $\rho_{cb} > \rho_{crit}$ implies that

$$C = \frac{2GM}{R} - \left(\dot{R}\right)^2 > 0 \tag{6.4}$$

Otherwise, the sub-universe will either be critical/flat as we saw above or subcritical/open ($C < 0$). Differentiating this expression, we see that

$$\dot{C} = -\frac{2GM}{R^2}\dot{R} - 2\dot{R}\ddot{R} = 0$$

where the latter equality comes from Eq. (6.2). Hence, the integration constant is time independent even when the universe is not flat. We could also have seen this by comparing Eqs. (2.23) and (6.3) directly, and then identifying

$$C = k$$

Hence, the integration constant is simply the curvature parameter k in natural units[7]. In any case, Eq. (6.3) has the solution

$$R = \frac{GM\left(1 - \cos\tau\right)}{k} \tag{6.5}$$

where the new parameter we have introduced is

$$\tau \equiv \arccos\left(1 - \frac{Rk}{GM}\right) \tag{6.6}$$

We may also write the constant k as

$$k = \frac{R_S}{R} - \left(\dot{R}\right)^2 \tag{6.7}$$

where $R_S = 2GM$ is the **Schwarzschild radius**[8] of the sphere, which remains constant as long as M does. Then the cycloid equation becomes

$$\left(\dot{R}\right)^2 = \frac{R_S}{R} - k \tag{6.8}$$

and the collapsing sphere becomes a black hole at $R = R_S$ or

$$\cos\left(\tau_S\right) = 1 - 2k$$

$$\tau_S = \arccos\left(1 - 2k\right) \tag{6.9}$$

[7]Remember that in a closed universe, we may take either $k = 1$ or $a_0 = 1$ to have absolute value, but not both.

[8]If we collapse the sphere to this radius, it becomes a black hole. For most of the collapse, $R_S \ll R$ is therefore a safe assumption.

6.1.1 Turnaround and virialization

This subsection is based on Elgarøy's lecture notes on spherical collapse[39].

The collapse reaches turnaround at $\tau_{turnaround} = \pi$, at which point $\left(\dot{R}\right)^2 = 0$:

$$R_{turnaround} = \frac{R_S}{k} = \frac{\Omega_{m0}}{\Omega_{m0} - 1} \tag{6.10}$$

and collapses to infinite density at $\tau_{coll} = 2\pi$. A more realistic criterion for collapse is that the virial theorem

$$2\langle E_k \rangle + \langle E_p \rangle = 0 \tag{6.11}$$

is satisfied. The kinetic energy of a body is given by

$$E_k = \int d^3x \, \frac{1}{2}\rho \dot{x}^2 \tag{6.12}$$

where for a top-hat distribution collapsing under its own gravity, the result of the integration is

$$E_k = \frac{3}{10} M \dot{R}^2 \tag{6.13}$$

In the absence of components other than matter, the potential energy of a top-hat is given by

$$E_p = -\frac{3GM^2}{5R} = -\frac{3M}{10}\frac{R_S}{R} \tag{6.14}$$

At turnaround the total energy is purely potential energy:

$$E_{tot} = E_{p,turnaround} = -\frac{3M}{10}\frac{R_S}{R_{turnaround}} = -\frac{3M}{10}k \tag{6.15}$$

From energy conservation[9] $E_k = E_{tot} - E_p$, we have that

$$E_k = \frac{3GM^2}{5}\left(\frac{1}{R} - \frac{1}{R_{turnaround}}\right) = \frac{3M}{10}\left(\frac{R_S}{R} - k\right)$$

[9] Or equivalently, by combing Eqs. (6.8) and (6.13)

so the virial theorem is satisfied when

$$2 \cdot \frac{3M}{10}\left(\frac{R_S}{R} - k\right) = \frac{3M}{10}\frac{R_S}{R}$$

$$R = R_{vir} = \frac{R_S}{2k} = \frac{1}{2}R_{turnaround} \tag{6.16}$$

Inserting this into Eq. (6.5), we see that

$$\cos\left(\tau_{vir}\right) = 0$$

And with $\tau_{turnaround} < \tau_{vir} < \tau_{coll}$,

$$\tau_{vir} = \frac{3\pi}{2} \tag{6.17}$$

As long as the distribution of baryons and CDM is uniform (i.e. remains a top-hat distribution), we may use Eqs. (6.4) and (6.6) along with the above result to determine virialization, provided we keep track of $\dot{R}$ during collapse. Unfortunately, the argument rests on mass conservation, which breaks down once we allow components other than CDM and baryons. Even if we assume no clustering and simply keep track of the background densities, these are not only time dependent through the evolution of the background, but will depend on R as well, unless the amount of clustering is such that it conserves the masses off all components simultaneously. This is certainly not the case for vacuum energy inside the sphere, which should remain proportional to the volume, and would seem to require excessive fine-tuning for the other components involved. Thus the argument leading to Eq. (6.3) does not hold in more complex models, and neither does the virialization result.

6.2 ΛCDM with massive neutrinos

This section is based on the spherical collapse articles by LoVerde[16] and Ichiki and Takada[33].

In a full ΛCDM background, we will assume that the universe is still flat, but now radiation and a cosmological constant are added. This has the following consequences:

- The background evolves differently (expanding more slowly in the radiation dominated era and accelerated expansion at late times).

- There is no analytical solution to the background - we have to compute it numerically.
- The results in 6.1 no longer hold.

Massive neutrinos are radiation-like at early times and dust-like at late times, with the crossover time for each eigenstate depending on its mass. The neutrinos introduce a scale dependence on the collapse that is not present in the bare ΛCDM model, as neutrinos can also cluster nonlinearly inside the collapsing sphere of CDM and baryons, and unlike the latter, the neutrino clustering is not limited by mass conservation inside the top-hat when we collapse baryons and CDM in a homogeneous and isotropic massive neutrino background. As the background neutrino density and the degree to which the massive neutrinos are relativistic change with time, this also introduces a time dependence: The collapse time of a top-hat perturbation depends in part on at what point in the evolution of the universe the collapse begins.

We will keep the simplifying assumption of an isolated sphere of CDM and baryons, whose mass M_{cb} remains constant throughout the collapse. However, the other components (photons, massive neutrinos, dark energy) will be present inside the collapsing sphere as well, making its total mass larger. Inserting the missing components into the second Friedmann equation (2.28), we now get

$$\frac{\ddot{\bar{R}}}{\bar{R}} = -\frac{4\pi G}{3}\sum_i \left(\bar{\rho}_i + 3\bar{P}_i\right) = -\frac{4\pi G}{3}\sum_i \left(1+3\omega_i\right)\bar{\rho}_i$$

where the latter equality comes from Eq. (2.32) in natural units. Inserting ω_i for the various components, we find that the unperturbed background evolves as determined by

$$\frac{\ddot{\bar{R}}}{\bar{R}} = -\frac{4\pi G}{3}\left[\bar{\rho}_{cb} + 2\bar{\rho}_\gamma + \bar{\rho}_\nu + 3\bar{P}_\nu - 2\bar{\rho}_\Lambda\right] \tag{6.18}$$

where we take advantage of already having calculated the background neutrino pressure in Eq. (4.24). For the perturbed sub-universe, we define the **density contrast** to be given by

$$\delta_i(\mathbf{x},t) \equiv \frac{\delta\rho_i}{\bar{\rho}_i} \equiv \frac{\rho_i(\mathbf{x},t) - \bar{\rho}(t)}{\bar{\rho}(t)} \tag{6.19}$$

This unitless quantity measures how overdense (or underdense, if negative) the sphere is[10]. We can use this to write

[10]Some textbooks prefer the notation $\Delta_i = \rho_i - \bar{\rho}_i$ instead of $\delta\rho_i$. I will restrict my use of

$$\rho_i = \bar{\rho}_i \left(1 + \delta_i\right) \tag{6.20}$$

Using this relation and replacing $\bar{\rho}_\nu$, $\bar{P}_\nu$ and $\bar{R}$ with their unbarred equivalents, Eq. (6.18) becomes

$$\frac{\ddot{R}}{R} = -\frac{4\pi G}{3}\left[\left(1 + \delta_{cb}\right)\bar{\rho}_{cb} + 2\bar{\rho}_\gamma + \rho_\nu + 3P_\nu - 2\bar{\rho}_\Lambda\right]$$

for the collapsing sphere. We have here assumed that the densities for photons and dark energy to be the same inside the sphere as outside, so that $\bar{\rho}_i = \rho_i$ for these components. For neutrinos, however, the reason for removing the bars is that we will allow a nonlinear clustering term. We define for a massive component inside a spherical volume V of radius R that the **mass perturbation**

$$\delta M_i \equiv \delta\rho_i V = \delta_i \bar{\rho}_i V \tag{6.21}$$

But by Eq. (6.20), we have that

$$\bar{\rho}_i = \frac{\rho_i}{\delta_i + 1}$$

and then

$$\delta M_i = \frac{\delta_i}{\delta_i + 1}\rho_i V = \frac{\delta_i}{\delta_i + 1} M_i \tag{6.22}$$

so that $\delta M_i \approx M_i$ at high overdensity when R is small[11].[29] By allowing the massive neutrinos to cluster in the same way, we get

$$\frac{\ddot{R}}{R} = -\frac{4\pi G}{3}\left[\left(1 + \delta_{cb}\right)\bar{\rho}_{cb} + 2\bar{\rho}_\gamma + \left(1 + \delta_\nu\right)\bar{\rho}_\nu + 3P_\nu - 2\bar{\rho}_\Lambda\right] \tag{6.23}$$

Analogously to Eq. (6.21), and inspired by Eq. (2.32), we may define a **pressure perturbation**

$$\delta P_i \equiv P_i - \bar{P}_i = \omega_i\left(\rho_i - \bar{\rho}_i\right) = \omega_i \bar{\rho}_i \delta_i \tag{6.24}$$

this notation to CAMB outputs, to be consistent with [28], but avoid it elsewhere.

[11] Alternately, $\delta M_i \equiv \delta\rho_i V = \left(\rho_i - \bar{\rho}_i\right) V = M_i - 4\pi R^3 \bar{\rho}_i/3$ if we wish to use the mass directly.

and we could then then use this with Eq. (5.11) to calculate the neutrino pressure, under the assumption that the clustering neutrinos are exactly as relativistic as those outside (thus sharing the same ω_i):

$$P_\nu = \bar{P}_\nu + \delta P_\nu = \bar{P}_\nu + \omega_{\nu,eff}\bar{\rho}_\nu\delta_\nu$$

Using the same simplification for the δM_ν terms as we did for M_{cb} in Eq. (6.20), we get

$$\frac{\ddot{R}}{R} = -\frac{4\pi G}{3}\left(\left[1+\delta_{cb}\right]\bar{\rho}_{cb} + 2\bar{\rho}_\gamma + \left[1+\delta_\nu\left(1+3\omega_{\nu,eff}\right)\right]\bar{\rho}_\nu - 2\bar{\rho}_\Lambda\right)$$

However, one may argue that neutrinos that cluster nonlinearly will essentially be nonrelativistic, so that $\omega_{\nu,eff} \approx 0$ for the clustering neutrinos (but not the background ones). We therefore obtain

$$\frac{\ddot{R}}{R} = -\frac{4\pi G}{3}\left[\left(1+\delta_{cb}\right)\bar{\rho}_{cb} + 2\bar{\rho}_\gamma + \left(1+\delta_\nu\right)\bar{\rho}_\nu + 3\bar{P}_\nu - 2\bar{\rho}_\Lambda\right] \tag{6.25}$$

which is fully equivalent to Eq. (8) in [16]. If we neglect neutrino clustering (setting $\delta_\nu = 0$), this becomes

$$\frac{\ddot{R}}{R} = -\frac{4\pi G}{3}\left[\bar{\rho}_{cb} + \delta_{cb}\bar{\rho}_{cb} + 2\bar{\rho}_\gamma + \bar{\rho}_\nu + 3\bar{P}_\nu - 2\bar{\rho}_\Lambda\right] \tag{6.26}$$

6.2.1 Virialization

Note that we have not included virialization results in this thesis. It is included for completeness, as this would be a logical next step.

The results from subsection 6.1.1 do not hold when more components are present. To be sure, the kinetic energy of the top-hat is still given by Eq. (6.13), and the total energy is conserved, but Eq. (6.14) does not hold under ΛCDM.

According to [40][12] the potential energy under ΛCDM is

$$E_p = -\frac{GM}{5}\left(\frac{3M}{R} + \frac{4\pi}{5}\rho_{\Lambda 0}R^2\right) \tag{6.27}$$

The virial theorem, Eq. (6.11), is then satisfied when

[12]In perfect agreement, I might add, with the result of [29] if one sets the modified gravity parameter from Eq. (6.36), ΔG_{DGP}, equal to 0 and neglects terms beyond first order in [40].

$$\dot{R}^2 = \frac{GM}{R} + \frac{4}{3}\pi G\rho_{\Lambda 0}R^2 \tag{6.28}$$

as long as $\dot{R} < 0$, ensuring that turnaround has already occurred. Note that we neglect massive neutrinos and radiation in this treatment, so the results are not accurate to high precision. However, according to [16], at this stage in the collapse the dynamics are dominated by the CDM and baryon components, so it should be good enough for our purposes.

6.3 DGP gravity

This chapter is based on [29] and [30].

Like in most theories of modified gravity, Birkhoff's theorem does not apply in DGP gravity. However, a cancellation effect similar to that of Birhkoff's theorem occurs inside a spherical mass distribution due to the extra dimension involved. Most importantly, the difference between using Birkhoff's theorem and Eq. (5.10) is small when used to describe growth of structure in the linear regime.

In particular, a top-hat overdensity will remain a top-hat during collapse: If the surrounding area (outside the top-hat radius R) contains the spatially averaged density, there will be swept out an underdensity outside R that still does not affect the shape of the top-hat. This is a unique property of the top-hat profile, and cannot be generalized to more general spherical distributions under DGP gravity.

What we need, then, is a version of Eq. (6.25) that has Eq. (5.10) as its starting point instead. [29] provides this for a universe with only modified gravity and matter:

$$\frac{\ddot{R}}{R} = -\frac{4\pi G}{3}\left[\bar{\rho}_m + (1+3\omega_{rc,eff})\bar{\rho}_{rc,eff}\right] - \frac{4\pi G_{DGP}\left(R/R_\star\right)}{3}\delta\rho_m \tag{6.29}$$

where $R_\star$ is the so-called **Vainshtein radius**:

$$R_\star = \left(\frac{16G\delta M r_c^2}{9\beta^2}\right)^{1/3} \tag{6.30}$$

below which nonlinear effects dominate and effectively recovers GR (see for instance [41]). Note that $\omega_{rc,eff} \neq \omega_{\nu,eff}$: The latter applies to massive neutrinos, whereas the former is related to modified gravity. We saw $\rho_{rc,eff}$ before in Eq. (5.3), and its equation of state is defined to be

$$-3\,(1+\omega_{rc,eff}) \equiv \frac{d\ln\bar{\rho}_{rc,eff}}{d\ln a} \tag{6.31}$$

Note further that while the background components evolve proportional to the usual gravitational constant G, the overdensity instead requires a modified effective gravitational function defined by

$$\frac{G_{DGP}(x)}{G} = 1 + \frac{2}{3\beta(a)}\frac{\sqrt{1+x^{-3}}-1}{x^{-3}} \tag{6.32}$$

where (in sDGP)

$$\beta(a) = 1 - 2H(a)r_c\left(1+\frac{\dot{H}(a)}{3H^2(a)}\right) \tag{6.33}$$

and the argument to the function in Eq. (6.32) is $x = R/R_\star$. δM is as before defined by Eq. (6.22) summed over all the components.

An important exception to the above is when the sphere has completely collapsed, in which case $x = R = 0$ and

$$\frac{\sqrt{1+x^{-3}}-1}{x^{-3}} = \sqrt{x^6+x^3} - x^3 = 0$$

so that

$$\frac{G_{DGP}(x)}{G} = 1 \tag{6.34}$$

which makes sense as Newtonian gravity is recovered as the scale grows smaller, even though Eq. (6.32) is undefined as written in this case. The extension to include radiation and massive neutrinos in Eq. (6.29) is then

$$\frac{\ddot{R}}{R} = -\frac{4\pi G}{3}\left[\bar{\rho}_{cb} + 2\bar{\rho}_\gamma + \bar{\rho}_\nu + 3\bar{P}_\nu + (1+3\omega_{rc,eff})\bar{\rho}_{rc,eff}\right]$$

$$-\frac{4\pi G_{DGP}\,(R/R_\star)}{3}\left[\delta_{cb}\bar{\rho}_{cb} + \delta_\nu\bar{\rho}_\nu\right] \tag{6.35}$$

6.3.1 Virialization in DGP gravity

Once again, we include virialization for completeness.

The results in subsection 6.2.1 only apply under GR. In modified gravity, potential energy is calculated differently. Furthermore, energy is not strictly conserved over a Hubble time in this scenario. We will follow [29] and outline how we can determine the virial radius in this instance.

While the kinetic energy of the sphere is still calculated using Eq. (6.13), potential energy now is given by

$$E_p = -\frac{M}{5}\left[\frac{3}{R}\left(GM - \Delta G_{DGP}\delta M\right) + 4\pi G\left(1+\omega_{rc,eff}\right)\bar{\rho}_{rc,eff}R^2\right] \tag{6.36}$$

where

$$\Delta G_{DGP} = \frac{2}{3\beta(a)}\frac{\sqrt{1+(R/R_\star)^{-3}}-1}{(R/R_\star)^{-3}} \tag{6.37}$$

as suggested by Eq. (6.32). The virial theorem, Eq. (6.11), is satisfied when

$$\dot{R}^2 = \frac{GM - \Delta G_{DGP}\delta M}{R} + \frac{4\pi G}{3}\left(1+\omega_{rc,eff}\right)\bar{\rho}_{rc,eff}R^2 \tag{6.38}$$

after turnaround. As in ΛCDM above, neutrinos and radiation are ignored in these calculations.

Part II

Algorithms

Chapter 7

Algorithms

> *"The test of the machine is the satisfaction it gives you. There isn't any other test. If the machine produces tranquility it is right. If it disturbs you, it is wrong until either the machine or your mind is changed."*
>
> — *Robert M. Pirsig, Zen and the Art of Motorcycle Maintenance*

In this section, we describe the methodology for reproducing the results in LoVerde's article[16]. This article has been used extensively as a source throughout the chapter.

As noted in chapter 4, if the sum of neutrino masses is greater than 0.3 eV, they are said to be degenerate, in the sense that when more than one neutrino species is present, they can all be said to have the same mass. In this chapter, it is everywhere assumed that there is only one massive neutrino species with a given mass m_ν (instead of several with separate masses $m_{\nu i}$) and no massless neutrinos.

If we want to consider the usual three species of neutrinos with this approach, we have to consider the masses degenerate, even for masses where they cannot normally be considered to satisfy this approximation. As fig. 7.3 and 7.4 show, even though neutrino masses down to 0.1 eV will be non-relativistic at the initial redshift of $z_{init} = 200$, three massive neutrinos whose sum is this mass will not be. We have still used this approximation, however, since even these less massive neutrinos become nonrelativistic early in the collapse process. In fig. 7.1 we see that a single massive neutrino with mass $m_\nu = 0.04\,\mathrm{eV}$ becomes nonrelativistic with $\omega_{\nu,eff} = 1/4$ at $z \approx 135$ in both ΛCDM and DGP gravity. In the massless limit, neutrinos are relativistic throughout, so we avoid the issue when looking at massless neutrinos.

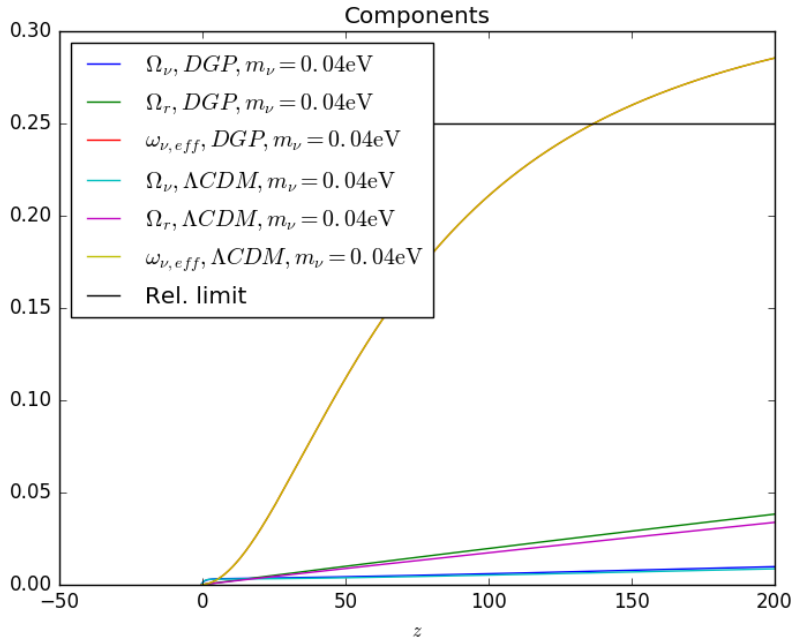

Figure 7.1: Relativistic background components and $\omega_{\nu,eff}$ for $m_\nu = 0.04\,\text{eV}$ in both cosmologies.

7.1 Unperturbed neutrino distributions

In order to find the unperturbed quantities $\bar{\rho}_\nu$ and $\bar{P}_\nu$, we could perform the integrations in Eqs. (4.22) and (4.24) on a grid of a and m_ν, but it is more convenient to choose $\mu(a, m_\nu)$ from Eq. (4.21) as a one-dimensional grid variable. We put the upper limit at $\mu_{max}(a_0, m_{\nu,max})$ and the lower limit at the massless limit $\mu_{min} = 0$. In the latter limit, Eq. (4.24) diverges, but we may instead use the known result

$$\bar{P}_\nu(\mu = 0) = \frac{1}{3}\bar{\rho}_\nu(\mu = 0) \tag{7.1}$$

to handle this particular case. To fix the upper integration limits for u in each case, the following analysis was performed:

1. Simply extending the integration to the point where overflow started to occur, which happened around $u \approx 700$.

2. Then, the integrations were performed up to different u values until increasing the upper limit stopped contributing to the integral[1]. This was found

[1]In other words, when integrating to u_{max} and $u_{max} + 1$ produces results that are identical

to happen consistently at $u \leq 120$ in the ΛCDM model for all relevant values of μ. The code performs this test automatically, so it can be re-used when there are changes to the code.

After this analysis, the LSODA[2]-based algorithm in the *scipy* package was used to calculate the two integrals for $\bar{\rho}_\nu$ and $\bar{P}_\nu$ at 10.000 grid points, after which the results were made continuous with cubic spline interpolation over μ.

7.1.1 Units

At this point, a quick dimensional analysis is beneficial. With m_ν given in units of eV and a being unitless, what are the rest of the units? In natural units, $\hbar = c = k_B = 1$, we measure T_ν in eV as well, so μ is a unitless quantity. Since velocities are unitless, momenta have the same units as masses (eV), hence u is also unitless. This means that the integrals in Eqs. (4.20), (4.22) and (4.24) are all unitless, and the units of $\bar{n}_\nu$, $\bar{\rho}_\nu$ and $\bar{P}_\nu$ are determined by the prefactors $\mathcal{P}(n)$ alone, which by definition have units $(\mathrm{eV})^n$: In this case $(\mathrm{eV})^3$, $(\mathrm{eV})^4$ and $(\mathrm{eV})^4$, respectively. To get the values of the remaining physical constants in natural units, we use

$$G = \left(6.67408 \cdot 10^{-11} \frac{\mathrm{m}^3}{\mathrm{kg} \cdot \mathrm{s}}\right) \left(6.582119 \cdot 10^{-16} \frac{\mathrm{eV}}{\mathrm{s}^{-1}}\right)^2$$

$$\times \left[\left(1.782662 \cdot 10^{-36}\right) \frac{\mathrm{kg}}{\mathrm{eV}}\right] \left[\left(1.97327 \cdot 10^{-7}\right)^{-1} \frac{\mathrm{m}^{-1}}{\mathrm{eV}}\right]^3 \tag{7.2}$$

and

$$H_0 = \left(100h \frac{\mathrm{km}}{\mathrm{s} \cdot \mathrm{Mpc}}\right) \left[\left(3.0856776 \cdot 10^{16}\right)^{-1} \frac{\mathrm{pc}}{\mathrm{m}}\right]$$

$$\times \left(10^3 \frac{\mathrm{m}}{\mathrm{km}}\right) \left(10^{-6} \frac{\mathrm{Mpc}}{\mathrm{pc}}\right) \left(6.582119 \cdot 10^{-16} \frac{\mathrm{eV}}{\mathrm{s}^{-1}}\right) \tag{7.3}$$

giving units of $(\mathrm{eV})^{-2}$ and eV, respectively.

The parameter ranges chosen were $a \in [a_{init}, 1]$ where $a_{init} = \frac{1}{1+z_{init}} = \frac{1}{201}$ and $m_{\nu i} \in [0.01\,\mathrm{eV}, 1\,\mathrm{eV}]$, which gives us the unitless interval

because of numerical lack of precision.

[2]LSODA is based on LSODE (Livermore Solver for Ordinary Differential Equations). The final A likely stands for "Automatic", as it automatically switches between stiff and non-stiff methods.[42]

$$\mu_i \in \left[\frac{T_{\nu i0}^{-1}}{20100}, T_{\nu i0}^{-1}\right]' \tag{7.4}$$

The reason for the high upper bound is to be able to compare results with [16]. As for the lower bound, we saw in chapter 4 that the lightest neutrino mass is $> 3 \cdot 10^{-3}$ eV[23]. Such a light neutrino would contribute very little to Ω_ν and is unlikely to have a large effect on structure formation at $a > a_{init}$ (see Fig. 7.3), so we set the lower bound at 0.01 eV. For the scale factor, the grid will be splined so we can get good values at arbitrary times. Such accuracy is not necessary for the neutrino masses, where we are content with 100 grid points, one for each integer multiple of 0.01 eV up to 1 eV.

7.2 Initial conditions

The unperturbed background evolution of the non-neutrino components are given by Eq. (2.37):

$$\bar{\rho}_i = \frac{\bar{\rho}_{i0}}{a^{3(1+\omega_i)}} = \frac{3H_0^2\Omega_{i0}}{8\pi G a^{3(1+\omega_i)}} \tag{7.5}$$

where the latter equality follows from Eq. (2.40). This allows us to use the cosmological parameters found by the **Planck mission**[6]. We will follow [16] and treat baryons and CDM as a single fluid, since the perturbations in baryon density have (nearly) caught up to the CDM perturbations. So, for $a \geq a_{init}$, we define $\bar{\rho}_{cb} \equiv \bar{\rho}_c + \bar{\rho}_b$, or directly:

$$\bar{\rho}_{cb} \equiv \frac{3H_0^2\left(\Omega_{c0} + \Omega_{b0}\right)}{8\pi G a^3} \tag{7.6}$$

The Planck data do not include a value for $\Omega_{\gamma 0}$. We can, however, use the CMB temperature measurements from $T_{\gamma 0}$ from [14] and Eq. (3.13) to find a value for $\bar{\rho}_{\gamma 0}$.

Before we proceed, we also need to take into account that neutrinos massive enough to be non-relativistic today look like CDM. Under the assumption that the Planck data are not sensitive to massive neutrinos, these will show up in the data as a contribution to the overall CDM density in the observations:

$$\Omega_{c0,obs} = \Omega_{c0} + \Omega_{\nu 0}$$

Hence, for a flat universe like the background:

$$\Omega_{c0} = \Omega_{c0,obs} - \frac{8\pi G\bar{\rho}_{\nu 0}}{3H_0^2} \tag{7.7}$$

The take-home message here is that the actual density of CDM (and in extreme cases, radiation) parameters depend to some (rather small) extent on the neutrino masses. Next, we choose mass scales M_{cb} for a halo, ranging from galaxy scales ($10^{11}\ M_\odot$) up to cluster scales ($10^{15}\ M_\odot$), also converted to eV. For each, the initial radius is given by

$$\bar{R}_{init}(M_{cb}) = \left(\frac{3M_{cb}}{4\pi\bar{\rho}_{cb}}\right)^{1/3} \tag{7.8}$$

After transforming Eq. (6.19) to Fourier space, we obtain

$$\delta_i(\mathbf{k}, t) = \int d^3\mathbf{x}\, e^{-i\mathbf{k}\cdot\mathbf{x}}\delta_i(\mathbf{x}, t)$$

so clearly $\delta_i(\mathbf{k}, t)$ has units of length cubed: $(\mathrm{eV})^{-3}$ in natural units. CAMB returns this quantity in units of Mpc^3, however, and we will use the CAMB code to obtain the initial conditions for the spherical collapse. Next, we define

$$\delta_{cb}(\mathbf{x}, a) \equiv \frac{\delta\rho_c + \delta\rho_b}{\bar{\rho}_c + \bar{\rho}_b} \equiv \frac{\delta\rho_{cb}(\mathbf{x}, a)}{\bar{\rho}_{cb}(a)} \tag{7.9}$$

as the density contrast for CDM + baryons in real space. As long as $\mathbf{x}$ is a position vector inside the collapsing sphere at the time a_{init}, we label the initial top-hat overdensity

$$\delta_{cb,init} \equiv \delta_{cb}(\mathbf{x}_{<R}, a_{init}) \tag{7.10}$$

We will initially pick the top-hat overdensity by hand. What CAMB will help us with is to find the other initial condition we need, $\dot{\delta}_{cb,init}$. To do this, I modified the CAMB code to provide $\Delta_{cb}(k, a_{init}) \equiv \delta_{cb}\bar{\rho}_{cb}$ and its derivative. Running CAMB for the range of neutrino masses needed, we obtain splined values of these quantities in Fourier space[3]. Note that $\bar{\rho}_{cb}$ in Eq. (7.9) will still

[3]Since Ω_{c0} and $\Omega_{\nu 0}$ depend on our choice of $m_{\nu i}$, my code generates files for each of these parameters as a function of neutrino mass. I modified the CAMB driver to read this file and run the CAMB code for each pair of these values (as well as having the other input parameters match those in my own code). In my modified version of CAMB, I made a crude change to

be calculated from the Planck data using Eq. (2.37), but I have verified that my code and CAMB agree on the critical density at a_{init} as a sanity check.

A subtle but important point is that CAMB does not give us the time derivative directly - instead, it provides us with derivatives with respect to conformal time[4] η measured in Mpc, that is,

$$\dot{\Delta}_{cb} = \frac{d\Delta_{cb}}{d\eta}\frac{d\eta}{dt} = \frac{d\Delta_{cb}}{d\eta}a^{-1} \tag{7.11}$$

where the latter equality follows from Eq. (2.12) in natural units. Thus, to work with the CAMB quantities, we transform them to

$$\delta_{cb}(k, a_{init}) = \frac{\Delta_{cb}(k, a_{init})}{\bar{\rho}_{cb}(a_{init})} \tag{7.12}$$

and

$$\dot{\delta}_{cb}(k, a_{init}) = \frac{d}{dt}\left(\frac{\Delta_{cb}}{\bar{\rho}_{cb}}\right) = \frac{\dot{\Delta}_{cb}}{\bar{\rho}_{cb}} - \frac{\Delta_{cb}}{\bar{\rho}_{cb}^2}\frac{d\bar{\rho}_{cb}}{dt} \tag{7.13}$$

Fortunately, we have an analytic expression for $\bar{\rho}_{cb}$ from Eq. (7.6), which upon differentiation yields

$$\frac{d\bar{\rho}_{cb}}{dt} = \frac{3H_0^2\left(\Omega_{c0} + \Omega_{b0}\right)}{8\pi G}\left(-3a^{-4}\right)\dot{a} = -3H\bar{\rho}_{cb}$$

Thus, combining this with Eqs. (7.11) and (7.13), we get

$$\dot{\delta}_{cb}(k, a_{init}) = \frac{\frac{d\Delta_{cb}}{d\eta}(k, a_{init})a_{init}^{-1} + 3H(a_{init})\Delta_{cb}(k, a_{init})}{\bar{\rho}_{cb}(a_{init})} \tag{7.14}$$

We will employ the top-hat window function in Fourier space (which weights the contribution to the top-hat overdensity from different scales):

---

the function that calculates the derivatives of the perturbation parameters, so that it writes the results of $\Delta_c + \Delta_b$ to file, along with the k and a values that produces them, but only for $a \approx a_{init}$. The tolerance for this selection, as well as z_{init}, can be changed in CAMB's parameter file without a need to recompile the program. My code then reads the files produces, makes a spline over a to hit a_{init} exactly, and finally makes a spline over k for the resulting values.

[4]We introduced this in section 2.3.

$$W(kR) = W_{\text{top-hat}}(kR) = \frac{3j_1(kR)}{kR} \tag{7.15}$$

with $R = \bar{R}_{init}$ given by Eq. (7.8) and j_1 being the spherical Bessel function of order 1. Using this, we could in principle do an inverse Fourier transform of the perturbation velocity and obtain

$$\dot{\delta}_{cb,R}(\mathbf{x}, a_{init}) = \int \frac{d^3\mathbf{k}}{(2\pi)^3} e^{i\mathbf{k}\cdot\mathbf{x}} W(kR) \dot{\delta}_{cb}(k, a_{init})$$

but we will instead exploit that $\delta_{cb,R}(\mathbf{x}, a)$ is a random variable with a Gaussian distribution with mean zero and variance

$$\sigma^2(R, a) = \left\langle \delta^2_{cb,R} \right\rangle = \int_0^{k_{max}} \frac{dk}{k} |W(kR)|^2 \frac{k^3 P_{cb}(k, a)}{2\pi^2} \tag{7.16}$$

where $P_{cb}(k, a)$ is the power spectrum, also obtained from CAMB. Similarly,

$$\dot{\sigma}^2(R, a) = \left\langle \dot{\delta}^2_{cb,R} \right\rangle = \int_0^{k_{max}} \frac{dk}{k} |W(kR)|^2 \left(\frac{\dot{\delta}_{cb}(k, a)_{cb}}{\delta_{cb}(k, a)_{cb}} \right)^2 \frac{k^3 P_{cb}(k, a)}{2\pi^2} \tag{7.17}$$

and we finally find the real space rate of change of the overdensity in real space by using the relation

$$\dot{\delta}_{cb,init} = \frac{\dot{\sigma}(R, a_{init})}{\sigma(R, a_{init})} \delta_{cb,init} \tag{7.18}$$

In order to calculate the integrals in Eqs. (7.16) and (7.17), we choose $k_{max} = 10\,\text{MPc}^{-1}$. While neither integral converges on its own, as [16] suggests, the ratio $\frac{\dot{\sigma}}{\sigma}(R, a_{init})$ will have reached an asymptote at this value for the relevant values of m_ν and M (see Fig. 7.2).

Now we use these initial conditions to find the initial top-hat radius and its derivative. By use of (6.19), one obtains

$$\rho_i = \bar{\rho}_i (1 + \delta_i)$$

and combining this with Eq. (7.8) gives us

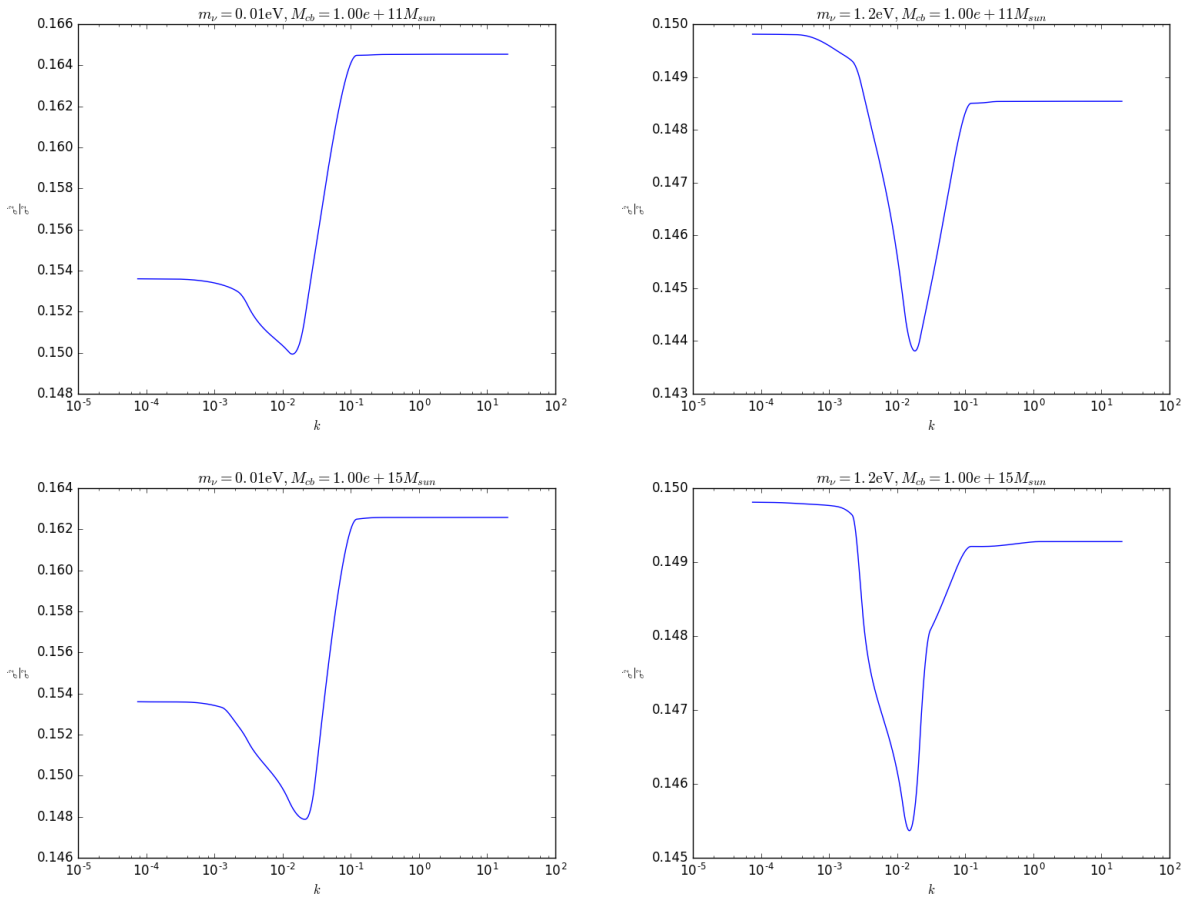

Figure 7.2: $\frac{\dot{\sigma}}{\sigma}(R, a_{init})$ plotted against k_{max}, the upper integration limit in Eqs. (7.16) and (7.17). The convergence was observed for the entire neutrino mass range - here we show the ΛCDM results for the cases $m_\nu = 0.01\,\mathrm{eV}$ and $m_\nu = 1.2\,\mathrm{eV}$, as well as the halo masses $M = 10^{11} M_\odot$ and $M = 10^{15} M_\odot$. $\delta_{cb,init}$ chosen to give collapse today.

$$R_{init} = \bar{R}_{init} \left(1 + \delta_{cb,init}\right)^{-1/3} \tag{7.19}$$

The evolution of $\bar{R}$ follows the background exactly (simply scaled by a constant with unit length), or more specifically

$$\bar{R} = \frac{\bar{R}_{init}}{a_{init}} a$$

so that

$$\dot{\bar{R}}_{init} = \frac{\dot{a}_{init}}{a_{init}} \bar{R}_{init} = H_{init} \bar{R}_{init}$$

and combining this with Eq. (7.19) and using the product rule, one gets

$$\dot{R}_{init} = \bar{R}_{init} \left(1 + \delta_{cb,init}\right)^{-1/3} \left(H_{init} - \frac{1}{3} \frac{\dot{\delta}_{cb,init}}{1 + \delta_{cb,init}} \right) \tag{7.20}$$

This result is not used in [16], which instead opts for the linear expansion[5]

$$R_{init} = \bar{R}_{init} \left(1 - \frac{1}{3} \delta_{cb,init}\right) \tag{7.21}$$

so that

$$\dot{R}_{init} = H_{init} \bar{R}_{init} \left(1 - \frac{1}{3} \delta_{cb,init} - \frac{1}{3} H_{init}^{-1} \dot{\delta}_{cb,init}\right) \tag{7.22}$$

7.2.1 Ensuring flatness

As Eq. (7.7) shows, we adjusted the value of Ω_{cb0} to account for the fact that non-relativistic neutrinos today would look like CDM. In ΛCDM, the sum of all Ω parameters are required to be 1 in a flat universe, hence we adjust $\Omega_{\Lambda 0}$ as follows:

[5] [16] claims that is justified by the fact that $\delta_{cb,init} \sim \mathcal{O}\left(10^{-2}\right)$. It turns out that an initial density contrast of this magnitude is indeed required to achieve collapse at the redshifts we are targeting here, but it is important to keep in mind that other choices of z_{coll} may well invalidate Eq. (7.21) because $\delta_{cb,init}$ would grow too large to justify a linear expansion.

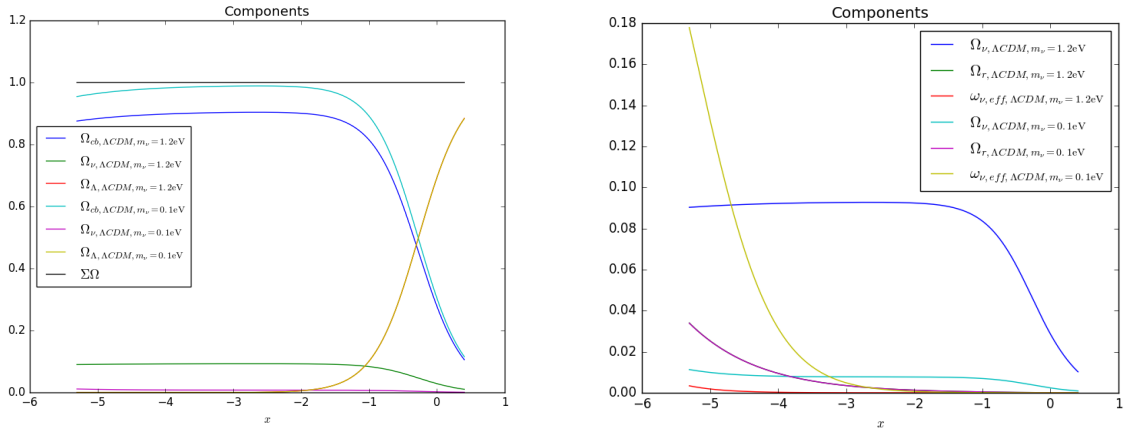

Figure 7.3: Evolution of density parameters in ΛCDM for $m_\nu = 0.1\,\text{eV}$ and $m_\nu = 1.2\,\text{eV}$, respectively. The rightmost plot includes radiation and the degree to which the massive neutrinos are relativistic (through $\omega_{\nu,eff}$). We see that $\omega_{\nu,eff} < \frac{1}{4}$ which was defined as the relativistic limit in Eq. (2.35).

$$\Omega_{\Lambda 0} = 1 - (\Omega_{r0} + \Omega_{\nu 0} + \Omega_{cb0}) \tag{7.23}$$

where Ω_{r0} accounts for photons and massless neutrino species, if any. For DGP gravity, we may not simply adjust Ω_{rc0} instead, since it depends directly on our chosen values of r_c and H_0. We do not want r_c to implicitly depend on m_ν. Since Ω_{r0} is calculated directly from CMB temperature, and $\Omega_{\nu 0}$ for the massive neutrinos is found by integrating the unperturbed Fermi-Dirac distribution, the only parameter left is Ω_{cb0}. In the DGP case, then, we do not employ Eq. (7.7), but instead use Eq. (5.12) to achieve the same effect (that massive neutrinos look like CDM today):

$$\Omega_{c0} = 1 - \left(\Omega_{r0} + \Omega_{\nu 0} + \Omega_{b0} + 2\sqrt{\Omega_{rc0}}\right) \tag{7.24}$$

The results of these adjustments can be seen in figures 7.3 and 7.4. The reason for choosing Ω_{c0} to adjust in DGP gravity is that we expect it to vary with neutrino mass, whereas Ω_{b0} shouldn't.

7.3 Collapse without neutrino clustering

By neutrino clustering, we are not referring to linear theory. We mean the non-linear clustering of massive neutrinos in the potential set up by the CDM+baryon

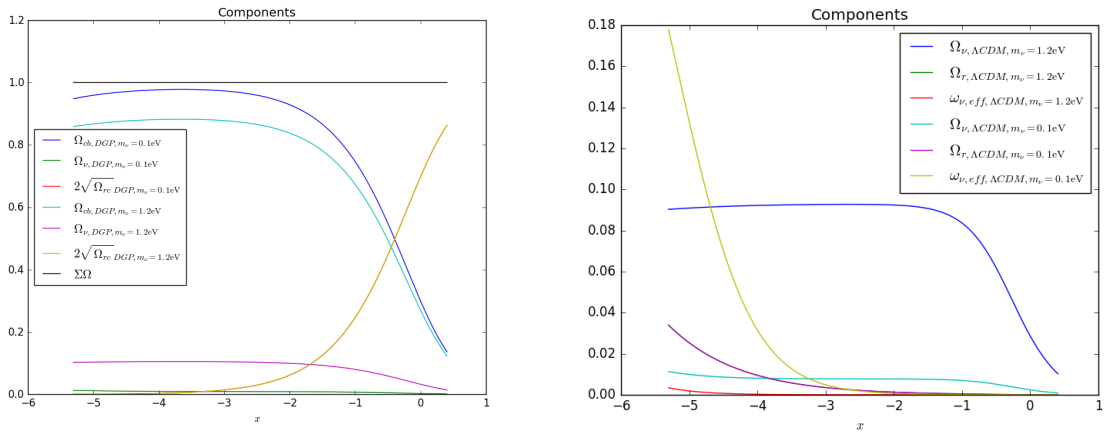

Figure 7.4: As fig. 7.3, for the DGP model.

collapsing sphere.

The approaches in [29] and [16] are not immediately compatible. What follows in this section is entirely my own work, where I combine them into a common framework that works with both massive neutrinos and DGP gravity together. An additional focus has been making the equations unitless to avoid complications with unit conversions.

Following [29] we introduce the time variable

$$x \equiv \ln\, a \tag{7.25}$$

and the dimensionless collapse parameter

$$y \equiv \frac{R\,(x)}{R_{init}} - \frac{a}{a_{init}} \tag{7.26}$$

where the x dependence of the last term is explicitly

$$\frac{a}{a_{init}} = e^{x - x_{init}} \tag{7.27}$$

so that $y(x_{init}) = 0$ and collapse has occurred when $y = -a/a_i$. The relation between derivatives may be expressed as

$$' \equiv \frac{d}{dx} = \frac{dt}{dx}\frac{d}{dt} = \left(\frac{d \ln\, a}{dt}\right)^{-1} \frac{d}{dt} = \left(\frac{\dot{a}}{a}\right)^{-1} \frac{d}{dt} = \frac{1}{H}\frac{d}{dt} \tag{7.28}$$

so that (since $a' = a$)

$$y' = \frac{R'}{R_{init}} - \frac{a}{a_{init}} \tag{7.29}$$

which for the initial condition $x = x_{init},\ R = R_{init}$ becomes

$$y'_{init} = \frac{\dot{R}_{init}}{R_{init} H_{init}} - 1 \tag{7.30}$$

We may combine this with Eq. (7.20) to get

$$y'_{init} = \frac{\bar{R}_{init}}{R_{init} H_{init}} \left(1 + \delta_{cb,init}\right)^{-1/3} \left(H_{init} - \frac{1}{3} \frac{\dot{\delta}_{cb,init}}{1 + \delta_{cb,init}} \right) - 1$$

which combined with Eq. (7.19) turns into

$$y'_{init} = -\frac{\dot{\delta}_{cb,init}}{3 H_{init} \left(1 + \delta_{cb,init}\right)} \tag{7.31}$$

We could also have followed [16] and use the linear expansion, combining Eqs. (7.21), (7.22) and (7.30) in the same way as above:

$$y'_{init} = -\frac{\dot{\delta}_{cb,init}}{3 H_{init} \left(1 - \frac{1}{3}\delta_{cb,init}\right)} \tag{7.32}$$

which is indeed close to the result in Eq. (7.31) when $\dot{\delta}_{cb,init} \ll 1$. Since $\dot{\delta}_{cb,init}$ is the output CAMB provides us with, we will use Eqs. (7.31) and (7.32) as they are.

Returning now to Eq. (7.29), note that we may also write it as

$$y' = \frac{1}{R_{init}} \left(R' - R\right) + y$$

Differentiating both sides, we obtain

$$y'' = \frac{1}{R_{init}} \left(R'' - R'\right) + y' = \frac{1}{R_{init}} \left(R'' - R\right) + y \tag{7.33}$$

With a little help from Eq. (7.28), we see that

$$R'' = \frac{1}{H}\frac{d}{dt}\left(\frac{1}{H}\dot{R}\right) = \frac{\ddot{R}}{H^2} - \frac{H'R'}{H}$$

but we already know from Eq. (7.29) that

$$R' = R_{init}\left(y' + \frac{a}{a_{init}}\right)$$

hence

$$R'' = \frac{R}{H^2}\frac{\ddot{R}}{R} - \frac{H'R_{init}}{H}\left(y' + \frac{a}{a_{init}}\right)$$

so Eq. (7.33) turns into

$$y'' = \left(y + \frac{a}{a_{init}}\right)\left(\frac{1}{H^2}\frac{\ddot{R}}{R} - 1\right) - \frac{H'}{H}\left(y' + \frac{a}{a_{init}}\right) + y$$

where we have applied Eq. (7.26) to replace a factor of R/R_{init}. Collecting terms, this turns into the differential equation we solve numerically, which is shown in fig. 7.5.

$$y'' = \frac{1}{H^2}\frac{\ddot{R}}{R}\left(y + \frac{a}{a_{init}}\right) - \frac{H'}{H}\left(y' + \frac{a}{a_{init}}\right) - \frac{a}{a_{init}} \tag{7.34}$$

H may be calculated directly from the Friedmann equation, which in ΛCDM is (2.42). After calculating values of H on a grid, we spline the results to obtain H' numerically. Then the only missing piece is $\ddot{R}/R$, which we obtain from Eq. (6.25) after making it unitless by multiplying each side by H^{-2}:

$$\frac{1}{H^2}\frac{\ddot{R}}{R} = -\frac{4\pi G}{3H^2}\left[(1+\delta_{cb})\,\bar{\rho}_{cb} + 2\bar{\rho}_\gamma + (1+\delta_\nu)\,\bar{\rho}_\nu + 3\bar{P}_\nu - 2\bar{\rho}_\Lambda\right] \tag{7.35}$$

7.3.1 Modified gravity solution

Eq. (7.34) also covers DGP gravity, where the only differences will be that

- The cosmological parameters common to both models (H_0, Ω_{m0}) may change.

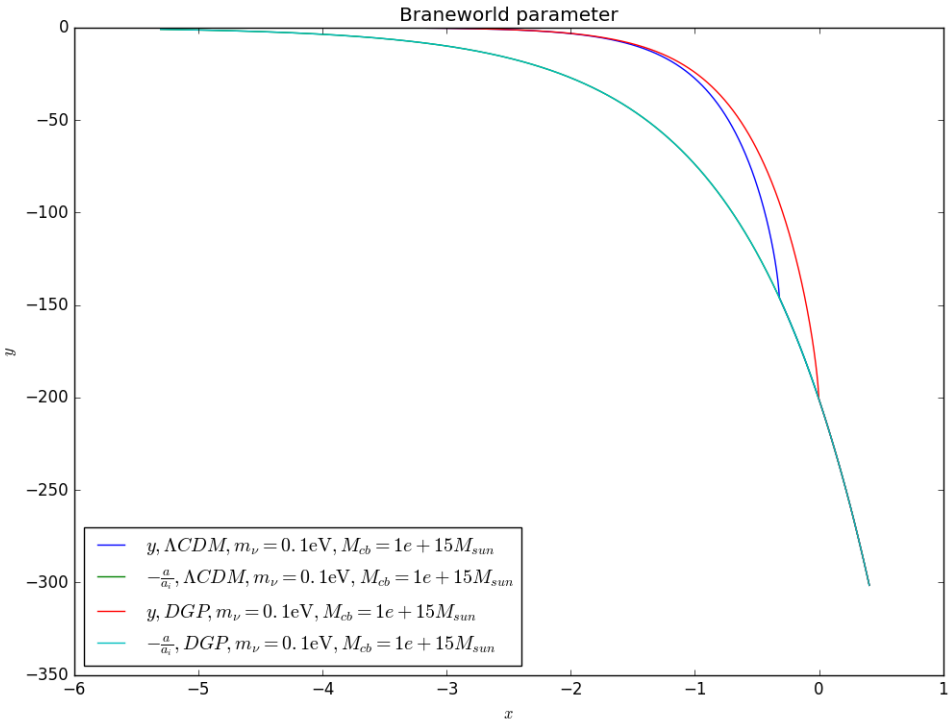

Figure 7.5: Solution to the differential equation (7.34) in ΛCDM and DGP gravity with $\delta_{cb,init} = 0.1317$ targeting collapse today ($x = 0$) for the DGP model. Also plotted for both models is the curve $y = -a/a_{init}$, representing complete collapse.

- H (and H' through a spline as before) is calculated using Eq. (5.10) instead (using $\Omega_{r_c 0}$ in place of $\Omega_{\Lambda 0}$).

- The calculation of $\ddot{R}/R$ is instead based on Eq. (6.35):

$$\frac{1}{H^2}\frac{\ddot{R}}{R} = -\frac{4\pi G}{3H^2}\left[\bar{\rho}_{cb} + 2\bar{\rho}_\gamma + \bar{\rho}_\nu + 3\bar{P}_\nu + (1+3\omega_{rc,eff})\bar{\rho}_{rc,eff}\right]$$

$$- \frac{4\pi G_{DGP}\left(R/R_\star\right)}{3H^2}\left[\delta_{cb}\bar{\rho}_{cb} + \delta_\nu\bar{\rho}_\nu\right] \tag{7.36}$$

where $\bar{\rho}_{rc,eff}$ is calculated using Eq. (5.3) and $\omega_{rc,eff}$ is calculated by using Eqs. (5.3) and (6.31) together:

$$-3\left(1+\omega_{rc,eff}\right) = \frac{H'}{H}$$

Here we have used the fact that r_c is not time dependent. As a result of this,

$$\omega_{rc,eff} = -\left(1 + \frac{1}{3}\frac{H'}{H}\right) \tag{7.37}$$

and the term that is put into Eq. (7.36) becomes

$$\left(1+3\omega_{rc,eff}\right)\rho_{rc,eff} = -\left(2 + \frac{H'}{H}\right)\rho_{rc,eff} \tag{7.38}$$

Inserting this result into Eq. (7.36), we obtain the unitless equation in its final form:

$$\frac{1}{H^2}\frac{\ddot{R}}{R} = \left(1 + \frac{1}{2}\frac{H'}{H}\right)\frac{1}{Hr_c}$$

$$- \frac{4\pi G}{3H^2}\left(\bar{\rho}_{cb} + 2\bar{\rho}_\gamma + \bar{\rho}_\nu + 3\bar{P}_\nu + \frac{G_{DGP}\left(R/R_\star\right)}{G}\left[\delta_{cb}\bar{\rho}_{cb} + \delta_\nu\rho_\nu\right]\right) \tag{7.39}$$

where Eq. (5.3) was also used to simplify the first term and $G_{DGP}\left(R/R_\star\right)/G$ is calculated as in Eq. (6.32), with

$$x^{-3} = \left(\frac{R_\star}{R}\right)^3 = \frac{16G\delta M r_c^2}{9\beta^2 R^3} \tag{7.40}$$

as given by Eq. (6.30), with

$$\beta(a) = 1 - 2Hr_c\left(1 + \frac{1}{3}\frac{H'}{H}\right) \tag{7.41}$$

by combining Eqs. (6.33) and (7.28).

7.3.2 Choice of y'_{init}

LoVerde[16] uses Eq. (7.22) to find $\dot{R}_{init}$. Through Eq. (7.30), we can make find the corresponding value of y'_{init}. However, Schmidt, Hu and Lima[29] instead use the much simpler linear initial condition

$$y'_{init} = -\frac{1}{3}\delta_{init} \tag{7.42}$$

The reason for using this is that [29] starts at the much earlier redshift of $a = 10^{-5}$, where this expression is easier to justify. Having followed LoVerde and done it the hard way, however, we might as well look into how applicable this initial condition would be compared to using the CAMB outputs, including massive neutrinos and starting at the much later initial time $z_{init} = 200$. From Figure 7.6, we see that while both the simple and the linear initial condition are decent approximations even in this case (the latter being slightly better at least for low neutrino masses). Still, there is no compelling reason not to use the full non-linear result.

7.4 Neutrino clustering inside the top-hat

The starting point in this section is again LoVerde's work[16]. However, I found Eq. (11) in that article cumbersome to work with numerically, due to the sheer number of dimensions and lack of unitless quantities. There were also some ambiguities in notation that required clearing up. Therefore, I have put considerable effort into expressing the calculation in a way that is more immediately applicable to solving the clustering problem numerically. What follows, therefore, beyond the first two equations, is entirely my own work.

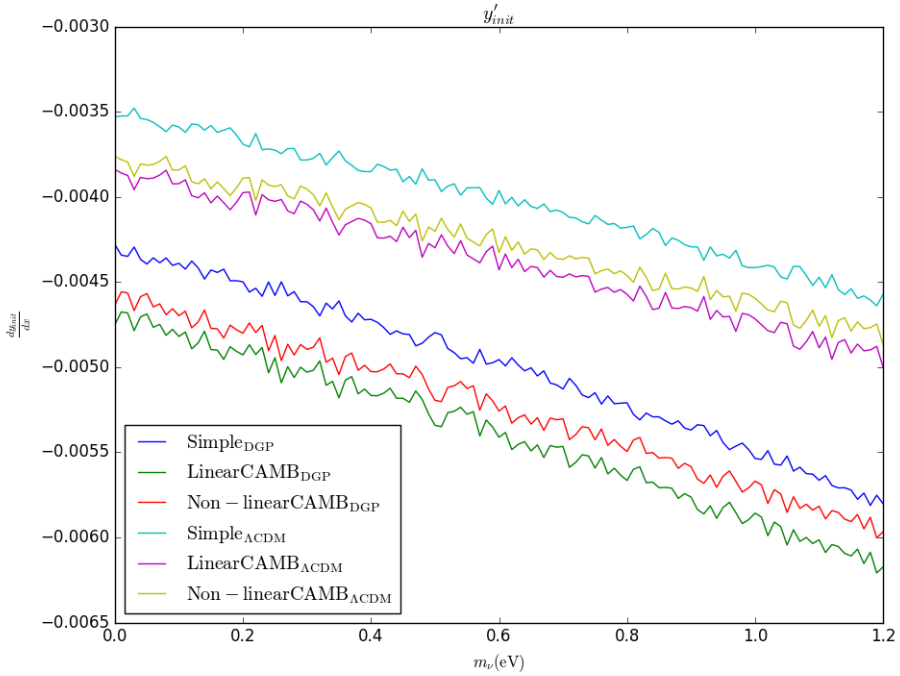

Figure 7.6: Initial conditions y'_{init} for different neutrino masses in ΛCDM and DGP gravity ($y_{init} = 0$ by definition). The simple case uses Eq. (7.42), whereas the linear and non-linear cases use Eqs. (7.32) and (7.31), respectively, with $\dot{\delta}_{cb,init}$ given by CAMB. In all three cases, $\delta_{cb,init}$ was chosen to ensure collapse today - the simulations used to target collapse used the full non-linear result, presumed to be the most accurate (which explains why even the simple case has a jagged curve).

In this entire section, r and R will both be given in co-moving coordinates[6]. As r is an integration variable with R as its upper limit[7], the key point is that whenever we input the proper radius R_{DP} of the collapsing sphere, we must employ Eq. (2.6):

$$R = \frac{R_{DP}}{a} = R_{init,DP}\left(\frac{y}{a} + \frac{1}{a_{init}}\right) \tag{7.43}$$

To find δ_ν inside a top-hat potential, we introduce a perturbation to the neutrino distribution $f = f_0 + f_1$, where f_0 is given by Eq. (4.13), and we get the following from Eq. (11) in [16]:

$$f_1 = 2\frac{m_\nu}{T_{\nu 0}}\int_{t_{init}}^{t}\frac{dt'}{a_{t'}}\frac{e^{q/T_{\nu 0}}}{\left(e^{q/T_{\nu 0}}+1\right)^2}\frac{G_{t'}\delta M_{t'}}{r^2}\left(\alpha\frac{q}{T_\nu} - \hat{q}\cdot\hat{r}\right)$$

$$\times\left[\mathcal{R}^{-3/2}\Theta\left(\mathcal{L}<\mathcal{R}\right) + \mathcal{L}^{-3/2}\Theta\left(\mathcal{L}\geq\mathcal{R}\right)\right] \tag{7.44}$$

where Θ is the Heaviside function. Variables that depend on t' are marked by a subscript for brevity (for instance $G(t') \equiv G_{t'}$ since in DGP gravity the effective gravitational constant will vary throughout the collapse). For convenience we have defined the following quantities, all unitless:

$$\mathcal{R} \equiv \frac{R_{t'}}{r} = \frac{R_{DP,t'}}{r a_{t'}} \tag{7.45}$$

$$\mathcal{L} \equiv 1 + \frac{q^2}{T_{\nu 0}^2}\alpha^2 - \frac{2q}{T_{\nu 0}}\alpha\hat{q}\cdot\hat{r} \tag{7.46}$$

$$\alpha \equiv \frac{T_{\nu 0}\left(\eta - \eta'\right)}{m_\nu r} \tag{7.47}$$

It should be well noted that η in Eq. (7.47) is **not** the conformal time we introduced in section 2.3. It is a new time variable defined by $a^2 d\eta = dt$, which describes the co-moving distance a non-relativistic neutrino travels along an unperturbed ($f_1 = 0$) path.[17] As this variable only appears in the difference $\eta - \eta'$, we are free to choose an initial condition $\eta = 0$ wherever we like. However,

[6] Unlike [16] and [17], where only r is co-moving

[7] See Eq. (7.48)

$\eta(a_{init}) = 0$ seems the most natural choice given this definition. Note that $\alpha \geq 0$, as $\eta \geq \eta'$ because $a' \leq a$ and all the other factors are positive.

Eq. (7.44) is the result of solving the linearized, non-relativistic Boltzmann equation for massive neutrinos, Eq. (3.19). Note that we have taken the liberty of introducing a small difference between Eq. (7.44) and Eq. (11) in [16] as written: We have replaced $a_{t'}^3 r^3/R^3$ with $a_{t'}^3 r^3/R_{t'}^3 = \mathcal{R}^{-3/2}$ in the first term of the Heaviside function for three reasons:

- As one crosses the step in the Heaviside function, f_1 should still be continuous, as the step originates from the peculiar potential Ψ_{pec} from Eq. (3.17), which is indeed continuous at the threshold $r = R$.
- The $a_{t'}^3$ in the nominator serves the purpose of making R^3 in the denominator co-moving, same as $r_{t'}^3$. To that end, one should use the correct time variable: The integration variable t' and not t.
- Without this change, we get very unrealistic results.

The quantity we seek, δ_ν, is then found by integrating over six more dimensions:

$$\delta M_\nu(< R, a) = m_\nu \int_{V_c} d^3\mathbf{r} \int \frac{d^3\mathbf{q}}{(2\pi)^3} f_1(\mathbf{q}, \mathbf{r}, a)$$

or, more suited to our purposes:

$$\delta_\nu(< R, a) = \frac{3m_\nu}{4\pi R_{PD}^3 \bar{\rho}_\nu} \int_{V_c} d^3\mathbf{r} \int \frac{d^3\mathbf{q}}{(2\pi)^3} f_1(\mathbf{q}, \mathbf{r}, a) \tag{7.48}$$

(where $V_c = \frac{4}{3}\pi \frac{R_{PD}^3(a)}{a^3} = \frac{4}{3}\pi R^3(a)$ is the co-moving volume of the sphere), all of which is the result of combining Eq. (8) in [16] with Eq. (6.21). We now introduce new, unitless integration variables:

$$dl^i \equiv T_{\nu 0} dr^i \qquad r = \frac{l}{T_{\nu 0}} \tag{7.49}$$

$$dk^i \equiv \frac{dq^i}{T_{\nu 0}} \qquad \frac{q}{T_{\nu 0}} = k \tag{7.50}$$

$$x' \equiv \ln\left(\frac{a'}{a_{init}}\right) \qquad a' = e^{x_{init} + x'} \tag{7.51}$$

The reasoning for writing x' in this form is that $x'_{init} = 0$ as a result. In practice, the ODE solver needs to take very small steps near the lower integration limit for several of the variables. This is no problem whenever the value of such an integration variable is very close to 0. If not, though, the new value after the first step will be $x' = x'_{init} + \Delta x' \approx x'_{init}$ when $\Delta x' \ll x'_{init}$. To avoid this, we will define our integration variables so they all have 0 as the lower limit. Then, we may use Eq. (7.28) to substitute

$$\frac{dt'}{a'} = \frac{dx'}{a' H_{a'}} \tag{7.52}$$

and we also get conveniently from Eqs. (7.49) and (7.50) that

$$d^3\mathbf{r}\, d^3\mathbf{q} = d^3\mathbf{k}\, d^3\mathbf{l} \tag{7.53}$$

$$\hat{q} \cdot \hat{r} = \frac{\mathbf{q} \cdot \mathbf{r}}{qr} = \frac{\mathbf{k} \cdot \mathbf{l}}{kl} = \hat{k} \cdot \hat{l} \tag{7.54}$$

Eq. (7.47) now becomes

$$\alpha \equiv \frac{T_{\nu 0}\,(\eta - \eta')}{m_\nu r} = \frac{T_{\nu 0}^2\,(\eta - \eta')}{m_\nu l} \tag{7.55}$$

We further define

$$L \equiv T_{\nu 0} R = \frac{T_{\nu 0}}{a} R_{DP} \tag{7.56}$$

which together with Eqs. (7.43) and (7.49) gives

$$\frac{R_{DP,a'}}{ra'} = \frac{a' R_{a'}}{ra'} = \frac{R_{a'}}{r} = \frac{L_{a'}}{l}$$

$$\mathcal{R} \equiv \frac{R_{DP,a'}^2}{r^2 (a')^2} = \frac{L_{a'}^2}{l^2} \tag{7.57}$$

For the left hand side of the Heaviside function, the same substitutions give

$$\mathcal{L} \equiv 1 + \frac{q^2}{T_{\nu 0}^2}\alpha^2 - \frac{2q}{T_{\nu 0}}\alpha \hat{r}\cdot\hat{q} = 1 + k^2\alpha^2 - 2k\alpha\hat{k}\cdot\hat{l} \tag{7.58}$$

so that we now have a completely unitless integrand:

$$f_1 = 2\frac{m_\nu}{T_{\nu 0}}\int_0^{x-x_{init}} \frac{dx'}{l^2}\frac{T_{\nu 0}^2 G_{a'}\delta M_{a'}}{a' H_{a'}}\frac{e^k}{\left(e^k+1\right)^2}\left(\alpha k - \hat{k}\cdot\hat{l}\right)$$

$$\times\left[\mathcal{R}^{-3/2}\Theta\left(\mathcal{L}<\mathcal{R}\right) + \mathcal{L}^{-3/2}\Theta\left(\mathcal{L}\geq\mathcal{R}\right)\right] \tag{7.59}$$

where $G_{a'} = G$ in ΛCDM and $G_{a'} \equiv (G_{DGP}(a')/G)\cdot G$ in DGP gravity[8].

By using Eq. (6.22) and exploiting that the total mass M for CDM + baryons is conserved, we can write

$$\frac{T_{\nu 0}^2 G_{a'}\delta M_{a'}}{a' H_{a'}} = \frac{T_{\nu 0}^2 GM}{a' H_{a'}}\frac{\delta_{cb}(a')}{\delta_{cb}(a')+1}\frac{G_{DGP}(a')}{G}$$

and we then move the time-independent unitless factor $T_{\nu 0}GM$ outside the integral over x' (where the factor $T_{\nu 0}$ conveniently cancels with its like in the denominator). For what remains inside the integral, we can define another unitless quantity:

$$\xi_{a'} \equiv \frac{T_{\nu 0}}{a' H_{a'}}\frac{\delta_{cb}(a')}{\delta_{cb}(a')+1}\frac{G_{DGP}(a')}{G} \tag{7.60}$$

After the overdensity has collapsed, in the limit $\delta_{cb}(a') \to \infty$, this becomes

$$\xi_{a'} \to \frac{T_{\nu 0}}{a' H_{a'}}\frac{G_{DGP}(a')}{G} \tag{7.61}$$

which we will use after collapse to avoid numerical problems.

An integral over seven dimensions is time-consuming to calculate, so we will see if we can simplify this somewhat. In spherical coordinates:

$$d^3\mathbf{l} = l^2\sin\phi_l dl\, d\theta_l d\phi_l \qquad d^3\mathbf{k} = k^2\sin\phi_k dk\, d\theta_k d\phi_k \tag{7.62}$$

[8] since $\delta M_{a'}$ follows the integration variable a' its scaling factor, $G_{a'}$, must do the same - this is the only halo mass term in the equation.

$$\hat{k}\cdot\hat{l} = (\cos\theta_k\cos\theta_l + \sin\theta_k\sin\theta_l)\sin\phi_k\sin\phi_l + \cos\phi_k\cos\phi_l$$

From the latter, it is easy to see that if we choose coordinates so that $\hat{l}$ points directly along the z axis, ϕ_k becomes the total angle between $\hat{l}$ and $\hat{k}$ and we get

$$\hat{k}\cdot\hat{l} = \cos\phi_k \equiv \beta - 1 \qquad \beta = \cos\phi_k + 1 \tag{7.63}$$

which is unchanged by rotating $\hat{k}$ around the z axis, so the dot product is independent of θ_k as well. Note that analogously to x' we have defined our new variable β so that $\beta = 0$ at the lower integration limit. Note that this has nothing whatsoever to do with the variable by the same name introduced in Eq. (6.33) in the context of DGP gravity. With this definition, we have

$$d\beta = \frac{d\beta}{d\phi_k}d\phi_k = -\sin\phi_k d\phi_k \tag{7.64}$$

The integrand is now completely independent of θ_l, ϕ_l and θ_k, but even though we just saved ourselves from a lot of redundant work, we must still integrate over these variables. Fortunately, we can do so analytically. For a generic function $g(\hat{k}\cdot\hat{l})$:

$$\int_0^{2\pi} d\theta_k \int_0^{2\pi} d\theta_l \int_0^{\pi} d\phi_l \sin\phi_l \int_0^{\pi} d\phi_k \sin\phi_k g(\hat{k}\cdot\hat{l})$$

$$= -\int_0^{2\pi} d\theta_k \int_0^{2\pi} d\theta_l \int_0^{\pi} d\phi_l \sin\phi_l \int_2^{0} d\beta g(\beta - 1)$$

$$= 8\pi^2 \int_0^2 d\beta g(\beta - 1) \tag{7.65}$$

Finally, we collect all the factors outside the x' integral that do not depend on integration variables (including the $T_{\nu 0}GM$ that we moved outside earlier) to get an unitless[9] outer factor:

$$\delta_\nu(< R, a) = \frac{3m_\nu^2 GM}{2\pi^2 R^3 \bar{\rho}_\nu}\int_0^{k_{max}} dk \int_0^2 d\beta \int_0^{L(a)} dl \int_0^{x-x_{init}} dx'\, I(k, l, \beta, x', a) \tag{7.66}$$

[9]Not surprising, as δ_ν itself is unitless.

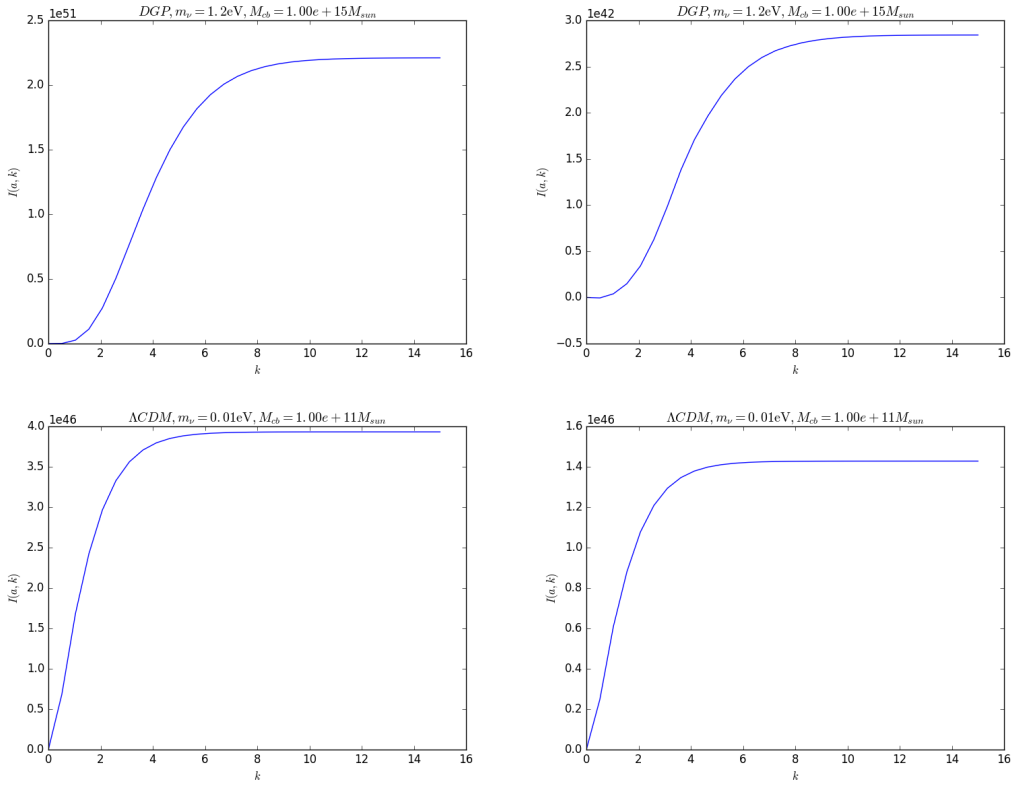

Figure 7.7: Examples of integrating Eq. (7.66) up to various values of k_{max}, demonstrating that the integral does reach an asymptote before $k = 15$ in each case. In each case, the figure to the left is the integral evaluated at $a = 5.54{\cdot}10^{-3}$, and the figure to the right is evaluated at $a = 1$. All simulations targeted collapse just slightly later than today.

where $k_{max} = 15$ is where we no longer have any significant contribution from extending the integral over k (see fig. 7.7).

We may of course also combine Eqs. (6.21) and (7.66) to find δM_ν directly if we wish:

$$\delta M_\nu = \frac{2m_\nu^2 GM}{\pi} \int_0^{k_{max}} dk \int_0^2 d\beta \int_0^{L(a)} dl \int_0^{x-x_{init}} dx'\, I(k, l, \beta, x', a) \qquad (7.67)$$

Our unitless integrand, with contributions from the surface elements in Eq. (7.62) and a factor $T_{\nu 0} GM$ moved outside, is then

$$I(k,l,\beta,a',a) = \xi_{a'}\frac{k^2e^k}{\left(e^k+1\right)^2}\left(\alpha k-\beta+1\right)$$

$$\times\left[\mathcal{R}^{-3/2}\Theta\left(\mathcal{L}<\mathcal{R}\right)+\mathcal{L}^{-3/2}\Theta\left(\mathcal{L}\geq\mathcal{R}\right)\right] \tag{7.68}$$

where, to summarize,

$$\mathcal{L} = 1+k\alpha\left[k\alpha+2\left(1-\beta\right)\right] \qquad \mathcal{R} = \frac{L_{a'}^2}{l^2} \qquad \alpha = \frac{T_{\nu0}^2\left(\eta-\eta'\right)}{m_\nu l} \tag{7.69}$$

There is a case where $\mathcal{R}$ has a singularity: $l=0$ results in $\mathcal{R}^{-3/2}=0$, which in itself is not an issue. However, it also causes the αk term to explode. In this case, we need to check the limit:

$$\lim_{l\to0}\alpha k\mathcal{R}^{-3/2} = \lim_{l\to0}\frac{T_{\nu0}\left(\eta-\eta'\right)kl^2}{\mu_\nu L_{a'}^3} = 0$$

whenever $L_{a'}^3\neq0$. However, in the case that $L_{a'}^3=0$, the entire integral over l becomes zero anyway, since the integration limits then coincide. The net result is easy to check for in the code:

$$l=0 \qquad \Rightarrow \qquad I(k,l,\beta,a',a)=0 \tag{7.70}$$

7.5 Overview of the code

This is a brief summary of how the code implements the algorithms presented in this chapter. The code is written in Python 2, chosen for its large number of publicly available libraries and plotting tools. To be sure, this incurs a performance penalty compared to Fortran, for example, but the simulations turned out to be quick enough in practice that there was no need to write performance-critical code in another language.

- First, parameter sets (DGP, ΛCDM) and grids (halo masses, neutrino masses, redshift) are set up (in natural units).

- Then, one calculates the density and pressure of unperturbed massive neutrinos as in section 7.1, performing cubic spline interpolation on the resulting grids and saving the results to file to improve performance.

- With these results, giving access to $\Omega_\nu(a)$, one adjusts the other parameters to ensure the universe is flat (section 7.2.1), and calculates the background densities with Eq. (2.37), with the exception of radiation, which uses Eq. (3.13). One then solves the appropriate Friedmann equation (2.42) or (5.10) to find $H(a)$.

- One then passes the adjusted cosmological parameters to CAMB, which is run once per neutrino mass (these results are saved to file, so this need not be repeated every run).

- Collecting the results from CAMB, one has the means to calculate $\dot{\delta}_{cb,init}$ for any choice of $\delta_{cb,init}$ (section 7.2)

- The code then calculates $\eta(a)$[10] and $t(a)$, again splining the results. The latter is used mostly for plotting and ensuring the universes in DGP and ΛCDM have the same age.

- One then solves the differential equations in section 7.3 without neutrino clustering. If one wants to target collapse today, this collapse is simulated on a grid of $\delta_{cb,init}$ values where collapse redshift is recorded. Using spline interpolation, one then picks the correct $\delta_{cb,init}$ for each set of parameters. One may also set a predetermined $\delta_{cb,init}$ for all simulations to better be able to compare them.

- Once all the results needed to calculate clustering are in place, we set up a coarse clustering grid, as this calculation is time intensive. On this grid, we calculate clustering as in section 7.4 and spline the results.

- Using the splined clustering results, the spherical collapse code is run again to include neutrino clustering.

- Plot data from all the simulations are saved to file, so that the code only runs the simulations that are not already on file. This way it is a quick process to re-run a simulation and display more plots than one wished to see the first time.

[10]The parameter from [16], not conformal time.

Part III

Results

Chapter 8

Results

> *Albert grunted. "Do you know what happens to lads who ask too many questions?"*
>
> *Mort thought for a moment. "No," he said eventually, "what?"*
>
> *There was silence.*
>
> *Albert straightened up. "Damned if I know. Probably they get answers, and serve 'em right."*
>
> *— Terry Pratchett, Mort*

In this chapter I present the results of the numerical simulations described in the preceding pages.

The first task the code was put to, was to compare the ΛCDM and s-DGP models in such a way that the background evolved similarly for both models. The process of ensuring similarly evolving backgrounds can be summarized as follows:

- Keep the ΛCDM model constant.
- Adjust Ω_{c0} and Ω_{b0} for the DGP model so that these agree with the ΛCDM model today.
- Adjust the Hubble parameter H_0 and the GR scale r_c for the DGP model until the age of the universe is the same in both models: $t(a_0)_{\Lambda\mathrm{CDM}} = t(a_0)_{\mathrm{DGP}}$.
- There are many combinations of H_0 and r_c that can do the above, and there is a degeneracy at work in this regard: Increasing H_0 and increasing r_c both make the universe younger. Several combinations of the two were investigated until one was found that overlaps nicely with ΛCDM using the Planck parameters, see fig. 8.1 and 8.2. Note that the shapes of the curves are not completely identical - this difference mainly stems from the

Parameter	ΛCDM	DGP	DGP (alternate)
h	$67.74 \cdot 10^{-2}$	$64.00 \cdot 10^{-2}$	$70.00 \cdot 10^{-2}$
$\Omega_{b0}h^2$	$2.230 \cdot 10^{-2}$	$2.498 \cdot 10^{-2}$	$2.088 \cdot 10^{-2}$
$\Omega_{c0}h^2$	$1.188 \cdot 10^{-1}$	$1.331 \cdot 10^{-1}$	$1.112 \cdot 10^{-1}$
$\Omega_{\Lambda 0}$	0.6911	0	0
r_c	∞	6717 Mpc	5500 Mpc
τ	0.066	0.066	0.066
n_s	0.9667	0.9667	0.9667
A_s	$2.142 \cdot 10^{-9}$	$2.142 \cdot 10^{-9}$	$2.142 \cdot 10^{-9}$

Table 8.1: Cosmological parameters. ΛCDM values picked from the "TT,TE,EE+lowP+lensing+ext" data set in [6]. DGP values adjusted by hand (see fig. 8.1 and 8.16).

Friedmann equations, and tinkering with parameters can only get you so far[1].

- The input to CAMB[2] (in order to get the initial conditions) were kept identical except for the above.

This resulted in the set of parameters shown in table 8.1 (before adjusting Ω_{c0} to account for massive neutrinos):

τ is the optical depth at reionization, n_s is the scalar spectral index, and A_s is the scalar amplitude. We refer to [5] for an explanation of these quantities. These inputs were only used for CAMB to get the initial conditions.

Onto this background, spherical collapse simulations were run for the same initial overdensity[3]. For each combination of halo mass and neutrino mass investigated, the following simulations took place:

- ΛCDM without neutrino clustering
- ΛCDM with neutrino clustering
- DGP gravity without neutrino clustering
- DGP gravity with neutrino clustering

[1] This is a subtle, but important point: Even though the scale factor itself evolves similarly in both cosmologies given our choice of parameters, the individual background densities of each component are not necessarily equal, as can be seen in fig. 8.2. This is due to the differences in the Friedmann equations

[2] Such as τ, n_s and other CMB-related properties, see table 8.1.

[3] Set so that the slowest collapse scenario, DGP gravity with maximal total neutrino mass $m_\nu = 1.2\,\mathrm{eV}$ and minimum halo mass $M_{cb} = 10^{10}\,\mathrm{M}_\odot$, collapses today at $a = a_0$. The other simulations then collapse earlier.

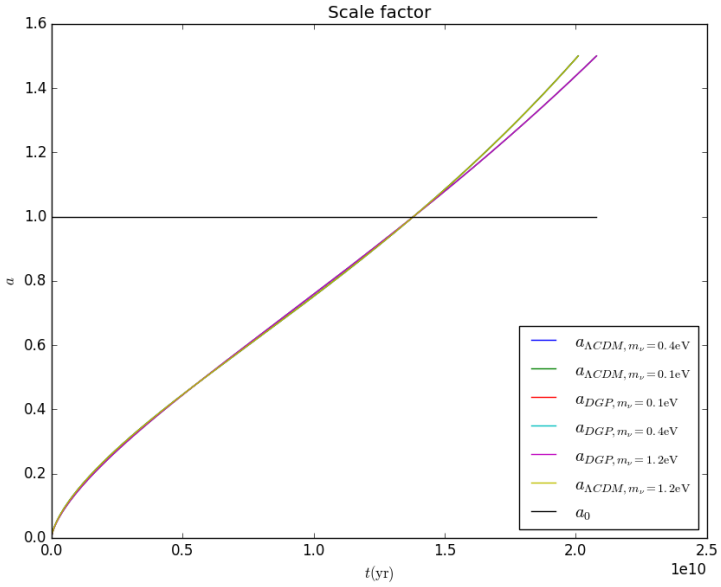

Figure 8.1: Background evolution: Scale factor plotted against time using Planck parameters, with the exception of DGP parameters set to $h = 64.0$, $r_c = 6717\,\mathrm{Mpc}$. Note that the neutrino mass has a very slight effect on the evolution of the scale factor.

- DGP gravity without neutrino clustering, without the effect of the modified gravitational constant ($G_{DGP}(a) = G$ at all times)

- DGP gravity with neutrino clustering, without the effect of the modified gravitational constant

The latter two cases were studied to see the effect of G_{DGP} on the mass perturbations δM_{cb} and δM_ν, compared to the effect of the background densities evolving differently.

The resulting plots of radii revealed that the major source of differences in spherical collapse stems from differences in the background densities and in the collapse equations (7.35) and (7.36) themselves. Even for large neutrino and halo masses, the effective gravitational constant $G_{DGP}(a)$ (plotted in fig. 8.4) turned out to be the lesser contributor to differences in collapse time, as fig. 8.3 suggests.

For low halo masses, however, the effect of clustering is all but absent, even for very heavy neutrinos (see fig. 8.5 and 8.6). As before, the background evolution has the greatest influence on collapse, with some additional contribution from the effective gravitational constant.

As mentioned in chapter 4, cosmological bounds on the sum of neutrino masses are close to 0.1 eV. We will now compare a universe with this neutrino mass to

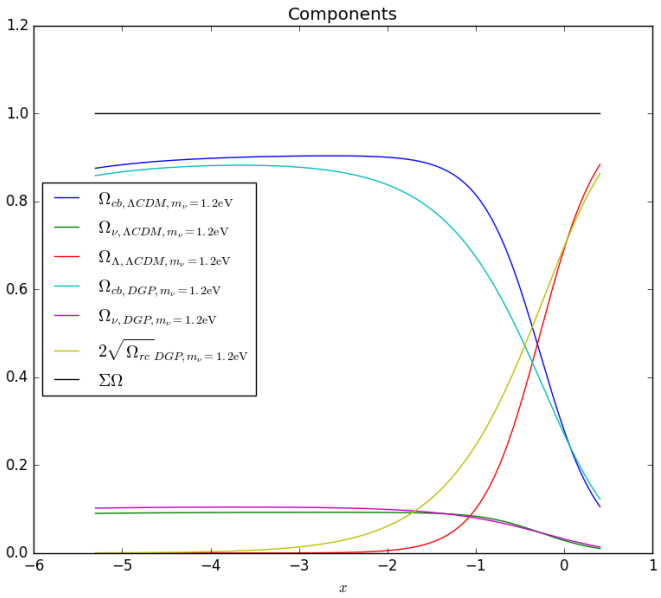

Figure 8.2: Comparison of components in ΛCDM and DGP cosmologies for $m_\nu = 1.2\,\mathrm{eV}$. Note that $2\sqrt{\Omega_{rc}} = \bar{\rho}_{rc}/\rho_{crit}$ is plotted instead of Ω_{rc} since the way the latter is defined would make the sum of components $\Sigma\Omega$ different from 1.

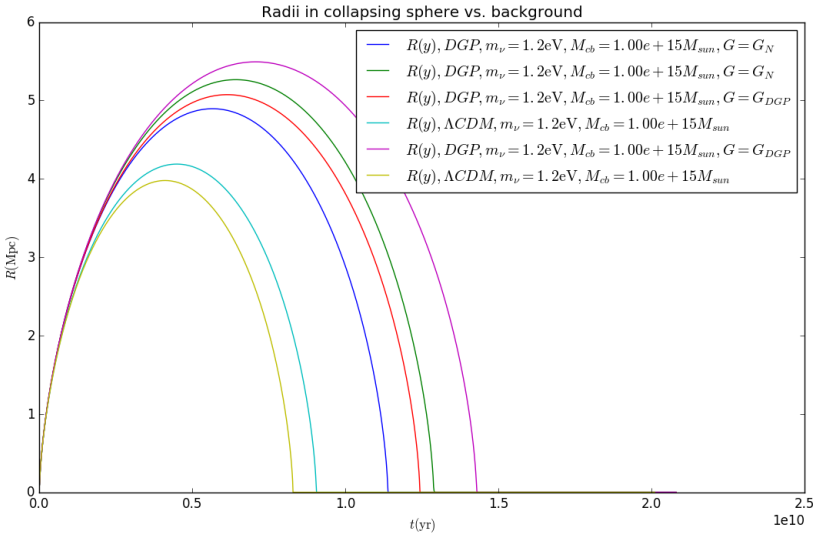

Figure 8.3: Spherical collapse in ΛCDM and DGP gravity: The latter first with invariant $G = G_N$ at all times, then with proper G_{DGP} calculated by Eq. (6.32). All simulations start at identical $\delta_{cb,init} = 1.7157 \cdot 10^{-2}$ so that only the slowest collapse occurs today. Each simulation is plotted with and without neutrino clustering - in all cases, the curve with neutrino clustering is the one that collapses first.

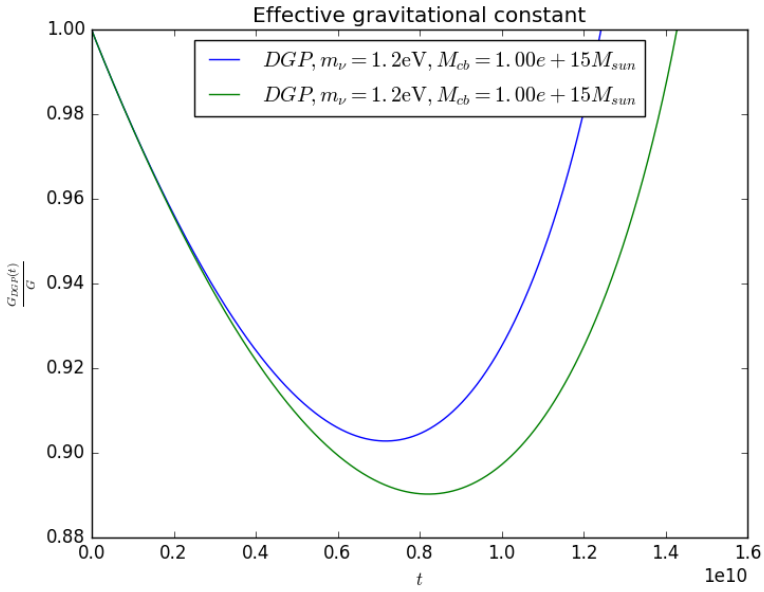

Figure 8.4: Ratio between the gravitational constants in DGP gravity and ΛCDM, $G_{DGP}(t)/G$, plotted throughout the collapse, with (blue) and without (green) neutrino clustering.

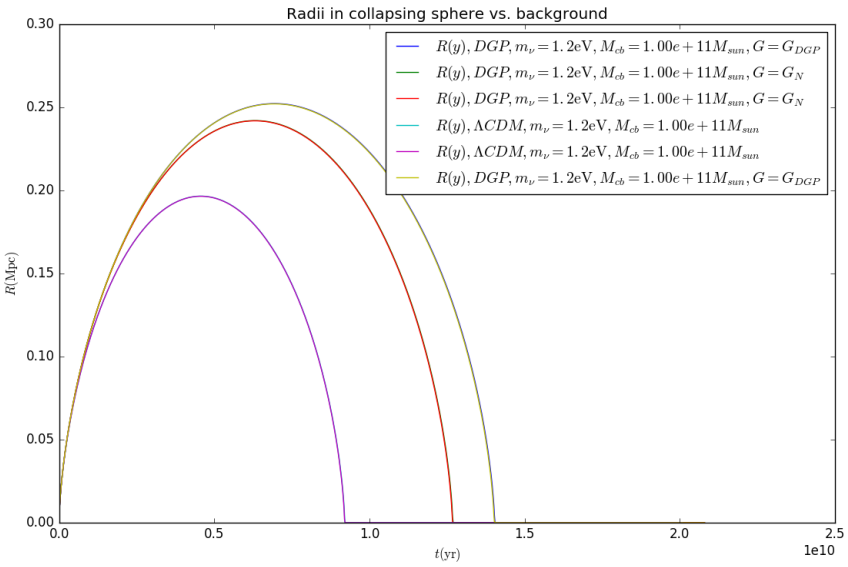

Figure 8.5: As fig. 8.3, with a lower halo mass.

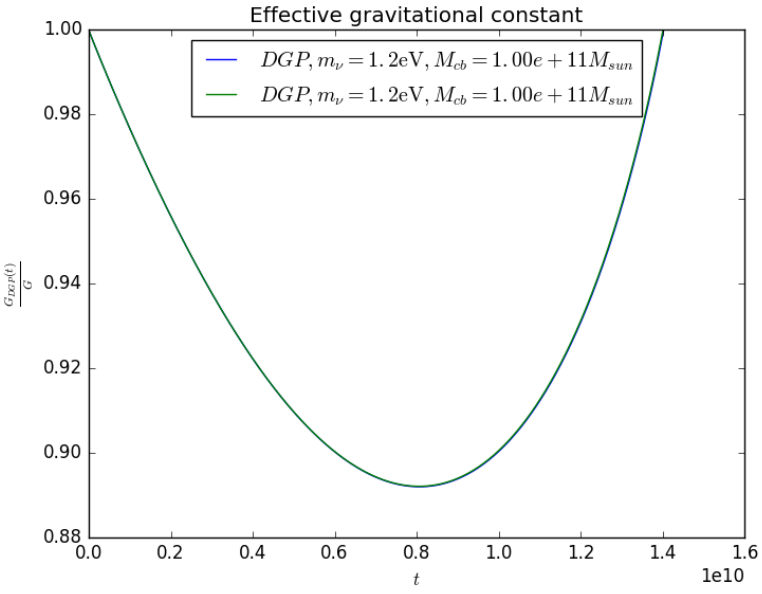

Figure 8.6: As fig. 8.4, with a lower halo mass.

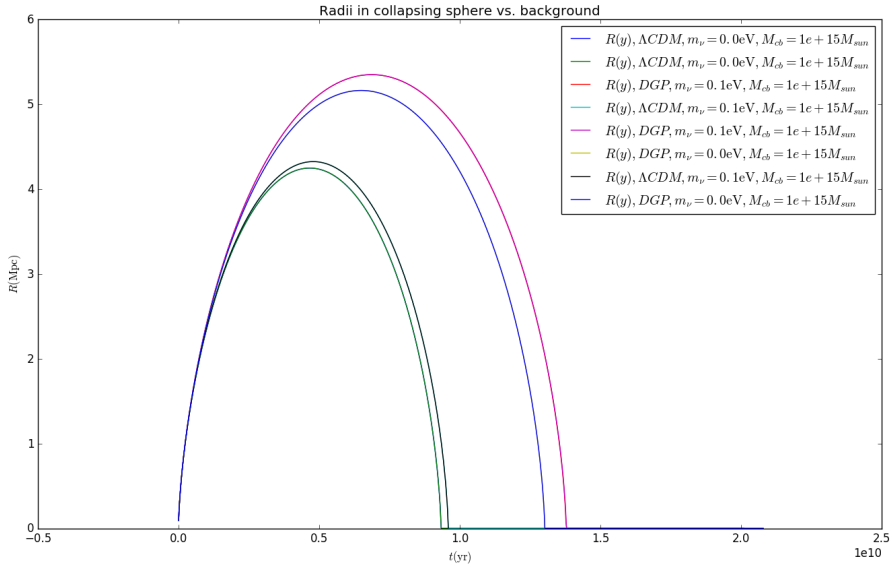

Figure 8.7: Comparison of ΛCDM and DGP gravity with massless neutrinos and a neutrino mass of $m_\nu = 0.1\,\text{eV}$, with and without clustering. Massive neutrino DGP gravity targets collapse today, giving $\delta_{cb,init} = 0.01317$, which was then used as input for all the simulations. Clustering has no visible impact here, only choice of cosmology.

a universe with massless neutrinos for both ΛCDM and DGP[4] for the maximal halo mass under consideration ($M = 10^{15}\,M_{sun}$). As we see in figures 8.7 to 8.10, the clustering effects are vanishingly small with such a small neutrino mass. More importantly, there is no confusing the two cosmologies in these cases - DGP gravity results in larger radii and later collapse times. Furthermore, in both cosmologies, the effect of heavier neutrinos delaying collapse can be clearly seen.

One may then ask, how massive need the neutrinos be in ΛCDM before the collapse starts to look like massless DGP gravity? As figures 8.11 to 8.14 show, increasing the neutrino mass to $m_\nu = 0.8\,\text{eV}$ allows massless neutrino DGP gravity to be confused with ΛCDM. The figure also reveals another interesting detail: When ΛCDM (without clustering) and massless neutrino DGP halos collapse at the same time, the DGP halo reaches a lower maximal radius. Not unexpectedly, the effects of clustering are even more pronounced with later (slower) collapse.

If we increase the neutrino mass by $0.3\,\text{eV}$ in both cosmologies[5], we see in figure 8.15 that an increase in total neutrino mass of $0.8\,\text{eV}$ is still required

[4]Even though said bounds assume ΛCDM.

[5]Thus avoiding the problem with mass degeneracies below this limit, as discussed in chapter 4.

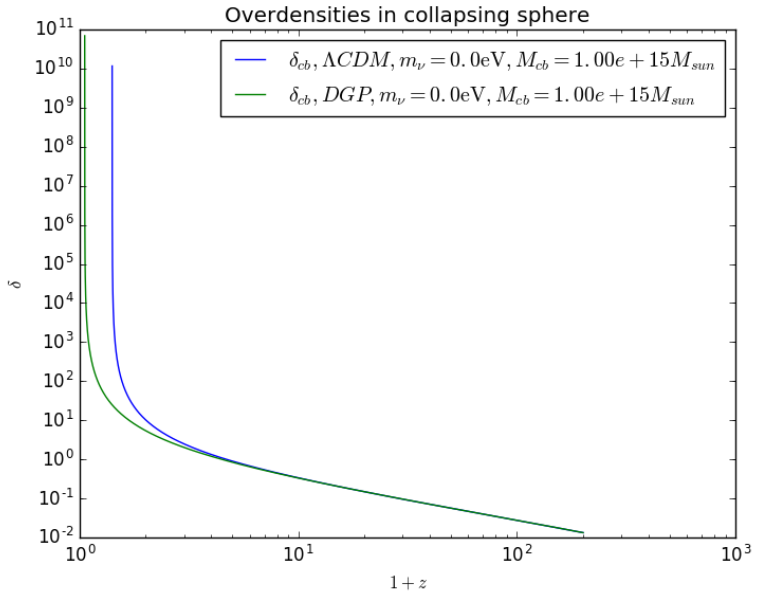

Figure 8.8: Comparison of overdensity $\delta_{cb}(1+z)$ for each cosmology with massless neutrinos ($\delta_{cb,init} = 0.01317$) as in fig. 8.7.

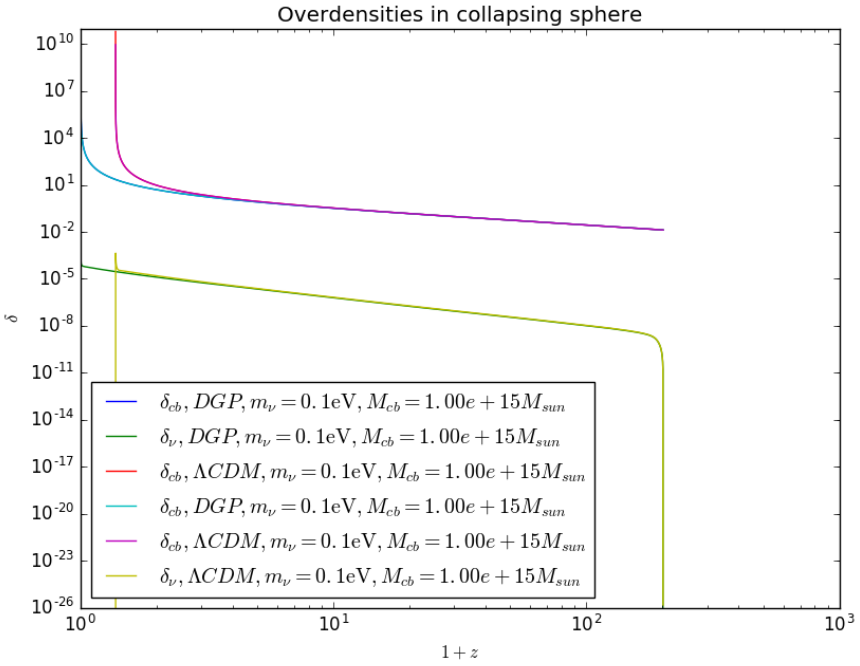

Figure 8.9: As fig. 8.8 with a neutrino mass of $m_\nu = 0.1\,\mathrm{eV}$. Both clustering and non-clustering collapse is plotted. $\delta_\nu(1+z)$ is plotted for clustering simulations.

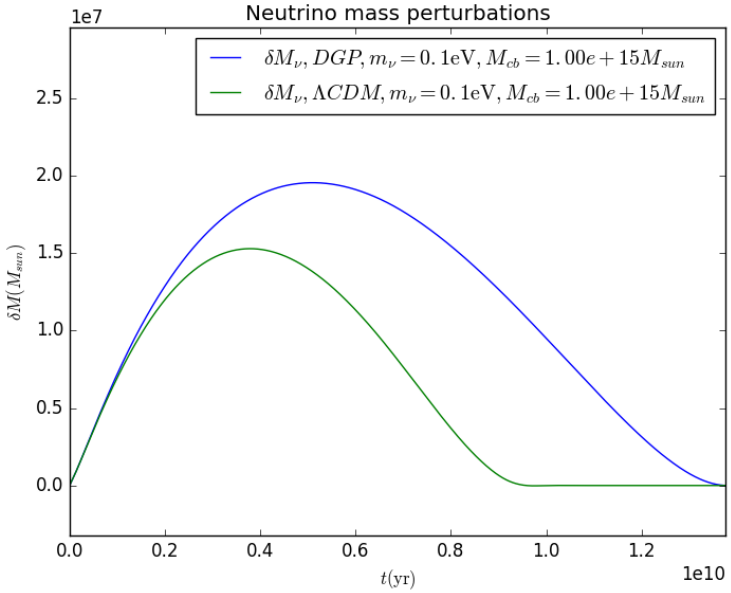

Figure 8.10: Neutrino mass perturbations $\delta M_\nu(t)$ for the neutrino overdensities in fig. 8.8 (clustering only).

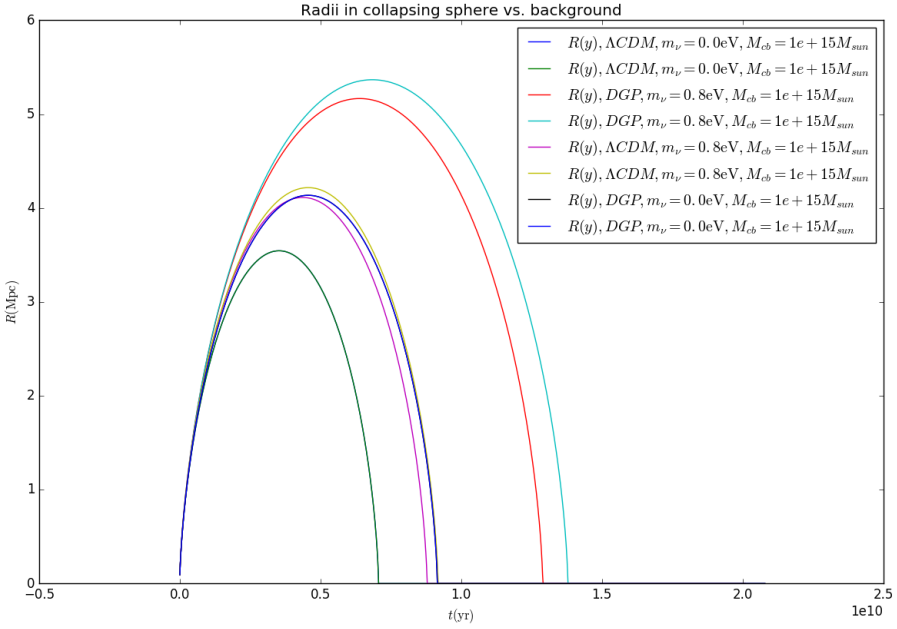

Figure 8.11: As figure 8.7, with more massive neutrinos and $\delta_{cb,init} = 0.1563$.

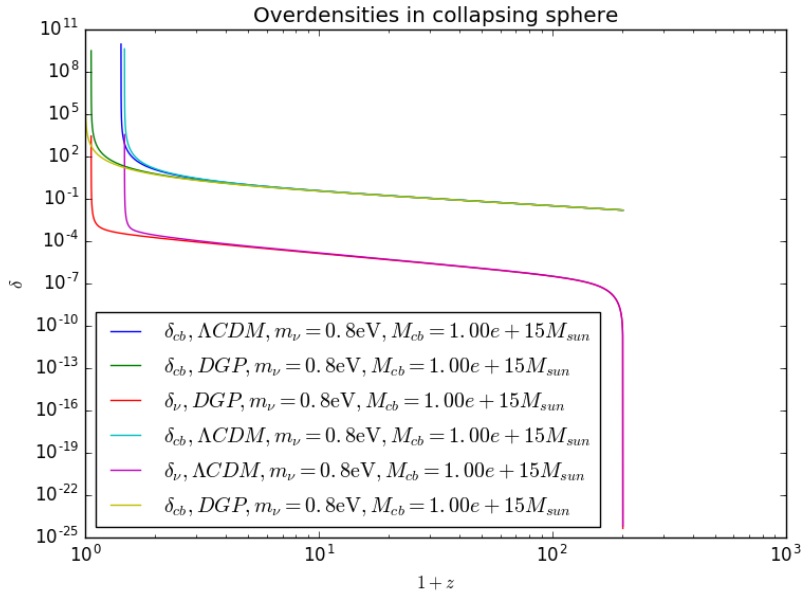

Figure 8.12: Overdensities with a neutrino mass of $m_\nu = 0.8\,\text{eV}$.

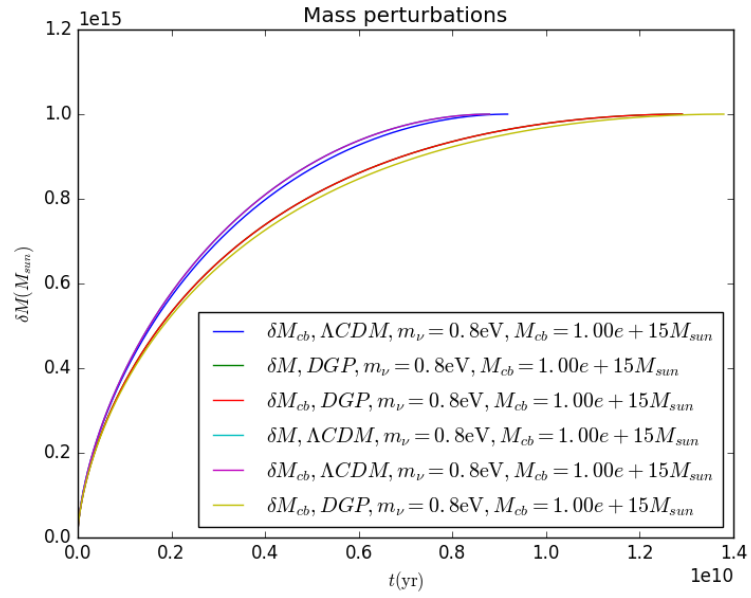

Figure 8.13: Mass perturbations (CDM+baryons and, if clustering, total) for $m_\nu = 0.8\,\text{eV}$.

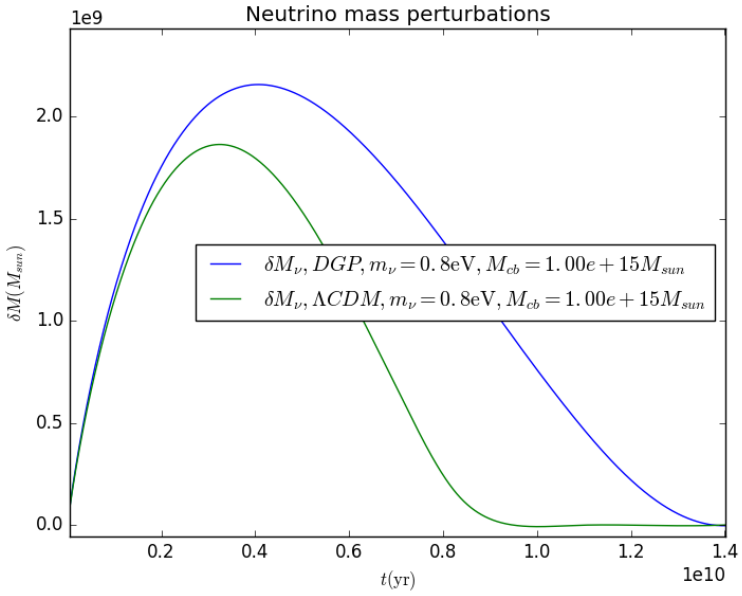

Figure 8.14: Neutrino mass perturbations (clustering only) for $m_\nu = 0.8\,\text{eV}$.

for ΛCDM to look like DGP. However, now this only applies without neutrino clustering. With neutrino clustering, we may still tell the cosmologies apart.

However, it turns out that another parameter combination of h and r_c in DGP gravity changes the result. We call this parameter set "DGP (alternate)" in table 8.1. In figures 8.16 and 8.17, we see that although the backgrounds still evolve similarly, the result is markedly different from fig. 8.11: We can now tell the two cosmologies apart (DGP collapses later than ΛCDM). Hence, the neutrino mass required to make the cosmologies indistinguishable is in this case even larger - we need a sum of neutrino masses greater than 0.8 eV to make the two look similar in this case.

With these results in hand, we conclude that DGP and ΛCDM cosmologies whose scale factors overlap from $z_{init} = 200$ until today will result in very different spherical collapse scenarios (a much larger difference than the effect of neutrino clustering). We observe the degeneracy between massive neutrinos and modified gravity, but note that the neutrinos need to be very massive to mask the choice of cosmological model completely, to the point that we go well above the current cosmological upper limits for the sum of neutrino masses. That said, as we discussed in chapter 4, we should take care not to put too much faith in cosmological constraints on neutrino masses.

The difference in total neutrino mass required to make one cosmology look like the other seems to be the same even when both cosmologies have massive neutrinos. However, this difference is clearly dependent on our choice of parameters in DGP gravity (the combination h and r_c), and so, even though the

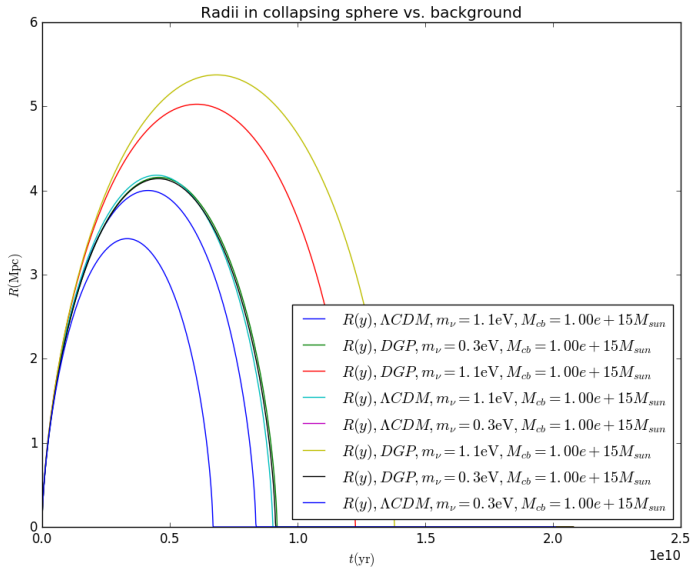

Figure 8.15: As figure 8.11, with massive neutrinos in both cosmologies, and a corresponding $\delta_{cb,init} = 0.01692$.

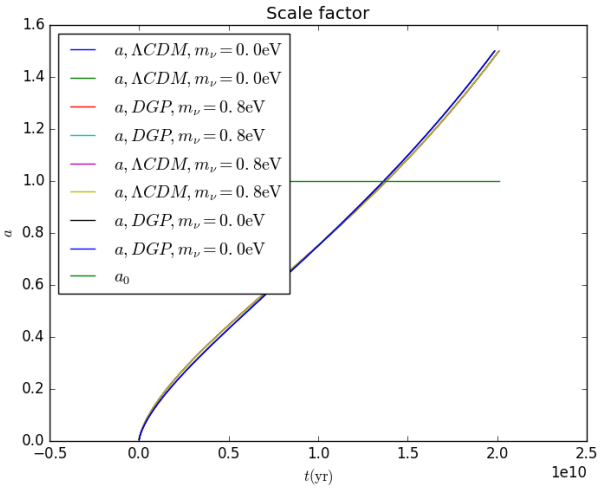

Figure 8.16: As fig. 8.1, with DGP parameters $h = 70.0$ and $r_c = 5500\,\mathrm{Mpc}$.

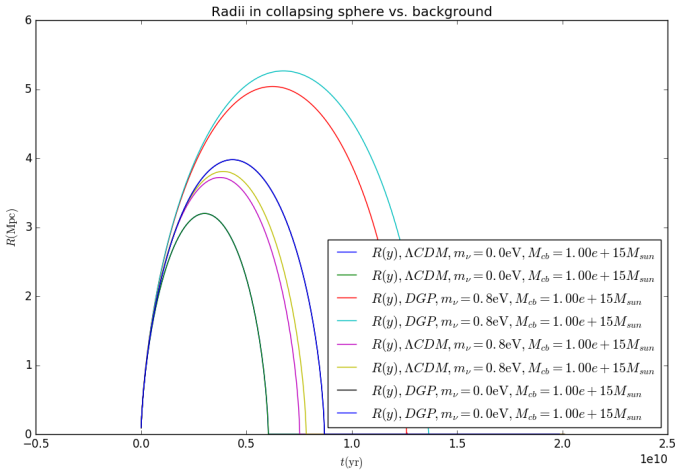

Figure 8.17: As fig. 8.11, with DGP parameters $h = 70.0$, $r_c = 5500\,\mathrm{Mpc}$ and $\delta_{cb,init} = 0.01721$. This corresponds to the slowest simulation collapsing today, as in fig. 8.11.

difference appears large, it is possible that one might make it arbitrarily small simply by picking the right parameter set.

Chapter 9

Discussion

> *"I make mistakes like the next man. In fact, being–forgive me–rather cleverer than most men, my mistakes tend to be correspondingly huger."*
>
> *— J.K. Rowling, Harry Potter and the Half-Blood Prince*

In this chapter, I discuss my results and try to pinpoint how trustworthy they are.

9.1 Approximations and assumptions

For convenience, we here list the assumptions and approximations used in this work:

- Spherical collapse is a crude model of structure formation, and should only be considered a first step on the way toward more accurate simulations. The price we pay for simplicity is that we sacrifice realism and accuracy. Furthermore, in DGP gravity there is no Birkhoff-like cancellation for non-top-hat profiles.
- For clustering, we use the linearized Boltzmann equation (BKT approximation), instead of the full solution in [17]. This should be all right as CDM and baryons dominate the spherical collapse at late times, even though it will underestimate the number of neutrinos whose trajectories are significantly altered by the overdensity, especially bound neutrinos.
- We use one massive neutrino, equivalent to three degenerate ones, even below 0.3 eV (0.1 eV per neutrino species) where the masses cannot be assumed to be degenerate.
- DGP gravity is shown (section 5.3) to be incompatible with observations. Hence, our parameter choices to get a ΛCDM-like evolution of the scale

factor for $a \leq a_0$ are most likely excluded by said observations as well. The large difference between the two cosmologies is therefore not guaranteed to be reproducible in more realistic modified theories of gravity. They could, in fact, be the result of our parameter choices, and it should be looked into whether we can achieve different results for spherical collapse with another combination of parameters that still make the scale factors in the two cosmologies evolve similarly.

- We assume the clustering neutrinos to be entirely nonrelativistic, with $\omega_{\nu,eff} = 0$ even though $\omega_{\nu,eff} < 1/4$ would be sufficient.

- We assume the background universe to be perfectly flat.

- We use ΛCDM in CAMB to get the initial conditions for DGP gravity as well, under the assumption that the cosmologies evolve similarly for $a < a_{init}$. We do, however, use change the parameters to match our DGP gravity parameters (else y'_{init} for both cosmologies would look identical in fig. 7.6).

- In ΛCDM we adjust $\Omega_{\Lambda 0}$ to keep the universe flat. In DGP gravity, we adjust Ω_{c0} to achieve the same thing so we are free to adjust Ω_{rc0} as a free parameter. We therefore assume that how we achieve flatness is relatively unimportant, given the small corrections that are involved ($\Omega_{\nu 0}$ is still subtracted from the observed Ω_{c0} in both cosmologies). The impact of this assumption increases for higher neutrino masses, however.

9.2 Comparison with the results in [16]

It proved difficult to reproduce the results in LoVerde's article exactly. For starters, an attempt to reproduce fig. 2 (a) in that work (with the same initial conditions, possibly excluding background cosmology parameters) resulted in fig. 9.1, where one notes that although the turnaround radius and time of collapse for the heaviest neutrinos (with a sum of 1.2 eV) is the same as in [16], the other neutrino masses (and the massless case) collapse too early and have slightly smaller turnaround radii. So we cannot claim to have reproduced this result exactly, even though these results are of the same order of magnitude. An important difference to note is that we have not simulated two massless neutrinos alongside the one massive neutrino, as LoVerde has done.

More worrying is our attempt to reproduce the right amount of clustering in fig. 2 (b) in the same article. Using 3 massive neutrinos, each with a mass of 0.4 eV (equivalent to a total mass of $m_\nu = 1.2\,\text{eV}$ in our simulations), we get significantly more clustering and a somewhat earlier collapse in fig. 9.2 compared

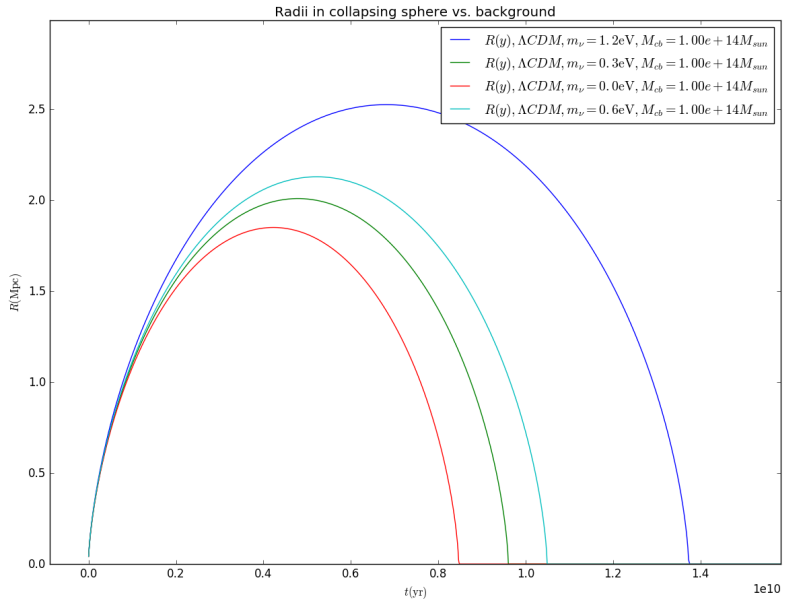

Figure 9.1: Equivalent to fig. 2 (a) in [16], with the same initial overdensity $\delta_{cb,init} = 1.377 \cdot 10^{-2}$ and halo mass $M = 10^{14}\, M_\odot$. Our simulation is run without two massless neutrinos.

to the article. Once again, we are not orders of magnitude off, but the difference is clearly noticeable.

Attempting to reproduce figure 1 in [16], showing plots for the overdensities δ_{cb} and δ_ν (fig. 9.3), as well as the mass perturbation δM_ν (fig. 9.4), reveals that the clustering effects on the collapse are caused by an amount of massive neutrinos that is far less than is the case in article. A by-eye reading of the plots at the turnaround point puts our result at $\delta_\nu \approx 5 \cdot 10^{-4}$, whereas figure 1 (b) in LoVerde's article gets $\delta_\nu \approx 0.25$, which is 500 times higher. Nonetheless, we achieve a slightly *greater* impact of clustering neutrinos in the output. It stands to reason that with neutrino overdensities such as in fig. 9.3, we would see a dramatic decrease in collapse time in our simulations: We have a maximal $\delta M_{\nu,max} \approx 2.8 \cdot 10^9\, M_\odot$, whereas the article gets $\delta M_{\nu,max} \approx 1.5 \cdot 10^{13}\, M_\odot$ - more than 5000 times higher.

This suggests that there are in fact *two* problems, either in the code used for this thesis or in that of [16]. First and foremost, the simulations clearly do not agree on how sensitive the collapse is to clustering neutrinos. Nonetheless, the collapse scenarios produced are much more similar than the overdensities and mass perturbations suggest they should be. Hence, the natural conclusion is that the work that gets the impact of clustering wrong also calculates an incorrect amount of clustering. It seems unlikely that both works get these two things

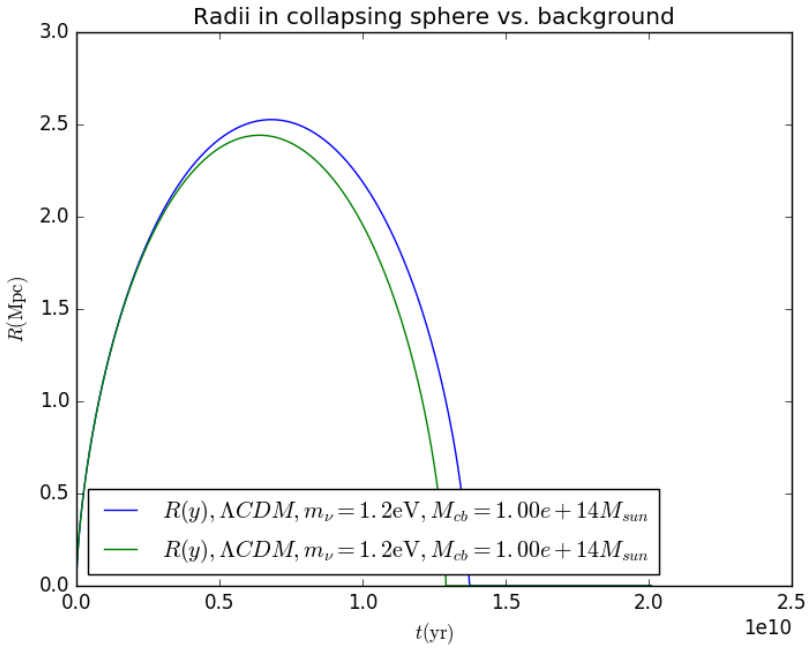

Figure 9.2: Equivalent to fig. 2 (b) in [16], with the same initial overdensity $\delta_{cb,init} = 1.377 \cdot 10^{-2}$ and halo mass $M = 10^{14}\, M_\odot$. Our simulation is run without two massless neutrinos. The green plot is with neutrino clustering in the halo, the blue is without.

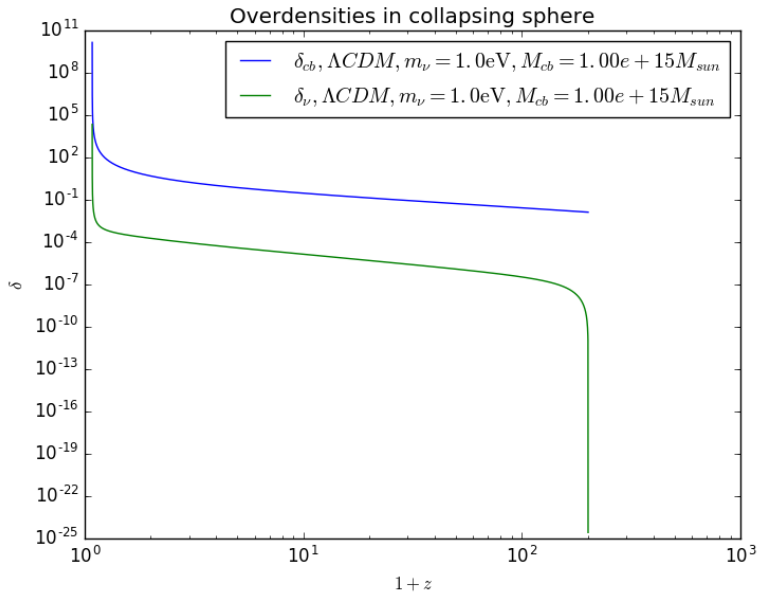

Figure 9.3: Equivalent to fig. 1 (b) in [16], with $z_{collapse} = 0.0$ for the non-clustering simulation.

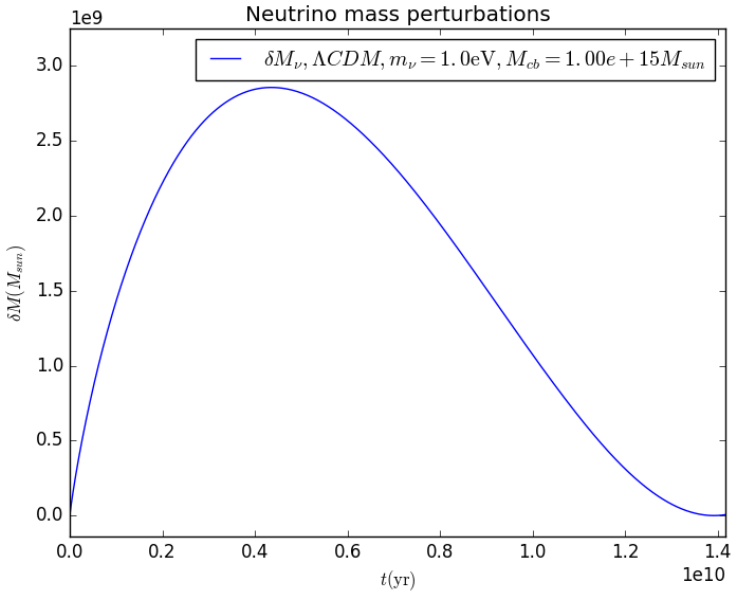

Figure 9.4: Equivalent to fig. 1 (a) in [16], with $z_{collapse} = 0.0$ without clustering.

exactly right.

It is also possible that the code used to extract the information in the figures 9.3 and 9.4 is not correct, whereas the final impact on collapse time is. Seeing as δ_ν is used explicitly to calculate $y(x)$ when clustering is switched on, however, this seems unlikely. And even if this were the case, we are still left with a discrepancy in fig. 9.2, in that we achieve the same amount of clustering with one neutrino species of mass $m_\nu = 0.4$ that [16] seems to achieve with three.

At first glance, mass perturbations as small as in fig. 9.4 seem unlikely to have a significant effect on the collapse time. From Eq. (7.9) we have that

$$\delta_{cb} = \frac{\rho_{cb}}{\bar{\rho}_{cb}} - 1 = \frac{1}{\bar{\rho}_{cb}} \frac{M_{cb}}{\frac{4}{3}\pi R^3} - 1 = \frac{3M_{cb}}{4\pi \bar{\rho}_{cb} R^3} - 1 \tag{9.1}$$

However, in ΛCDM, according to Eq. (6.25), the clustering (cl) and non-clustering (ncl) differential equations can differ only by a neutrino mass perturbation term

$$\ddot{R}_{cl} - \ddot{R}_{ncl} = -\frac{4\pi G}{3}\delta_\nu \bar{\rho}_\nu R = -\frac{4\pi G}{3}\delta\rho_\nu R = -\frac{4\pi G}{3}\frac{3\delta M_\nu}{4\pi R^3}R = -\frac{G\delta M_\nu}{R^2} \tag{9.2}$$

In fig. 9.5, we have plotted the CDM+baryon and massive neutrino terms

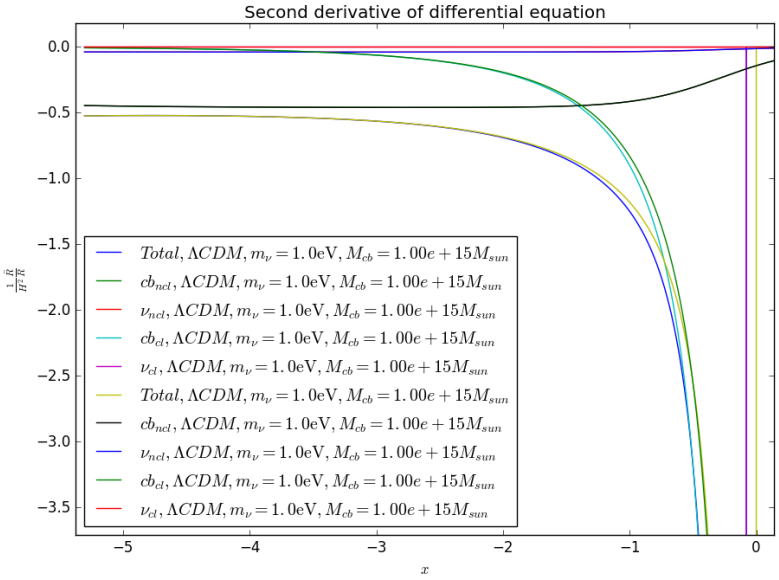

Figure 9.5: Contribution of the different terms in Eq. (6.25) for the collapse in figs. 9.3 and 9.4, including also the no-clustering version.

on the right hand side of Eq. (7.35) to see how much the clustering and non-clustering terms contribute. For CDM+baryons, the non-clustering (background) term dominates early on, but is then completely overtaken by the clustering term as we approach collapse. This happens both with and without neutrino clustering, but at a later stage in the latter case. We can also see how the background CDM+baryon terms dominate initially, only to be overtaken by the collapse of M_{cb} later on.

Are the clustering neutrinos really responsible for this behaviour? Zooming in on their contributions (fig. 9.6), we see that they in fact contribute much less than the difference between the sum of terms in the two simulations (in fig. 9.5). Thus they cannot directly explain the difference. Indirectly, however, it is conceivable that even this minuscule effect will change the radius noticeably. Since $\delta_{cb} \propto R^{-3}$, a slightly smaller radius will lead to a higher δ_{cb}, which in the next step affects the radius even more, causing the simulations to differ visibly after enough steps. δ_{cb} is definitely the primary driver of the collapse throughout. However, with the δ_ν term being the only difference between the clustering and non-clustering simulations, we must conclude that its effect on the radius is what causes δ_{cb} to evolve differently.

The question then becomes: Is the differential equation sensitive enough that a neutrino mass perturbation as small as the one in fig. 9.4 can have such a noticeable effect on collapse time? We certainly do not see such an instability in the plots of [16], and it would be premature to rule out a numerical problem in

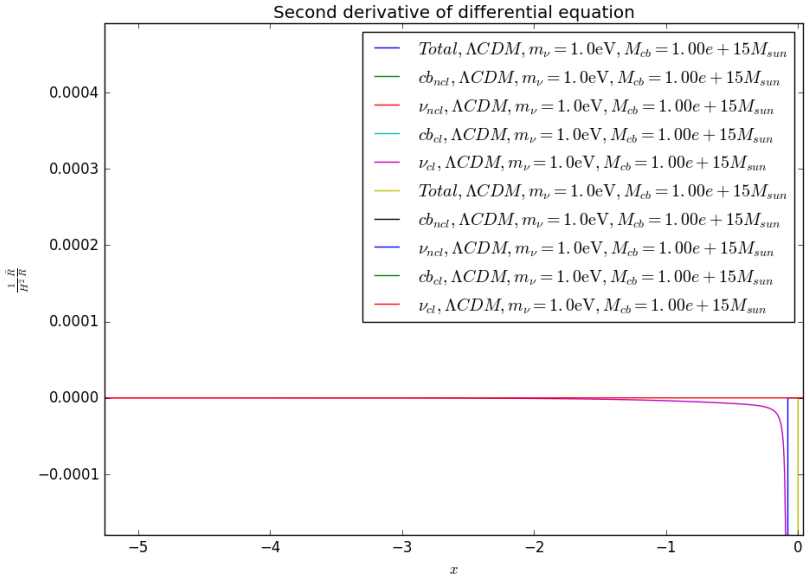

Figure 9.6: Contribution of the clustering neutrino terms (enlarged version of the top part of fig. 9.5).

the code. Further testing is necessary to determine whether this result is in fact incorrect, and if so, why.

A redeeming feature, however, is that the final impact of clustering on the radius R is not very far from what we would expect, even if the effect is a little more pronounced. For a realistic sum of neutrino masses in the neighbourhood of $m_\nu = 0.1\,\text{eV}$, clustering is hardly present at all, which is indeed consistent with [16]. Thus, even though it is disheartening to be unable to reproduce these results, we are unlikely to jump to wrong conclusions regarding the impact of clustering for small neutrino masses.

There remains, however, the question of being unable to reproduce the non-clustering scenario (fig. 9.1) exactly. Whereas the cosmological parameters leading to this plot's counterpart in [16] are unknown, they are unlikely to be very different from the Planck parameters. Can we then trust our conclusions regarding DGP gravity? It is somewhat comforting that the heaviest neutrino result in this figure agrees, but a little worrisome that the lighter ones do not match, even though they are the correct order of magnitude. We are thus forced to conclude that more investigation is necessary to uncover why we were unable to reproduce these results as well.

Chapter 10

Conclusions and future prospects

> *"It's the questions we can't answer that teach us the most. They teach us how to think. If you give a man an answer, all he gains is a little fact. But give him a question and he'll look for his own answers."*
>
> — *Patrick Rothfuss, The Wise Man's Fear*

In this final chapter, we look at what's next, for this model, its successors and observations. Here we assume that the model has been thoroughly tested and corrected where necessary.

10.1 Conclusions

Based on the findings in chapter 8, it may seem tempting to claim that at least in DGP gravity, we expect to see a large impact of the cosmological model on halo abundance, given that DGP halos collapse significantly later unless we are dealing with neutrinos almost 8 times heavier than the cosmological upper bound. However, we caution that DGP gravity is not consistent with observations, and it remains to be seen whether more realistic models of modified gravity will be able to reproduce the results. What is clear is that our choice of DGP parameters (the combination of h and r_c, especially) had a noticeable impact on collapse time in that cosmology, which is an interesting result in itself. Investigating a broader range of possible parameter combinations and their implications for spherical collapse seems worthwhile. Specifically, how small the difference in neutrino masses can get while still making the two cosmologies produce similar collapse scenarios. This could lead us closer to the expected degeneracy between massive neutrinos and modified gravity mentioned in chapter 1.

In any event, the inconsistencies with the results presented here and those of [16] needs to be cleared up before the results presented here can be trusted. Discovering why the non-clustering simulations do not agree on the collapse times

for lighter neutrinos should be the priority here. The clustering results should also be looked into, but since both works conclude that the impact is very small for realistic neutrino masses, the conclusion does not appear to stand or fall on this point alone. It is at best a small correction to the results, and we should keep in mind that spherical collapse is not precision cosmology on the best of days.

Nevertheless, we have shown how the approaches in [16] and [29] may be combined for collapse scenarios that obey Birkhoff's theorem. This applies even if we include neutrino clustering, where we have shown how to implement the approach outlined in [16] numerically.

10.2 Building upon and refining this methodology

The obvious next step is to include virialization in addition to collapse, to investigate at what radii the halos virialize. While the methods outlines in chapter 6 do not include massive neutrinos, one should investigate whether it is prudent to include them in the mass terms of Eqs. (6.28) and (6.38), especially the clustering ones.

Multiple (non-degenerate) neutrino species is another aspect of the simulations that need fleshing out. Being able to accurately model three non-degenerate neutrino masses whose sum is less than 0.3 eV would add realism to the model. This could lead to some corrections early in the collapse process, where the lightest neutrino species may be close to relativistic, and investigating how sensitive the collapse time and radii are to this change would be interesting. While it seems unlikely that one could distinguish between the normal and inverted hierarchy from halo observations (who at best are expected to help constrain the sum of neutrino masses[2]), it could be instructive to see how the model responds to a change in hierarchy when the sum of neutrino masses is small.

When it comes to clustering, we have calculated the potential for the massive neutrinos using only the non-clustering solution. We have neglected that the clustering neutrinos also change the potential. For heavy neutrinos, these corrections could become important. The slow way to do this is to include clustering calculations for every step of the collapse. This is slow because we would then no longer run clustering on a coarse grid and then spline it (as in section 7.5), but do the most time-intensive calculations on the full collapse grid.

A quicker way would be to simply run the clustering calculations more than once on the coarse grid, each time using the previous result as input. As long as the difference between non-clustering and clustering simulations are small, this should converge fairly quickly to the point where additional runs produce negligible changes.

There is also the potential to integrate Press-Schechter formalism[43]. This is the most important way one can link the results to observations of the abundance of collapsed/virialized dark matter halos (i.e. galaxies). Some pieces of the groundwork has already been done due to the way we extracted initial conditions from the CAMB output in section 7.2.

Finally, extending the model beyond DGP gravity to modified theories of gravity that do not obey Birkhoff's theorem[1] would be an interesting challenge. One should take care not to overcomplicate the model so that its appealing relative simplicity is sacrificed, though - with added complexity, N-body simulations become more attractive.

10.3 N-body simulations and the Euclid mission

And indeed, the simplicity of spherical collapse is also its greatest limitation: Observed dark matter halos in general most certainly do not have top-hat profiles, and there may be important physical effects hiding beyond spherical collapse. For one thing, even a top-hat could accrete CDM and baryon mass from outside the sphere, and sweep out an underdensity around it in the process, both of which we have neglected in this thesis. To get accurate results on modified gravity and massive neutrinos together, one needs to run computationally intensive N-body simulations. These may even simulate more than a single overdensity at at time, so that the effects of halos merging with one another can be seen. Such N-body simulations already exist for some theories of modified gravity[1] - one can then test the predictions we make here and see whether they still hold.

In such a scenario, where Birkhoff's theorem is no longer required, one may test other theories of modified gravity that unlike DGP gravity are consistent with observations (see section 5.3). If some modified gravity theories are detectable with massive neutrinos and some are not, we are getting closer to using halo abundance to probe the underlying cosmology. As neutrino mass constrains from other experiments become more accurate, it may be easier to determine what to look for in the search for deviations from ΛCDM cosmology.

Finally, the Euclid mission[2] aims to map halos and their redshift (as well as use weak gravitational lensing) to constrain the neutrino masses and look for signs of modified gravity at the same time. N-body simulations such as described above will be an invaluable tool in determining how well the instrument is able to detect the cosmological properties of the model. In that regard, the simple model of this thesis is but a modest first step.

[1] $f(R)$ gravity is one example.

Bibliography

[1] M. Baldi, F. Villaescusa-Navarro, M. Viel, E. Puchwein, V. Springel, and L. Moscardini. Cosmic degeneracies - I. Joint N-body simulations of modified gravity and massive neutrinos. *Mon. Not. Roy. Astron. Soc.*, 440:75–88, May 2014.

[2] L. Amendola, S. Appleby, D. Bacon, T. Baker, et al. Cosmology and fundamental physics with the Euclid satellite. *Living Reviews in Relativity*, 16:13–17, 2013. arXiv:1206.1225 [astro-ph.CO].

[3] G. Dvali, G. Gabadadze, and M. Porrati. 4D gravity on a brane in 5D Minkowski space. *Physics Letters B*, 485:208–214, July 2000.

[4] Ø. Elgarøy. AST4220: Cosmology I. https://www.uio.no/studier/emner/matnat/astro/AST4220/h09/course-material/lectures.pdf, 2009. Lecture notes in AST 4220: Cosmology I (University of Oslo).

[5] S. Dodelson. *Modern Cosmology*. Academic Press, 2003.

[6] Planck Collaboration, P. A. R. Ade, N. Aghanim, M. Arnaud, M. Ashdown, J. Aumont, C. Baccigalupi, A. J. Banday, R. B. Barreiro, J. G. Bartlett, et al. Planck 2015 results. XIII. Cosmological parameters. *ArXiv e-prints*, February 2015. 1502.01589.

[7] Y. Chen, B. Ratra, M. Biesiada, S. Li, and Z.-H. Zhu. Constraints on non-flat cosmologies with massive neutrinos after Planck 2015. *ArXiv e-prints*, March 2016. 1603.07115.

[8] T. M. Davis and C. H. Lineweaver. Expanding Confusion: Common Misconceptions of Cosmological Horizons and the Superluminal Expansion of the Universe. *Proc. Astron. Soc. Austral.*, 21:97–109, 2004.

[9] Ø. Grøn. *Lecture Notes on the General Theory of Relativity: From Newton's Attractive Gravity to the Repulsive Gravity of Vacuum Energy*. Lecture Notes in Physics. Springer New York, 2010.

[10] Joseph C. Kolecki. An introduction to tensors for students of physics and engineering. http://www.grc.nasa.gov/WWW/k-12/Numbers/Math/documents/Tensors_TM2002211716.pdf.

[11] S. Reynaud, A. Lambrecht, C. Genet, and M.-T. Jaekel. Quantum vacuum fluctuations. *Academie des Sciences Paris Comptes Rendus Serie Physique Astrophysique*, 2:1287–1298, 2001.

[12] H. Li and J.-Q. Xia. Testing Dvali-Gabadadze-Porrati gravity with Planck. *Physics Letters B*, 726:549–553, November 2013.

[13] Julien Lesgourgues and Sergio Pastor. Massive neutrinos and cosmology. *Phys. Rept.*, 429:307–379, 2006.

[14] D. J. Fixsen. The Temperature of the Cosmic Microwave Background. *The Astrophysical Journal*, 707:916–920, December 2009.

[15] L. Bergström and A. Goobar. *Cosmology and Particle Astrophysics*. Springer Praxis Books. Springer Berlin Heidelberg, 2006.

[16] Marilena LoVerde. Spherical collapse in $\nu\Lambda$CDM. *Phys. Rev. D*, 90:083518, Oct 2014.

[17] Marilena LoVerde and Matias Zaldarriaga. Neutrino clustering around spherical dark matter halos. *Phys. Rev.*, D89(6):063502, 2014.

[18] Robert H. Brandenberger, Nick Kaiser, and N. Turok. Dissipationless Clustering of Neutrinos Around a Cosmic String Loop. *Phys. Rev.*, D36:2242, 1987.

[19] S. Eidelman, K.G. Hayes, K.A. Olive, et al. Review of Particle Physics. *Physics Letters B*, 592:1+, 2004.

[20] M. Maltoni and A. Y. Smirnov. Solar neutrinos and neutrino physics. *ArXiv e-prints*, July 2015. 1507.05287.

[21] R.N. Mohapatra and P.B. Pal. *Massive Neutrinos in Physics and Astrophysics*. Lecture Notes in Physics Series. World Scientific, 2004.

[22] K. A. Olive et al. Review of Particle Physics. *Chin. Phys.*, C38:090001, (2014) and 2015 update.

[23] Rohit Verma. Lower bound on neutrino mass and possible CP violation in neutrino oscillations. *Phys. Rev.*, D88:111301, 2013.

[24] A. J. Cuesta, V. Niro, and L. Verde. Neutrino mass limits: Robust information from the power spectrum of galaxy surveys. *Physics of the Dark Universe*, 13:77–86, September 2016.

[25] YONG-YEON KEUM. Neutrino mass bounds from neutrinoless double beta-decays and cosmological probes. *Pramana*, 86(2):437–451, 2016.

[26] Edward W. Kolb and Michael S. Turner. The Early Universe. *Front. Phys.*, 69:1–547, 1990.

[27] Gianpiero Mangano, Gennaro Miele, Sergio Pastor, Teguayco Pinto, Ofelia Pisanti, and Pasquale D. Serpico. Relic neutrino decoupling including flavor oscillations. *Nucl. Phys.*, B729:221–234, 2005.

[28] Antony Lewis. CAMB Notes. http://cosmologist.info/notes/CAMB.pdf.

[29] Fabian Schmidt, Wayne Hu, and Marcos Lima. Spherical collapse and the halo model in braneworld gravity. *Phys. Rev. D*, 81:063005, Mar 2010.

[30] G. Dvali and M. S. Turner. Dark Energy as a Modification of the Friedmann Equation. *ArXiv Astrophysics e-prints*, January 2003. astro-ph/0301510.

[31] W. Fang, S. Wang, W. Hu, Z. Haiman, L. Hui, and M. May. Challenges to the DGP model from horizon-scale growth and geometry. *Phys. Rev. D*, 78(10):103509, November 2008.

[32] K. Koyama. TOPICAL REVIEW: Ghosts in the self-accelerating universe. *Classical and Quantum Gravity*, 24:R231–R253, December 2007.

[33] Kiyotomo Ichiki and Masahiro Takada. Impact of massive neutrinos on the abundance of massive clusters. *Phys. Rev. D*, 85:063521, Mar 2012.

[34] N. Voje Johansen and F. Ravndal. On the discovery of Birkhoff's theorem. *ArXiv Physics e-prints*, August 2005. physics/0508163.

[35] M. Kopp, S. A. Appleby, I. Achitouv, and J. Weller. Spherical collapse and halo mass function in f(R) theories. *Phys. Rev. D*, 88(8):084015, October 2013.

[36] S. Carroll. *Spacetime and Geometry: An Introduction to General Relativity*. Always learning. Pearson Education, Limited, 2013.

[37] S. Weinberg. *Cosmology*. Cosmology. OUP Oxford, 2008.

[38] L. Amendola and S. Tsujikawa. *Dark Energy: Theory and Observations*. Cambridge University Press, 2010.

[39] Ø. Elgarøy. The spherical collapse model. https://www.uio.no/studier/emner/matnat/astro/AST4320/h12/undervisningsmateriale/spherecollapse.pdf, 2012. Lecture notes in AST 4320: Cosmology and Extragalactic astronomy (University of Oslo).

[40] S. Meyer, F. Pace, and M. Bartelmann. Relativistic virialization in the spherical collapse model for Einstein-de Sitter and ΛCDM cosmologies. *Phys. Rev. D*, 86(10):103002, November 2012.

[41] E. Babichev and C. Deffayet. An introduction to the Vainshtein mechanism. *Classical and Quantum Gravity*, 30(18):184001, September 2013.

[42] John Burkardt. Odepack: Ordinary differential equation solvers. https://people.sc.fsu.edu/~jburkardt/f77_src/odepack/odepack.html, 2012. Online resource.

[43] Ø. Elgarøy. The Press-Schechter mass function. https://www.uio.no/studier/emner/matnat/astro/AST4320/h12/undervisningsmateriale/psmassfunction.pdf, 2012. Lecture notes in AST 4320: Cosmology and Extragalactic Astronomy (University of Oslo).